



NUREG/CR-6965
ANL-07/11

Irradiation-Assisted Stress Corrosion Cracking of Austenitic Stainless Steels and Alloy 690 from Halden Phase-II Irradiations

AVAILABILITY OF REFERENCE MATERIALS IN NRC PUBLICATIONS

NRC Reference Material

As of November 1999, you may electronically access NUREG-series publications and other NRC records at NRC's Public Electronic Reading Room at <http://www.nrc.gov/reading-rm.html>. Publicly released records include, to name a few, NUREG-series publications; *Federal Register* notices; applicant, licensee, and vendor documents and correspondence; NRC correspondence and internal memoranda; bulletins and information notices; inspection and investigative reports; licensee event reports; and Commission papers and their attachments.

NRC publications in the NUREG series, NRC regulations, and *Title 10, Energy*, in the Code of *Federal Regulations* may also be purchased from one of these two sources.

1. The Superintendent of Documents
U.S. Government Printing Office
Mail Stop SSOP
Washington, DC 20402-0001
Internet: bookstore.gpo.gov
Telephone: 202-512-1800
Fax: 202-512-2250
2. The National Technical Information Service
Springfield, VA 22161-0002
www.ntis.gov
1-800-553-6847 or, locally, 703-605-6000

A single copy of each NRC draft report for comment is available free, to the extent of supply, upon written request as follows:

Address: U.S. Nuclear Regulatory Commission
Office of Administration
Mail, Distribution and Messenger Team
Washington, DC 20555-0001

E-mail: DISTRIBUTION@nrc.gov

Facsimile: 301-415-2289

Some publications in the NUREG series that are posted at NRC's Web site address <http://www.nrc.gov/reading-rm/doc-collections/nuregs> are updated periodically and may differ from the last printed version. Although references to material found on a Web site bear the date the material was accessed, the material available on the date cited may subsequently be removed from the site.

Non-NRC Reference Material

Documents available from public and special technical libraries include all open literature items, such as books, journal articles, and transactions, *Federal Register* notices, Federal and State legislation, and congressional reports. Such documents as theses, dissertations, foreign reports and translations, and non-NRC conference proceedings may be purchased from their sponsoring organization.

Copies of industry codes and standards used in a substantive manner in the NRC regulatory process are maintained at—

The NRC Technical Library
Two White Flint North
11545 Rockville Pike
Rockville, MD 20852-2738

These standards are available in the library for reference use by the public. Codes and standards are usually copyrighted and may be purchased from the originating organization or, if they are American National Standards, from—

American National Standards Institute
11 West 42nd Street
New York, NY 10036-8002
www.ansi.org
212-642-4900

Legally binding regulatory requirements are stated only in laws; NRC regulations; licenses, including technical specifications; or orders, not in NUREG-series publications. The views expressed in contractor-prepared publications in this series are not necessarily those of the NRC.

The NUREG series comprises (1) technical and administrative reports and books prepared by the staff (NUREG-XXXX) or agency contractors (NUREG/CR-XXXX), (2) proceedings of conferences (NUREG/CP-XXXX), (3) reports resulting from international agreements (NUREG/IA-XXXX), (4) brochures (NUREG/BR-XXXX), and (5) compilations of legal decisions and orders of the Commission and Atomic and Safety Licensing Boards and of Directors' decisions under Section 2.206 of NRC's regulations (NUREG-0750).

DISCLAIMER: This report was prepared as an account of work sponsored by an agency of the U.S. Government. Neither the U.S. Government nor any agency thereof, nor any employee, makes any warranty, expressed or implied, or assumes any legal liability or responsibility for any third party's use, or the results of such use, of any information, apparatus, product, or process disclosed in this publication, or represents that its use by such third party would not infringe privately owned rights.



United States Nuclear Regulatory Commission

Protecting People and the Environment

NUREG/CR-6965
ANL-07/11

Irradiation-Assisted Stress Corrosion Cracking of Austenitic Stainless Steels and Alloy 690 from Halden Phase-II Irradiations

Manuscript Completed: February 2007

Date Published: September 2008

Prepared by

Y. Chen, O.K. Chopra, W.K. Soppet, N.L. Dietz Rago

W.J. Shack

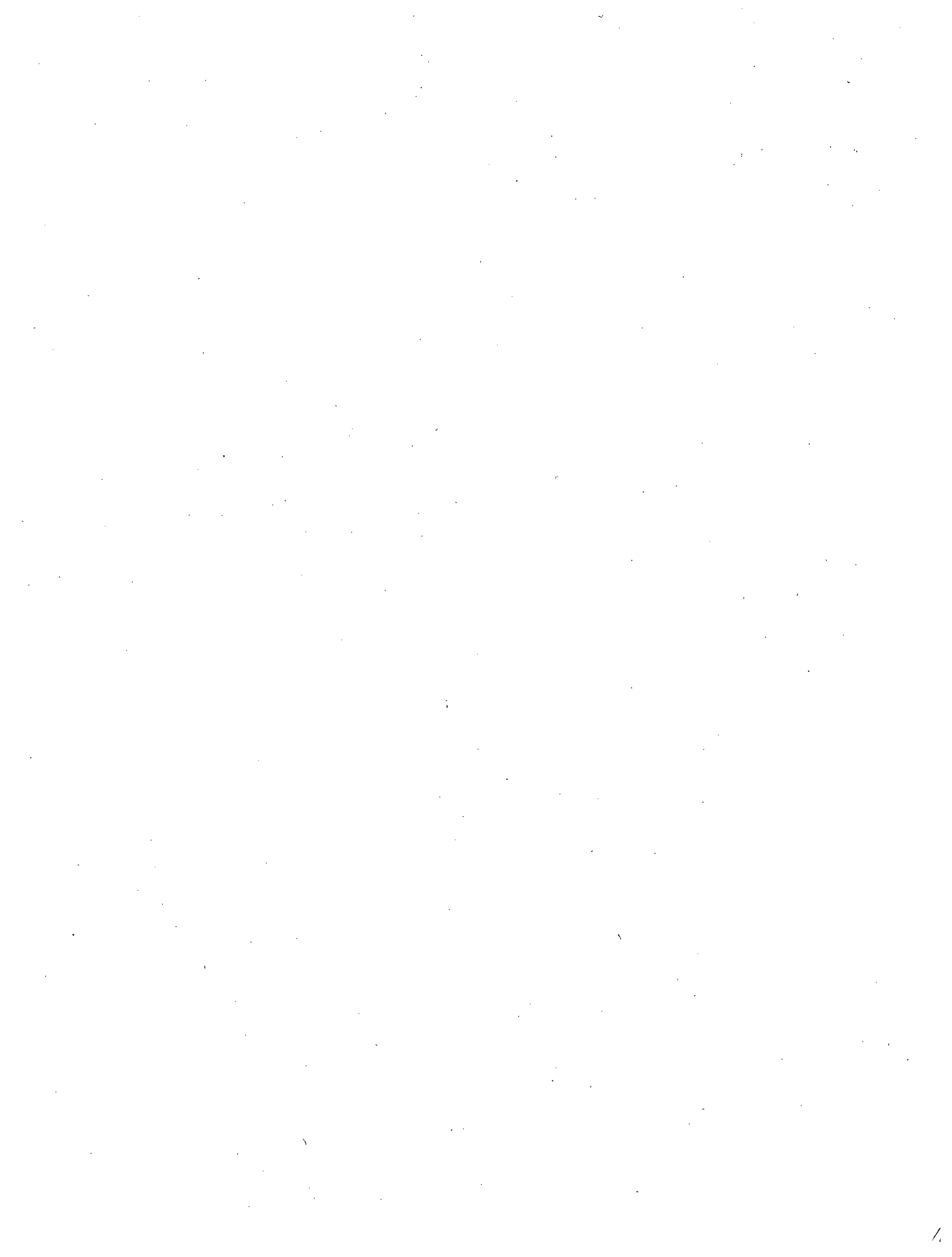
Argonne National Laboratory

Argonne, IL 60439

A.S. Rao, NRC Project Manager

NRC Job Code Y6388

Office of Nuclear Regulatory Research



Abstract

This work is an ongoing effort at Argonne National Laboratory on the mechanistic study of irradiation-assisted stress corrosion cracking (IASCC) in the core internals of light water reactors. Phase II in this effort focused on determining the influence of grain boundary engineering (GBE), alloying elements, and neutron dose on the IASCC susceptibility of austenitic stainless steels (SSs) and Alloy 690. Flat dog-bone specimens irradiated in the Halden boiling heavy water reactor to neutron doses of ≈ 2 displacements per atom (dpa) were subjected to slow strain rate tensile (SSRT) tests in high dissolved oxygen water at 289°C. The areas of the fracture surfaces with brittle fracture morphology (intergranular and transgranular cleavage cracking) were measured with a scanning electron microscope. All materials showed significant irradiation hardening and loss of ductility. Some strain hardening was observed in the normal-Carbon (C) content SSs (Types 304 and 316) and Alloy 690, but not in the low-C content SSs (Types 304L and 316L). The area fraction of the intergranular cracking increased with decreasing uniform elongation and was used to rank the IASCC susceptibility of the alloys. The GBE process did not seem to have a significant effect on the IASCC behavior of Type 304 and 304L SSs, at least at a dose level of about ≈ 2 dpa, but did affect the cracking behavior of Alloy 690. A minimum-C content and a low-sulfur (S) content (< 0.002 wt.%) may be required for IASCC resistance. By analysis of the results from the Halden Phase-II specimens along with previous results on Halden Phase-I specimens, the effect of neutron dose on IASCC behavior was determined. While irradiation hardening and embrittlement start below 0.4 dpa, IG cracking appears between 0.4 and 1.3 dpa for most commercial austenitic SSs in this study.

Paperwork Reduction Act Statement

This NUREG does not contain information collection requirements and, therefore, is not subject to the requirements of the Paperwork Reduction Act of 1995 (44 U.S.C. 3501 et seq.).

Public Protection Notification

The NRC may not conduct or sponsor, and a person is not required to respond to, a request for information or an information collection requirement unless the requesting document displays a current valid OMB control number.

Foreword

This report examines the effects of simulated light-water reactor coolant, irradiation damage, material chemistry, and grain boundary engineering (GBE) on the irradiation-assisted stress-corrosion cracking (IASCC) susceptibility of austenitic stainless steels (SSs) and Alloy 690. This report is one of a series dating back nearly 10 years describing such results, and supports analysis of the structural integrity of reactor internal components, many of which are subject to IASCC. These earlier reports present results on specimens irradiated in Phases I and II in the Halden test reactor.

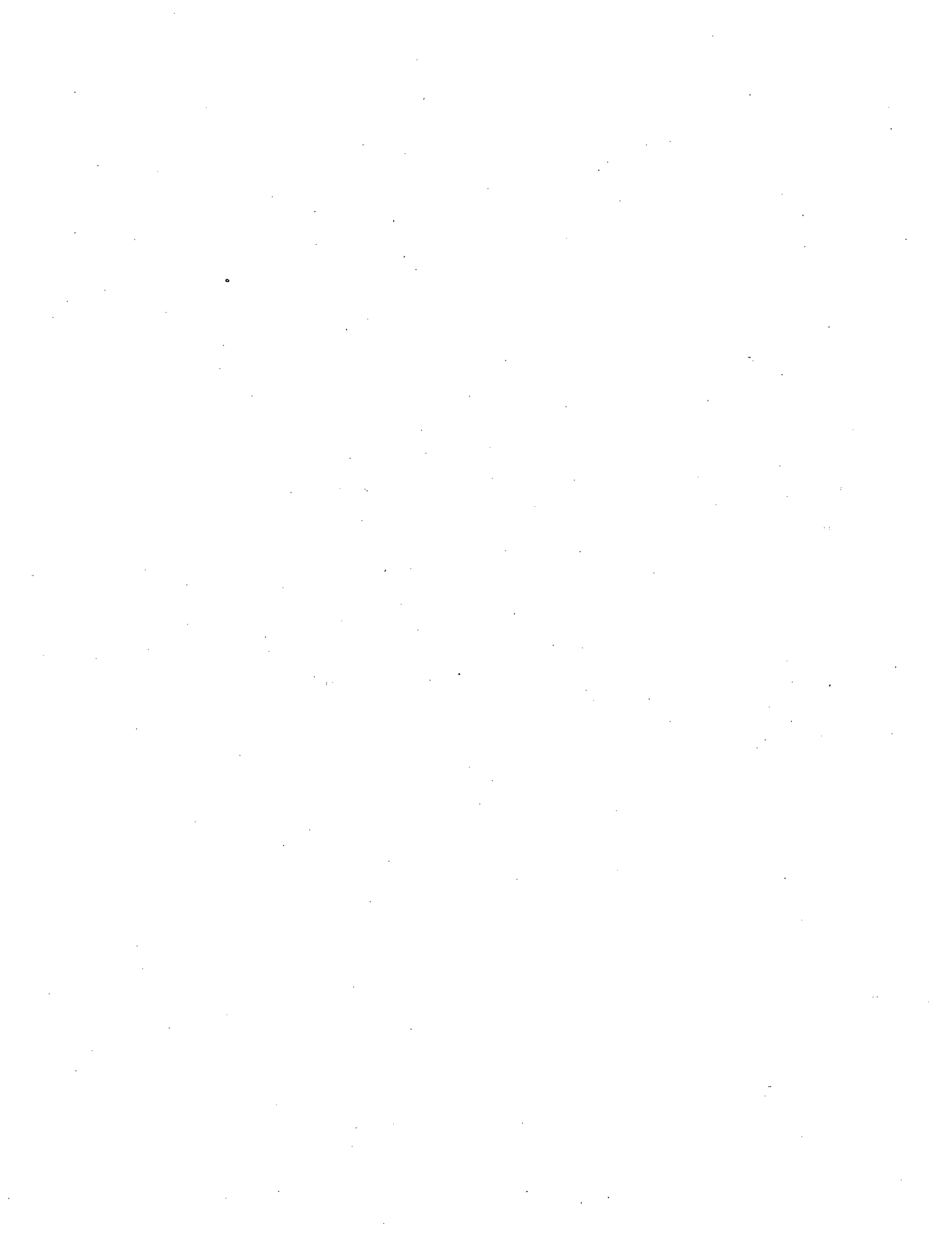
This report is built upon specimens irradiated to approximately 2 displacements per atom (dpa) in Phase II in the Halden test reactor. Phase I irradiations included SSs of wide-ranging chemistry (including commercial steels of typical SS chemistry) and conventional thermomechanical processing. Phase II irradiations include several innovatively fabricated and engineered alloys that are designed to (possibly) be more resistant to IASCC. Future reports will detail the results of ongoing and future tests of higher fluence Phase II irradiations.

As in earlier reports, alloying elements have an effect on IASCC susceptibility. This study shows that high oxygen content contributes to the IASCC susceptibility by enhancing intergranular crack initiation. In addition, low carbon content is associated with a poor ductility in high-dissolved-oxygen (DO) water for all irradiated austenitic SSs, which was shown through the linear increase in uniform elongation with carbon content up to 0.06 weight percent (wt.%). Carbon and sulfur content contribute to the IASCC susceptibility of austenitic SSs. Reducing the sulfur content to less than about 0.002 wt.% protects against IASCC; however, this alone is not a sufficient material condition to ensure resistance to IASCC. With a similar sulfur composition, a low-carbon austenitic SS is more susceptible to IASCC than a normal-carbon SS. Thus, there may be a tradeoff in minimizing susceptibility to IASCC and minimizing susceptibility to intergranular stress-corrosion cracking resulting from conventional sensitization.

The GBE process used in this study did not show a significant, beneficial effect for Type 304 or 304L SS. However, the GBE treatment did result in a smaller reduction in uniform elongation for Alloy 690 at 2 dpa and did reduce its IASCC susceptibility in high-DO water.

In part, the results of this report form the technical basis for Title 10, Section 50.55a, "Codes and Standards," of the *Code of Federal Regulations* (10 CFR 50.55a). In addition, the results of this research, including crack growth rates, may be reviewed, and if applicable, used as a basis for deciding whether to approve or deny requests for relief or requests for reductions in the inspection requirements of 10 CFR 50.55a.

Jennifer L. Uhle, Director
Division of Engineering
Office of Nuclear Regulatory Research
U.S. Nuclear Regulatory Commission



Contents

Abstract.....	iii
Foreword.....	v
Executive Summary.....	xiii
Acknowledgments.....	xv
Acronyms and Abbreviations.....	xvii
1 Introduction.....	1
2 Experimental.....	3
2.1 Specimens and Irradiation.....	3
2.2 Test Facility and Procedure.....	4
3 Results.....	7
3.1 SSRT Tests.....	7
3.2 Fracture Surface and Gauge Surface Observations.....	9
3.2.1 Baseline Specimens.....	9
3.2.2 Irradiated Type 304 SS.....	11
3.2.3 Irradiated Type 304L SSs.....	13
3.2.4 Irradiated Type 316 and 316L SSs.....	18
3.2.5 Irradiated Alloy 690.....	21
3.3 Measurements of IG and TG Cracking on Fracture Surfaces.....	22
4 Discussion.....	25
4.1 SSRT Tests.....	25
4.1.1 Effect of Irradiation and High-DO Water Environment on the SSRT Behavior....	25
4.1.2 Influence of GBE Processing on the SSRT Behavior.....	27
4.1.3 Influence of Alloying Elements on the SSRT Behavior of Austenitic SSs.....	28

4.2	Fractographic Analyses.....	30
4.2.1	Influence of Irradiation and High-DO Water on the Fracture Morphology	30
4.2.2	IASCC Susceptibility of Halden Phase-II Specimens	31
4.2.3	Effect of GBE Process on the IASCC Behavior.....	33
4.2.4	Effects of Alloying Elements on the IASCC Behavior of Austenitic SSs.....	34
4.2.5	Irradiation Dose and IASCC Behavior	41
5	Summary	43
	References.....	45
	Appendix A.....	A-1

Figures

1.	Halden SSRT test specimen geometry.....	3
2.	Schematic diagram of the recirculating water system.....	5
3.	Schematic for determining SSRT properties.....	7
4.	Stress-strain curves of SSRT specimens tested in high-DO water environment: Type 304 SS, Type 304L SS, Type 316 and 316L SS, and Alloy 690.....	8
5.	Ductile dimple morphology on the fracture surface of nonirradiated GBE Type 304L SS tested in high-DO water at 289°C.....	9
6.	Ductile dimple morphology on the fracture surface of irradiated GBE Type 304L SS tested in air at 287-292°C.....	10
7.	Similar appearance of gauge surfaces for nonirradiated GBE Type 304L SS tested in high-DO water at 289°C and irradiated GBE Type 304L SS tested in air.	10
8.	IG and mixed-mode cracks on the fracture surface of Type 304 SS tested in high-DO water at 289°C.....	11
9.	Fracture surface of GBE Type 304 SS tested in high-DO water at 289°C.....	12
10.	Comparison of gauge surface for Type 304 and GBE Type 304 SSs tested in high-DO water at 289°C.....	13
11.	Fracture surface of Type 304L SS tested in high-DO water at 289°C.....	14
12.	Fracture surface of irradiated GBE Type 304L SS tested in high-DO water at 289°C.....	15
13.	Comparison between gauge surface of Type 304L and GBE Type 304L SSs tested in high-DO water at 289°C.....	15
14.	Fracture surfaces of two high-purity Type 304L SSs with low-O content tested in high-DO water at 289°C.....	16
15.	Fracture surface of high-purity Type 304L SS with high-O content tested in high-DO water at 289°C.....	17
16.	Moderate plastic deformation and occasional surface cracks on the gauge surfaces of high-purity Type 304L SSs: low-O content and high-O content.....	17
17.	Fracture surface of GBE Type 316 SS tested in high-DO water at 289°C.....	18
18.	A surface crack on the gauge surface of GBE Type 316 SS tested in high-DO water at 289°C.....	19

19.	Fracture surfaces of Type 316LN SS tested in high-DO water at 289°C.	19
20.	Fracture surfaces of Ti-doped Type 316LN SS tested in high-DO water at 289°C.	20
21.	Gauge surfaces of Type 316 LN SS and Ti-doped Type 316 LN.	20
22.	Fracture surfaces of Alloy 690 and GBE Alloy 690 tested in high-DO water at 289°C.	21
23.	Gauge surfaces of Alloy 690 and GBE Alloy 690 tested in high-DO water at 289°C.	22
24.	Schematic for fracture surface characterization and measurement.	22
25.	Effects of irradiation and high-DO water on the SSRT behavior of GBE Type 304L SS.	25
26.	Variation in yield strength with irradiation dose in high-DO water at 289°C.	26
27.	Variation in ultimate tensile strength with irradiation dose in high-DO water at 289°C.	26
28.	Variation in uniform elongation with irradiation dose in high-DO water at 289°C.	27
29.	Variation in total elongation with irradiation dose in high-DO water at 289°C.	27
30.	The influence of GBE treatment on the increase in YS and decrease in UE in high-DO water at 289°C.	28
31.	The influence of alloy elements on the uniform elongation for austenitic SSs with and without GBE treatment.	29
32.	Fraction of IG and TG fracture in the Halden Phase-II specimens tested in high-DO water at 289°C.	31
33.	Uniform elongations of the Halden Phase-II specimens tested in high-DO water at 289°C.	32
34.	Correlation between IG fraction and UE among Halden Phase-I and Phase-II specimens.	32
35.	Number of IG and TG cracks observed in Halden Phase-II specimens.	33
36.	Number of IG cracks normalized by the UE in Halden Phase-II specimens.	33
37.	Comparisons of Type 304 and 316 SSs for the IG area fraction and the number of IG cracks normalized by uniform elongation.	35
38.	The influence of Cr and Ni content on the IG cracking for austenitic SSs.	36
39.	The influence of C content on the IG cracking behavior for austenitic SSs.	37
40.	The influence of S content on the IG cracking behavior for austenitic SSs.	37

41.	Range of bulk S and C contents in which Type 304 or 316 steels are resistant or susceptible to IASCC in BWR-like oxidizing water.	38
42.	Ranges in the sulfur-carbon content map that austenitic SSs are resistant and susceptible to IASCC in high-DO aqueous environment.	38
43.	The influence of P content on the IG cracking behavior for austenitic SSs.....	39
44.	The influence of Mn content on the IG cracking behavior for austenitic SSs.	39
45.	The influence of N content on the IG cracking behavior for austenitic SSs.....	40
46.	The influence of Si content on the IG cracking behavior for austenitic SSs.....	40
47.	Dose dependence of IG area fraction for Halden Phase-I and Phase-II specimens tested in high-DO water at 289°C.	41
48.	Dose dependence of number of IG cracks per UE for Halden Phase-II specimens tested in high-DO water at 289°C.	42

Tables

1.	Chemical compositions of Halden Phase-II SSRT specimens.....	3
2.	Irradiation conditions for Halden Phase-II SSRT specimens.....	4
3.	Results of Halden Phase-II SSRT tests.....	8
4.	Measurements of IG and TG cracking on the fracture surfaces of Halden Phase-II specimens.	23
5.	Chemical compositions of commercial heats in Halden Phase-I study.....	26
6.	Comparison of SSRT results with tensile properties obtained before irradiation.....	28
7.	Percentages of CSL boundaries (Σ) in GBE materials irradiated in Halden Phase-II study.....	34

Executive Summary

Non-sensitized austenitic stainless steels (SSs) and nickel (Ni) alloys used in the core internals of light water reactors (LWRs) have experienced intergranular (IG) cracking after extended neutron exposure. This form of material degradation is commonly referred to as irradiation-assisted stress corrosion cracking (IASCC). This complex phenomenon involves simultaneous actions of irradiation, stress, and corrosion. As nuclear power plants age, IASCC becomes an important issue for the reliable continuous operation of LWRs. A research program was established at Argonne National Laboratory (ANL) to evaluate the IASCC susceptibility of core internal materials and to further the understanding of the IASCC mechanism. The current research at ANL involves experimental testing and evaluation of various austenitic SSs, Alloy 690, and grain boundary engineered (GBE) materials irradiated in the Halden boiling heavy water reactor. This report summarizes the results of SSRT tests conducted in high purity water with high dissolved oxygen (DO). The influences of GBE treatment, alloying elements, and neutron dose on IASCC susceptibilities are discussed.

As part of the Halden Phase-II project, flat dog-bone tensile specimens of several austenitic SSs and Alloy 690 were irradiated to a fast neutron fluence of $\approx 1.6 \times 10^{21}$ n/cm² (>1 MeV) (≈ 2 dpa). The irradiated specimens underwent SSRT testing in high-DO water at 289°C. The fracture surfaces of the test specimens were examined, and the area fractions of the regions with intergranular cracking were measured with a scanning electron microscope (SEM). The area fractions of IG cracking, along with the uniform elongation (UE) obtained from the SSRT tests, were used to evaluate the IASCC susceptibility of the examined alloys.

Irradiation hardening and embrittlement were observed in all irradiated specimens. At the dose level of ≈ 2 dpa, the SSRT yield strengths of irradiated specimens were about three times higher than those of nonirradiated specimens, and the UE of irradiated specimens was less than 10%. Some strain hardening was observed in the normal-C content SSs (Types 304 and 316) and Alloy 690, but not in the low-C content SSs (Types 304L and 316L). A low-C content is associated with a poor ductility in high-DO water for all irradiated austenitic SSs, and the UE obtained from SSRT tests in high-DO water increases linearly with C content up to 0.06 weight percent (wt.%).

Regions with intergranular (IG) or transgranular (TG) cracking were observed in all irradiated specimens except GBE Alloy 690. A general correlation can be seen between the IG area fraction and UE. Fractographic analysis also showed that IG cracks always initiated on the surface of an SSRT specimen and then extended into the specimen's interior under stress. Transgranular cracks observed in SSRT specimens did not necessarily originate from IG crack sites.

The GBE process employed in this study increased the coincident site lattice boundaries ($\Sigma < 29$) to $\approx 66\%$ for austenitic SSs and to $\approx 70\%$ for Alloy 690. For Alloy 690, the GBE treatment results in a smaller reduction in UE after irradiation and reduces the IG susceptibility in high-DO water. However, little beneficial effect of the current GBE process was observed for Type 304 and 304L SSs.

Similar to the Halden Phase-I results, a higher IG area fraction is often seen in low-C and high-S austenitic SSs. An S content below 0.002 wt.% is a critical requirement for IASCC resistance in austenitic SSs. With a similar S composition, a low-C austenitic SS is more susceptible to IASCC than a normal-C SS. Thus, there may be a trade-off in minimizing susceptibility to IASCC and minimizing susceptibility to IGSCC resulting from conventional sensitization.

Type 316 SSs tested in this study showed more resistance to IASCC than Type 304 SSs. The presence of Mo or the higher Ni concentrations in Type 316 SSs may contribute to the difference in IASCC susceptibility between Type 304 and 316 SSs. By comparing the results between two high-purity Type 304L SSs, we found that the oxygen (O) content is also critical for IASCC susceptibility. The high-O content contributes to the IASCC susceptibility by enhancing IG crack initiation.

Although irradiation hardening and loss of ductility are evident at 0.4 dpa for all alloys, IG cracking only starts to appear between 0.4 and 1.3 dpa in the commercial austenitic SSs. This dose range is consistent with the threshold value reported by other researchers. The threshold dose may also vary among materials.

Acknowledgments

The authors thank T. M. Karlsen, OECD Halden Reactor Project, Halden, Norway, for specimen irradiations in the Halden reactor; D. O. Pushis for specimen retrieval; and L. A. Knoblich, E. E. Gruber, R. Clark, and E. J. Listwan for their contributions to the experimental effort. The authors are also grateful to W. H. Cullen, Jr. and S. Crane for many helpful discussions. This work is sponsored by the Office of Nuclear Regulatory Research, U.S. Nuclear Regulatory Commission, under Job Code Y6388; Program Manager: Appajosula S. Rao.

Acronyms and Abbreviations

ABB	Asea Brown Boveri Ltd.
ANL	Argonne National Laboratory
BWR	Boiling Water Reactor
CSL	Coincident Site Lattice
DO	Dissolved Oxygen
dpa	Displacements per atom
dpm	Disintegrations per minute
ECP	Electrochemical Potential
FS	Fracture Strength
GBE	Grain Boundary Engineered
IASCC	Irradiation-Assisted Stress Corrosion Cracking
IG	Intergranular
kV	kilovolt
LWR	Light Water Reactor
MATMs	Melting Alloy Temperature Monitors
MeV	Million electronvolt
MPa	Megapascal
mm	Millimeter
ml/min	Milliliter / minute
mV	Millivolt
$\mu\text{s/cm}$	Microsiemens / centimeter
n/cm^2	Neutron / centimeter ²
ppm	Parts per million
psig	Pound per square inch gauge
PWR	Pressurized Water Reactor
RIS	Radiation-Induced Segregation
SCC	Stress Corrosion Cracking
SEM	Scanning Electron Microscope
SHE	Standard Hydrogen Electrode
SS	Stainless Steel
SSRT	Slow Strain Rate Tensile
TE	Total Elongation
TG	Transgranular
UE	Uniform Elongation
UTS	Ultimate Tensile Strength
YS	Yield Strength
wt.%	Weight percent %



1 Introduction

As nuclear power plants age and exposure to neutron irradiation increases, failures of reactor core internal components have increased. Examples of such failures include cracking of the core shroud, jet pump assembly, top guide, and core plate in boiling water reactors (BWRs)¹⁻⁷ and baffle former bolts in pressurized water reactors (PWRs).⁸ When exposed to neutron irradiation for extended periods, various nonsensitized austenitic stainless steels (SSs) and Ni alloys become susceptible to intergranular (IG) failure. This form of degradation is commonly referred to as irradiation-assisted stress corrosion cracking (IASCC). This complex process involves simultaneous actions of irradiation, stress, and corrosion. In recent years, to address issues related to plant aging and license renewal, IASCC studies have attracted increased attention.

Neutron irradiation plays a key role in IASCC of internal components in light water reactors (LWRs). A characteristic rise in IASCC susceptibility is observed above a "threshold" neutron fluence. This threshold is often taken to be $\approx 5 \times 10^{20}$ n/cm² ($E > 1$ MeV)* (≈ 0.75 dpa) in BWR environments,^{9,10} and approximately one order of magnitude higher in PWRs.¹¹ Some studies show that IASCC could occur even at a dose as low as $\approx 2 \times 10^{20}$ n/cm² (≈ 0.3 dpa) in water with high dissolved oxygen (DO).¹² Irradiation-induced microstructural (e.g., radiation defects) and microchemical (e.g., radiation-induced segregation) changes in the material combined with changes in water chemistry (e.g., radiolysis) contribute to the increased susceptibility of IG cracking.^{13,14}

Early mechanistic studies of IASCC focused mainly on the depletion of Cr at grain boundaries and its influence on the grain boundary oxidation.¹⁵⁻¹⁷ Radiation-induced segregation (RIS) was considered as the main reason for the sharp Cr depletion at grain boundaries. It is believed that the absence of protective oxide layers stimulates cracking along grain boundaries in the IASCC process. More recently, the roles of impurity elements such as Si, P, and S on IASCC susceptibility have also been investigated.^{14,18} Although redistribution of impurities to grain boundaries due to RIS clearly does occur, no clear correlations have yet been found between the original concentration of impurities in the bulk material and IASCC susceptibility. The Halden Phase-I study was an effort to investigate the contributions of alloying and impurity elements to IASCC susceptibility in various austenitic SSs.¹⁹⁻²¹ The Halden Phase-I study indicates that the S content contributes to the IASCC susceptibility in low-C SSs but is less critical in the high-C SSs.^{21,22} Recent studies on IASCC have also attributed a greater role to radiation hardening and the development of localized deformation modes in the increase of susceptibility.²³ The localized plastic deformation induced by irradiation contributes to the rupture of the oxide film near the grain boundary and, therefore, is a critical factor for IASCC susceptibility.²⁴

Based on the progress in the mechanistic understanding of IASCC, various engineering methods have been proposed to mitigate the effect of IASCC on LWR core internal components. Because of the strong dependence of IASCC susceptibility on the corrosion potential between -100 and 0 mV with a standard hydrogen electrode (SHE),¹⁸ the most effective way to mitigate IASCC may be to control the electrochemical corrosion potential (ECP). In addition, because of the predominately IG nature of IASCC, considerable attention has been paid to the role of grain boundary properties. It is believed that coincident site lattice (CSL) grain boundaries with low Σ numbers[§] (≤ 29) are more resistant to IG cracking.²⁵⁻²⁸ Grain boundary engineering (GBE), a thermomechanical treatment that systematically

* All references to fluence levels are calculated for fast neutron $E \geq 1$ MeV.

§ Σ is the reciprocal of the density of coincident sites. For example, Σ of 17 means that one in every 17 sites in one grain coincides with a site from the neighboring grain, and the density of coincident sites is 1/17.

increases the population of low Σ CSL grain boundaries, is therefore considered as another potential approach to improve the material's resistance to IASCC.

In the Halden Phase-II effort, additional studies were performed on the effects of alloy composition and the GBE process on the IASCC behavior. Slow strain rate tensile (SSRT) tests were conducted in high-DO water at 289°C on several austenitic SSs, Alloy 690, and their GBE counterparts after having been irradiated to the same dose level in the Halden boiling heavy water reactor in Norway. The IASCC susceptibility of the materials was determined by fractographic analyses using a scanning electron microscope (SEM). The Halden Phase-II test matrix also provided opportunities to investigate the effects of bulk O content and Ti doping on the IASCC behavior of austenitic SSs. The results obtained from the Halden Phase-II study also enlarged the Halden Phase-I database, in which the effect of C and S contents on IASCC behavior was determined for austenitic SSs.

2 Experimental

2.1 Specimens and Irradiation

As part of the Halden Phase-II experiment, 32 alloy specimens from 13 heats were irradiated in helium capsules, between August 2001 and October 2004, in the Halden boiling heavy water reactor in Norway. The tensile specimens had a flat dog-bone geometry whose dimensions are given in Fig. 1. All specimens were packed in two irradiation capsules and loaded in the Halden reactor at core position 1-00. The specimens were removed from the reactor in December 2004 and transferred to ANL for SSRT testing in March 2005. Table 1 shows the chemical compositions of the specimens.

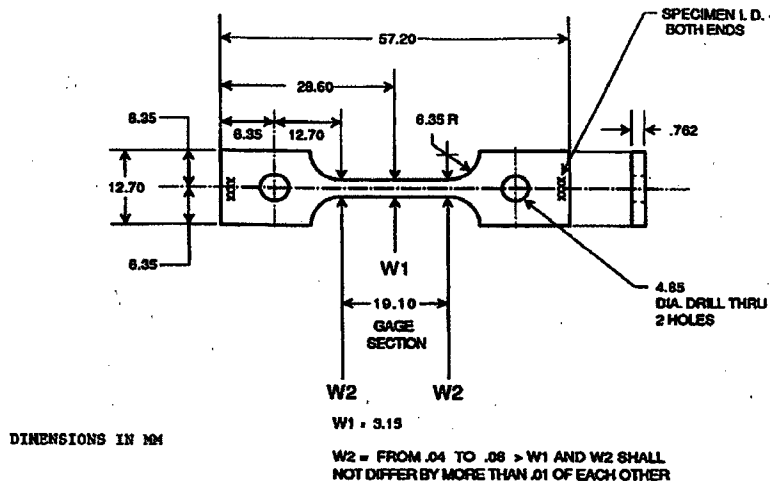


Figure 1.
Halden SSRT test
specimen geometry.

Table 1. Chemical compositions of Halden Phase-II SSRT specimens.

Material Type	Heat ID	Composition (wt.%)								
		Ni	Si	P	S	Mn	C	N	Cr	Others
Type 304 SSs	333	8.45	0.68	0.027	0.019	1.38	0.04	0.068	18.54	Mo 0.37
	GBE304	8.19	0.41	0.029	0.006	1.73	0.054	0.052	18.28	Mo 0.23, Co 0.10, Cu 0.31
	304L	8.33	0.45	0.028	0.007	1.74	0.023	0.090	18.35	Mo 0.37, Co 0.13, Cu 0.35
Type 304L SSs	GBE304L	8.33	0.45	0.028	0.007	1.74	0.020	0.090	18.35	Mo 0.37, Cu 0.35
	327	9.54	0.01	0.001	0.002	1.12	0.006	<0.001	19.71	Mo 0.02, O 0.008
	945	9.03	0.03	<0.005	0.005	1.11	0.005	0.003	19.21	Mo <0.005, O 0.047
	L15	8.00	1.82	0.010	0.013	1.07	0.02	0.085	17.80	O 0.011
Type 316 SSs	GBE316	11.16	0.35	0.029	0.025	1.59	0.041	0.050	16.34	Mo 2.07, Cu 0.37, Co 0.09
	623	12.20	0.7	0.007	0.002	0.97	0.019	0.103	17.23	Mo 2.38, Cu 0.21
	625	12.30	0.72	0.007	0.002	0.92	0.012	0.064	17.25	Mo 2.39, Ti 0.027, Cu 0.21
Alloy 690	690	61.49	0.05	-	0.001	0.15	0.030	-	29.24	Fe 9.02, Co 0.007, Cu 0.01
	GBE690	59.40	0.42	0.026	0.003	0.42	0.010	-	29.10	Fe 10.26, Al 0.22, Ti 0.29
Fe-Cr-Ni model alloy	151	23.49	0.06	0.006	0.005	1.39	0.004	0.001	24.02	Mo 0.002

The target irradiation dose was ≈ 1.8 dpa for all specimens. The actual neutron fluence was monitored by an Al/1% Co wire for thermal neutrons and by Fe and Ni wires for fast neutrons; these wires were attached to the external surface of each of the irradiation capsules. During the irradiation, specimen temperature was monitored by two sets of Melting Alloy Temperature Monitors (MATMs) in each irradiation capsule. The post-irradiation analyses of the dosimeter wires and MATM results provided the actual conditions of the Halden Phase-II irradiation, and the results are summarized in Table 2.

Table 2. Irradiation conditions for Halden Phase-II SSRT specimens.

Heat ID	Material Description	Available Specimens	Neutron Fluence E > 1 MeV ($\times 10^{21}$ n/cm ²)	Damage Dose (dpa)	Irr. Temp. (°C)
333	Type 304 SS from ABB ^a	3	1.63	2.44	290-296
GBE304	GBE Type 304 SS	3	1.31	1.96	296-305
304L	304L SS, commercial heat	2	1.31	1.96	296-305
GBE304L	GBE Type 304L SS	3	1.31	1.96	296-305
327	High-purity Type 304L SS, low O	3	1.63	2.44	290-296
945	High-purity Type 304L SS, high O	3	1.63	2.44	290-296
L15	Type 304 SS, laboratory heat	1	1.63	2.44	290-296
GBE316	GBE Type 316 SS	3	1.31	1.96	296-305
623	Type 316LN (high N, low C)	2	1.63	2.44	290-296
625	Type 316LN (high N, low C), Ti-doped	2	1.63	2.44	290-296
690	Alloy 690	2	1.31	1.96	296-305
GBE690	GBE Alloy 690	3	1.31	1.96	296-305
151	Fe-Cr-Ni model alloy, Fe-20Cr-24Ni	2	1.63	2.44	290-296

^aProcured from Asea Brown Boveri Ltd. (ABB).

2.2 Test Facility and Procedure

The SSRT tests were carried out in a test facility that is located in hot cell #1 of the ANL's Irradiated Materials Laboratory. It is equipped with a worm gear actuator, a set of gear reducers, and a variable speed motor with speed control. A high-purity, high-DO aqueous environment was provided by the recirculating water loop, as shown in Fig. 2. This water loop consists of a storage tank, 0.2 micron filter, high-pressure pump, regenerative heat exchanger, autoclave preheater, test autoclave, electrochemical potential (ECP) cell preheater, ECP cell, air-cooled heat exchanger, Mity MiteTM back-pressure regulator, two ion-exchange cartridges, another 0.2-micron filter, and a return line to the storage tank. The high-pressure portion of the system extends from the high-pressure pump (item 10) to the back-pressure regulator (item 27). Overpressurization of the loop due to temperature excursions is prevented by a rupture disk (set at 2300 psig) installed upstream from the high-pressure pump.

Most SSRT tests on the Halden Phase-II specimens were conducted at 289°C in high-purity water containing ≈ 8 ppm DO, and another test was conducted in laboratory air at ≈ 290 °C to obtain baseline data. For all tests in water, the system pressure was maintained at ≈ 9.31 MPa (≈ 1350 psig). The flow rate of the system was 15-30 ml/min, and water samples were taken periodically from ports 7 and 29B to monitor the resistivity, pH, and DO level in the effluent. The conductivity and pH of water at room temperature were 0.06-0.10 μ S/cm and 6.4-7.2, respectively. The ECPs of a Pt electrode and a SS sample located downstream from the autoclave were monitored continuously during the test. Another

nonirradiated specimen was also tested in water with ≈ 8 ppm DO at 289°C for comparison. The strain rate during for all SSRT tests was held at about $\approx 3.31 \times 10^{-7} \text{s}^{-1}$.

- | | | |
|--------------------------------------|----------------------------------|---|
| 1. Cover gas supply tank | 14. Heat exchanger | 27. Back-pressure regulator |
| 2. Two stage high-pressure regulator | 15. Autoclave preheater | 28. Outlet vent port |
| 3. Low-pressure regulator | 16. Tube autoclave | 29. Loop water sampling port (not used) |
| 4. Compound vacuum & pressure gauge | 17. Thermocouple well | 29B. Loop water sampling port (new) |
| 5. Feed water storage tank | 18. ECP cell preheater | 30. Ion exchange bed |
| 6. Sparger | 19. Preheater thermocouple | 31. 2 nd ion exchange bed |
| 7. Tank water sample port | 20. ECP cell | 32. 0.2 micron filter |
| 8. Solenoid valve | 21. ECP cell thermocouple | 33. Feed water fill port |
| 9. 0.2 micro filter | 22. SS electrode | 34. Recirculating pump |
| 10. High-pressure pump | 23. Standard reference electrode | 35. Check valve |
| 11. Rupture disk | 24. Platinum electrode | 36. Pressure relief valve to tank |
| 12. Check valve | 25. Heat exchanger | 37. Check valve |
| 13. High-pressure gauge | 26. Cooling fan | 38. Bypass pressure relief valve |

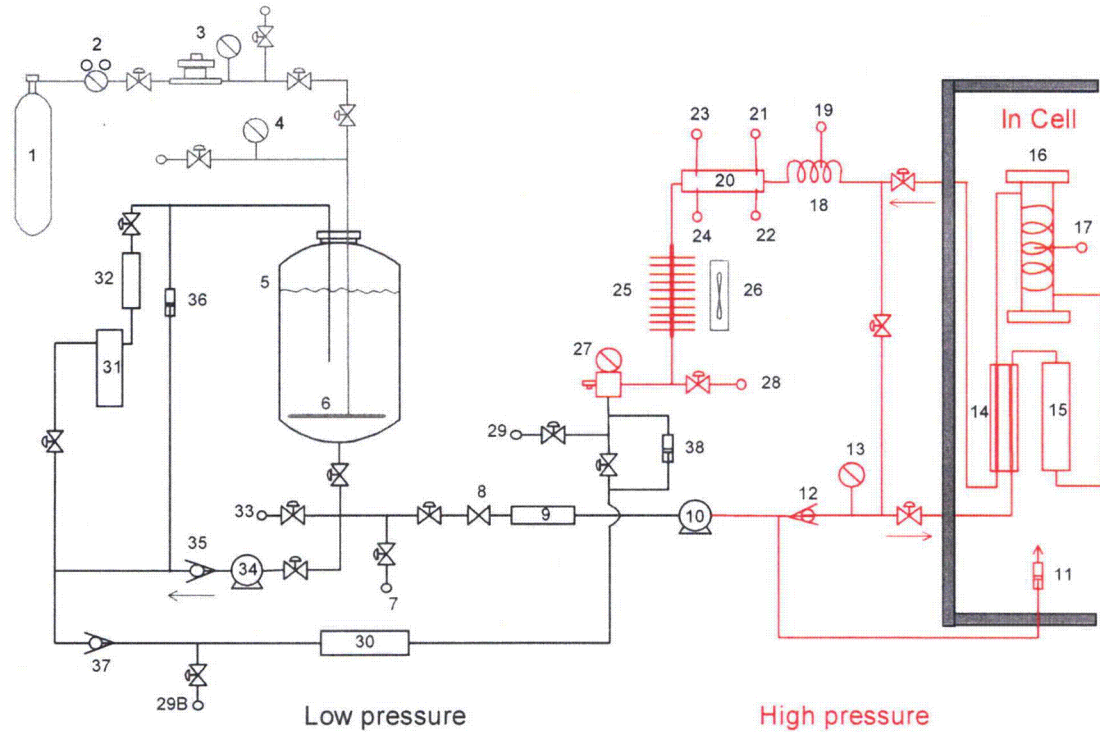


Figure 2. Schematic diagram of the recirculating water system.

Because of the relatively small thickness (≈ 0.76 mm) and cross sectional area (≈ 2.4 mm²) of the SSRT specimens, precautions were taken during specimen installation and pressurization of the autoclave to prevent their premature straining. Each specimen was first loaded in a sample grip and then inserted into the tube autoclave. After tightening of the flanges of the autoclave, both upper and lower pull rods were engaged with the sample grip. The assembled autoclave was then installed in the test frame without having the lower pin in place to maintain a stress-free condition on the specimen. The subsequent pressurization generates about ≈ 120 MPa tensile stress on the specimen. Once the desired temperature and pressure were achieved, the lower pin was inserted to connect the loading train with the lower pull rod. The specimen was then soaked in the autoclave (at 289°C and ≈ 9.3 MPa) for about 24 hours to stabilize the environmental conditions.

To evaluate the IASCC susceptibility, the fracture surfaces of the SSRT test specimens were examined with an SEM. Because of the high radioactivity and loose contamination, safety precautions were taken to prepare the SEM specimens. A fracture tip, about 3 mm (0.12 in.) long, was first cut remotely from a tested SSRT specimen using a shear device installed inside the hot cell. Then, the fracture tip was cleaned with an ultrasonic cleaner and moved out of the hot cell. The obtained fracture tip was manually wiped several times with a damp cloth in a fume hood to further reduce the loose contamination. Once a smear test result was below 200 disintegrations per minute (dpm), the fracture tip was moved to the SEM facility for examination. A Hitachi S-3000N variable pressure microscope was used for the fractographic examinations. A secondary electron image at 30-kV acceleration voltage with 25-mm (1.0 in.) work distance was used for most observations.

3 Results

3.1 SSRT Tests

An SSRT test on a nonirradiated GBE Type 304L SS specimen was carried out in high-DO (≈ 8 ppm DO) water to establish a baseline for irradiated specimens. Another SSRT test on an irradiated GBE Type 304L SS specimen was performed in air around $\approx 290^\circ\text{C}$ as a baseline for the tests in water. All the other SSRT tests were conducted on irradiated specimens in high-DO water at 289°C .

The characteristic SSRT properties were determined by using the scheme illustrated in Fig. 3. If a well-defined upper yield point was present in an SSRT test stress vs. strain curve, the stress at the upper yield point was selected as the yield strength (YS). Otherwise, the stress at 0.2% plastic strain was defined as the yield strength ($YS_{0.2\%}$). If no strain hardening was observed in a stress vs. strain curve, the ultimate tensile strength (UTS) was considered the same as the YS. Accordingly, the uniform elongation (UE) in this case was taken as the plastic strain at the point where the stress vs. strain curve starts to deviate from a linear strain softening. If a small amount of strain hardening remained in a SSRT test, the nominal definition of UE (i.e., the plastic strain at UTS) was used. The fracture strength (FS) was taken at the end of the SSRT test when the specimen was broken. Accordingly, the plastic strain at the fracture was defined as the total elongation (TE). The characteristic SSRT properties determined using this scheme for all Halden SSRT tests performed in this study are summarized in Table 3. The complete SSRT test results, including the engineering stress vs. strain results, are given in Appendix A.

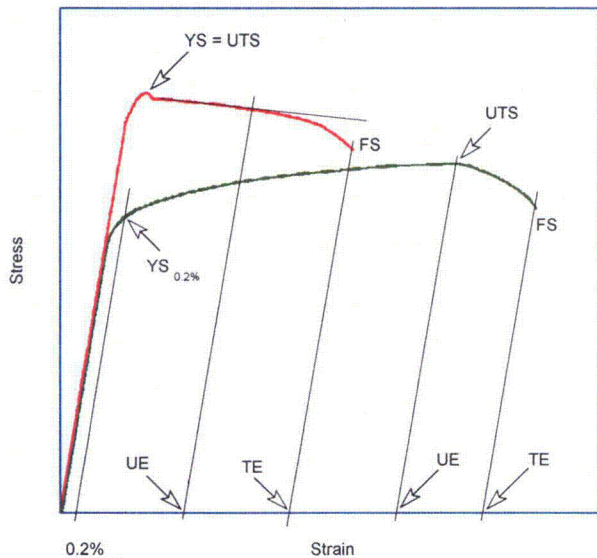


Figure 3. Schematic for determining SSRT properties.

The stress vs. strain curves on the SSRT specimens tested in high-DO water are shown in Fig. 4. A significant amount of irradiation hardening was observed in all the specimens. Irradiation embrittlement was also evident, except for the GBE Alloy 690, where more than 22% uniform elongation remained in this alloy after irradiation. For austenitic SSs, a minimum amount of strain hardening occurred in Type 304 and 316 SSs, while no strain hardening occurred for Type 304L and 316L SSs. For Alloy 690, a considerable amount of strain hardening occurred in the GBE alloy, whereas only limited strain hardening was found in the alloy without the GBE treatment. Dynamic strain aging was observed in both Alloy 690 materials, with and without GBE treatment.

Table 3. Results of Halden Phase-II SSRT tests.

Material	Heat ID	Dose (dpa)	YS (MPa)	UTS (MPa)	FS (MPa)	UE (%)	TE (%)
Type 304 SS	333	2.44	711	711	628	4.06	5.34
	GBE304	1.96	750	750	581	5.80	8.22
	304L	1.96	677	677	282	2.18	4.65
	GBE304L	1.96	747	747	581	1.11	2.22
	GBE304L ^a	1.96	750	750	621	9.41	11.30
	GBE304L ^b	-	231 (0.2%)	532	454	32.20	36.10
Type 304L SS	327	2.44	703	703	334	1.51	3.10
	327	2.44	690	690	333	1.25	2.59
	945	2.44	666	666	443	1.22	2.20
	GBE316	1.96	640 (0.2%)	644	378	4.44	6.80
Type 316 SS	623	2.44	883	883	729	1.94	4.00
	625	2.44	890	890	725	0.75	2.59
Alloy 690	690	1.96	837 (0.2%)	868	743	5.94	7.29
	GBE690	1.96	677 (0.2%)	801	704	22.80	27.60

^aTested in air.

^bNonirradiated specimen, tested in high-DO water.

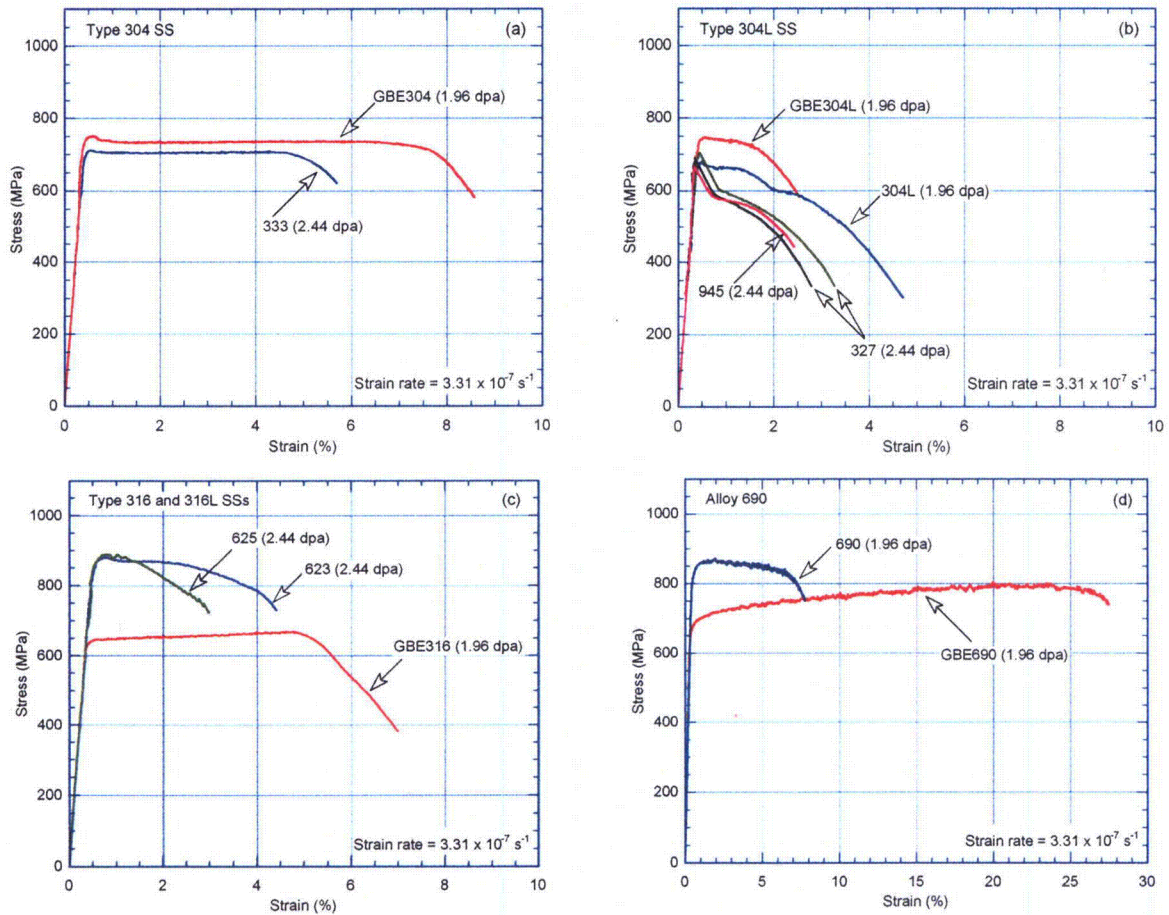


Figure 4. Stress-strain curves of SSRT specimens tested in high-DO water environment: (a) Type 304 SS, (b) Type 304L SS, (c) Type 316 and 316L SS, and (d) Alloy 690.

3.2 Fracture Surface and Gauge Surface Observations

3.2.1 Baseline Specimens

The two baseline specimens, a nonirradiated GBE Type 304L SS tested in water and an irradiated GBE Type 304L SS tested in air, were examined with the SEM. The fracture surfaces of these two specimens are shown in Figs. 5 and 6, and their gauge surfaces appear in Fig. 7. The cross sections of both the nonirradiated and irradiated specimens indicate fully ductile dimple fracture despite their different testing conditions. The gauge surfaces of these two specimens are also very similar. Surface steps resulting from heavy plastic deformation can be seen on both gauge surfaces.

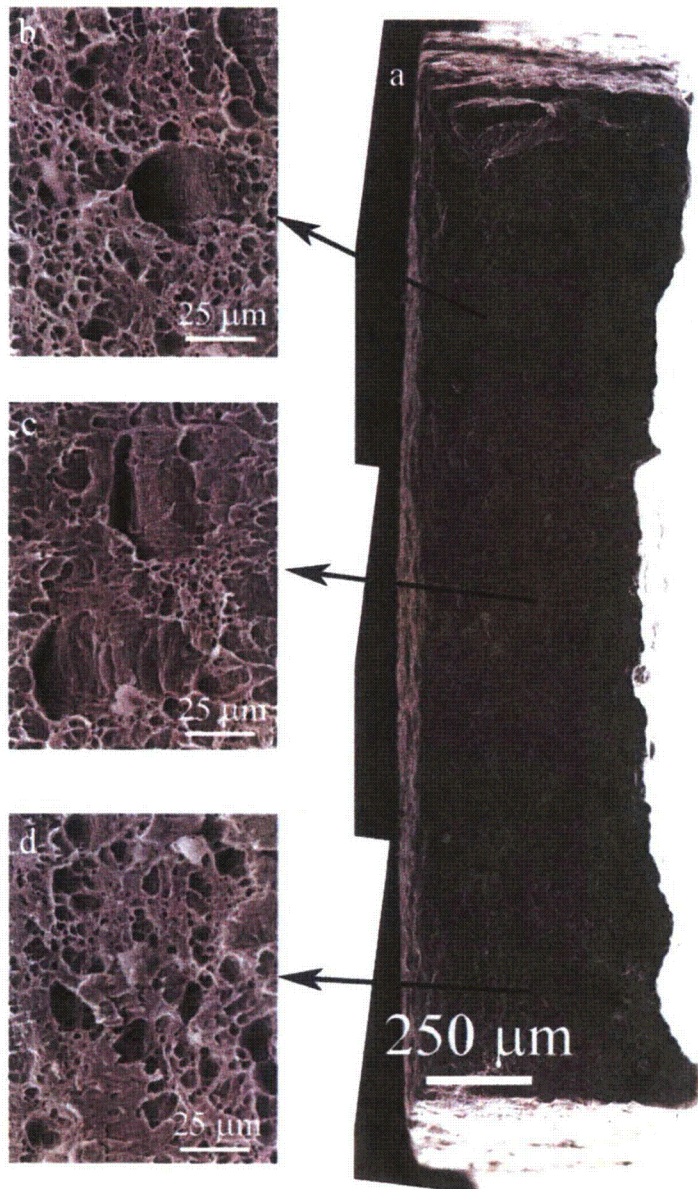


Figure 5.
Ductile dimple morphology on the fracture surface of nonirradiated GBE Type 304L SS tested in high-DO water at 289°C. (a) fracture surface; (b)-(d) ductile fracture with large dimples.

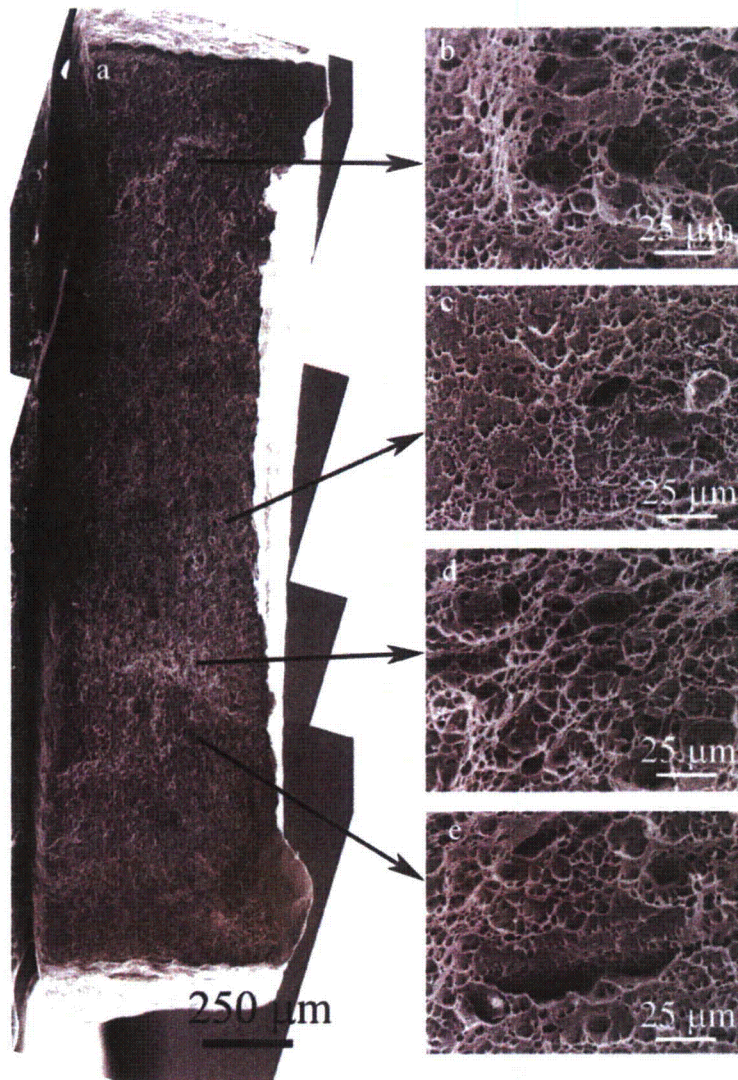


Figure 6. Ductile dimple morphology on the fracture surface of irradiated GBE Type 304L SS tested in air at 287-292°C. (a) fracture surface; (b)-(d) ductile fracture; (e) ductile fracture with a few linked deep dimples.

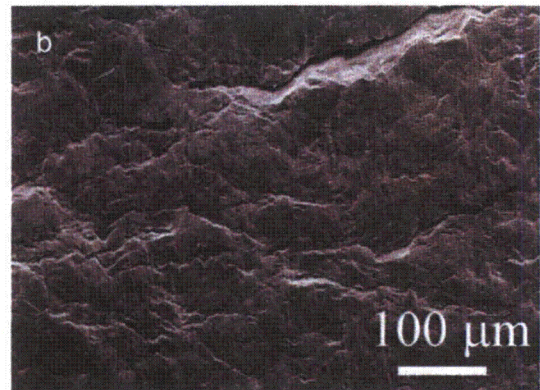
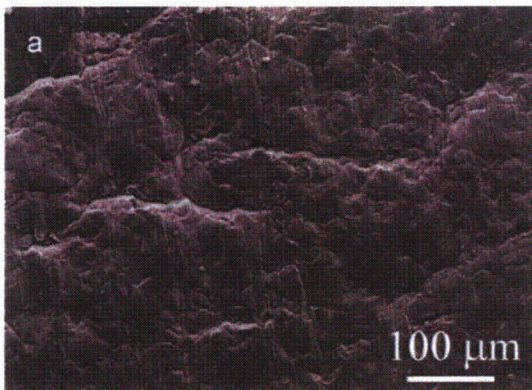


Figure 7. Similar appearance of gauge surfaces for (a) nonirradiated GBE Type 304L SS tested in high-DO water at 289°C and (b) irradiated GBE Type 304L SS tested in air.

3.2.2 Irradiated Type 304 SS

The fracture surface of Type 304 SS (Heat 333) tested in high-DO water in 289°C is shown in Fig. 8. Four separate regions of cracking are seen on this fracture surface. Two regions show full IG fracture, and the other two consist of a mixture of IG and TG fracture. All the IG and mixed-mode cracks start from the surface, but three of them are just a few grains deep. One small IG crack is completely surrounded by a TG region whose area is significantly larger than its IG initiation site. Another IG crack has progressed deeper into the interior of specimen, and a TG region is observed ahead of the IG cracking. An isolated TG area is also seen at the interior of the specimen. It is believed that this TG area is caused by the irradiation embrittlement rather than IASCC, because contact with water is not expected in this region before the failure of the specimen.

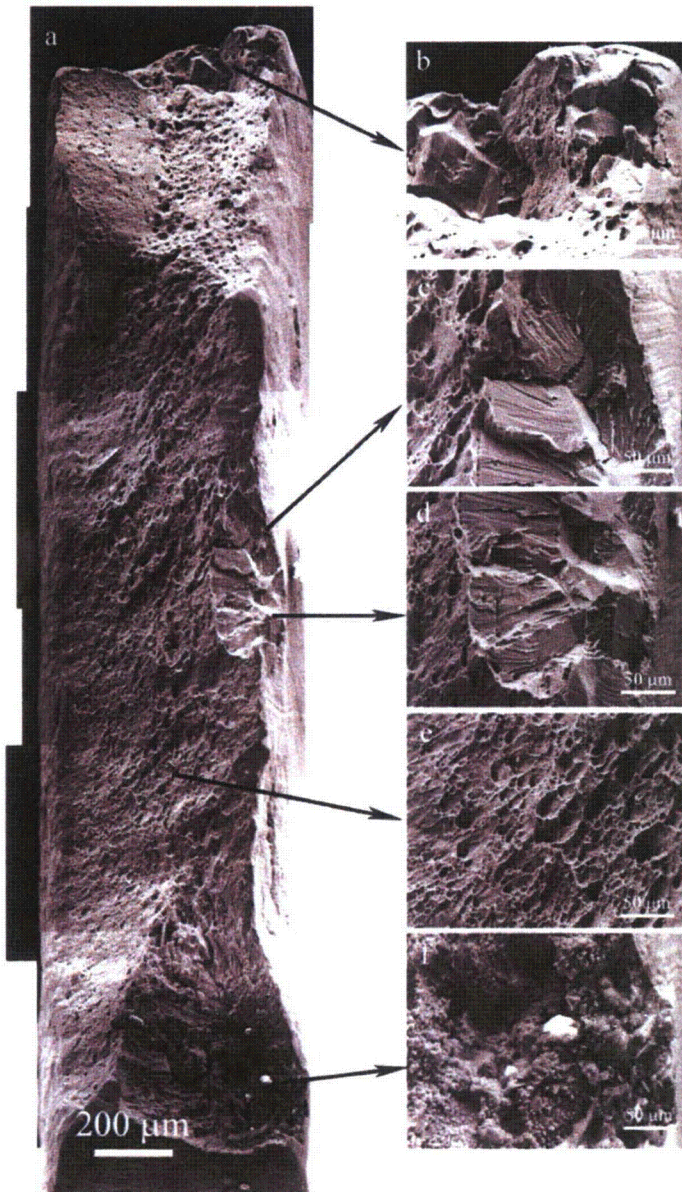


Figure 8.
IG and mixed-mode cracks on the fracture surface of Type 304 SS (Heat 333 from ABB) tested in high-DO water at 289°C. (a) fracture surface; (b) IG cracks; (c) and (d) small IG area surrounded by TG cracking; (e) ductile fracture with elongated dimples; (f) IG cracking area covered by corrosion products.

The fracture surface of the GBE Type 304 SS is shown in Fig. 9; it contains only one large non-ductile region, which is nearly all IG. The IG region starts from one side of the specimen surface and covers more than the half of the specimen thickness. A small region of TG and mixed-mode fracture morphology is seen next to the initial IG crack, and the rest of the cross section has a ductile failure appearance.

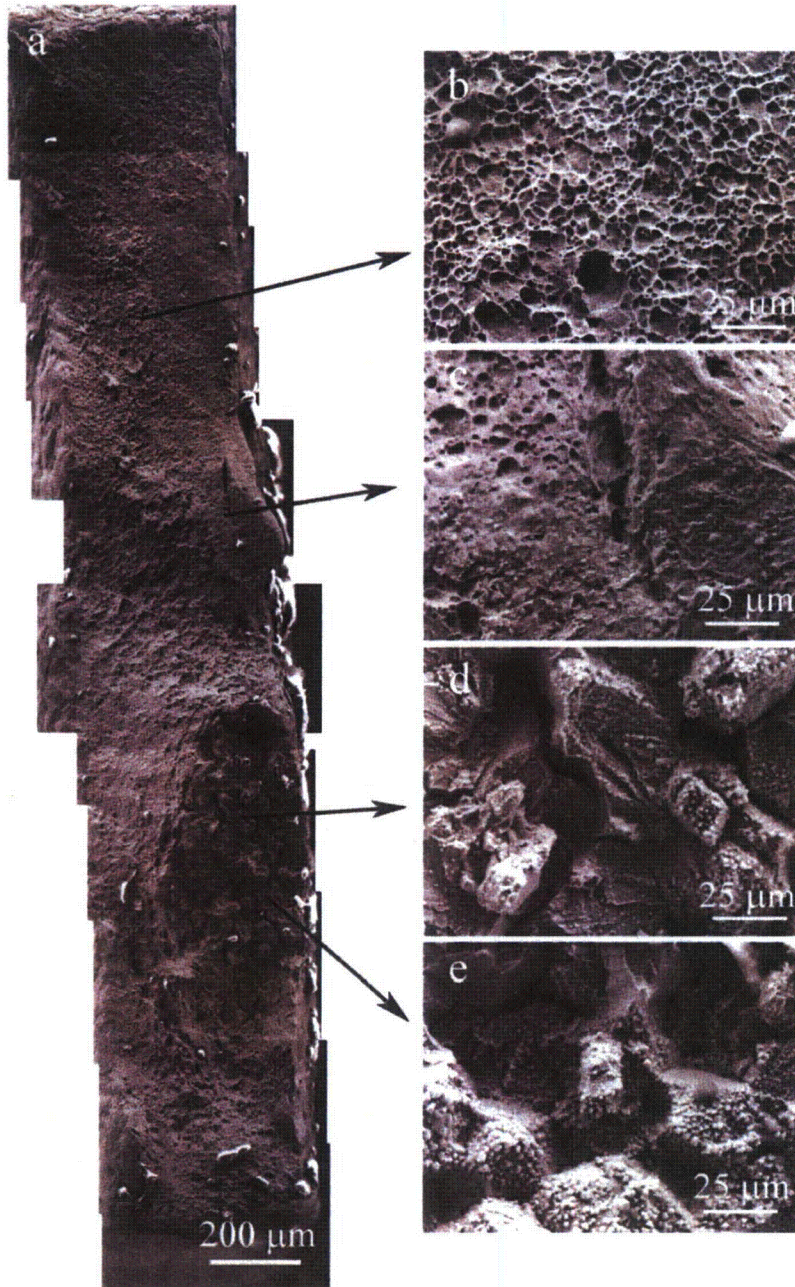


Figure 9. Fracture surface of GBE Type 304 SS tested in high-DO water at 289°C. (a) fracture surface; (b) ductile dimple fracture; (c) ductile fracture with linked deep dimples; (d) and (e) IG cracking with some TG cleavage morphology covered with corrosion products.

Figure 10 shows the gauge surfaces of the Type 304 SS and GBE Type 304 SS specimens. Large surface cracks can be seen on the Type 304 SS specimen, while only small cracks can be identified on the heavily deformed gauge surface in the GBE Type 304 SS specimen.

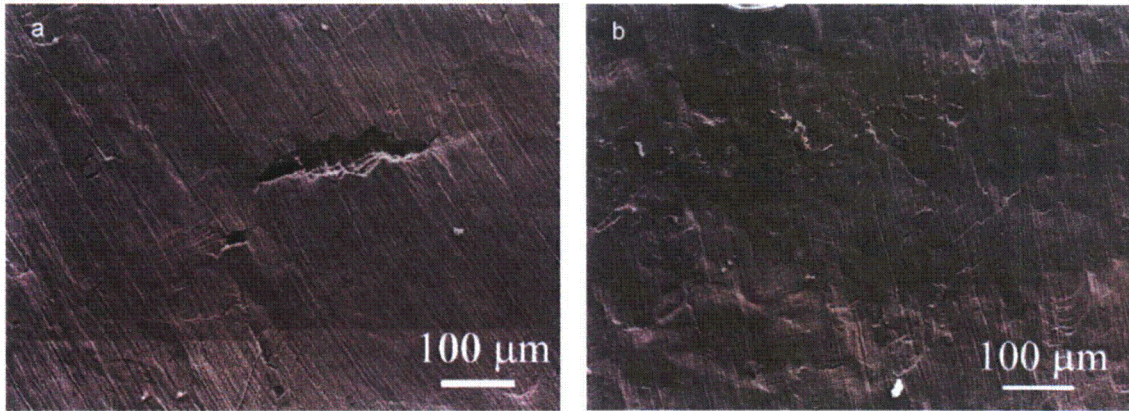


Figure 10. Comparison of gauge surface for Type 304 and GBE Type 304 SSs tested in high-DO water at 289°C. (a) a large surface crack on gauge surface of Type 304 SS (Heat 333 from ABB); and (b) heavily deformed gauge surface of GBE Type 304 SS.

3.2.3 Irradiated Type 304L SSs

The fracture surface of a Type 304L SS specimen is shown in Fig. 11. Two isolated regions of IG cracking are apparent. One is a small region on the specimen gauge surface, and the other is a large, through-thickness IG crack that initiates from the specimen edge. A region of TG cracking is also seen in the center. The major non-ductile feature that contributes to the failure of this specimen is the large IG crack. Considerable necking occurred in the center portion, as seen in Fig. 11.

The fracture surface of GBE Type 304L SS is shown in Fig. 12. Significant IG cracking can be seen on the fracture surface. Two separate IG cracks initiated from the periphery of the fracture surface and moved inwards to the interior. Some TG or mix-mode cracking can be seen at the edge of the IG region.

Figure 13 shows the gauge surfaces of both Type 304L SS and GBE Type 304L SS. The plastic flow in Type 304L SS is highly localized in a narrow band around the necked region. No signs of large deformation can be seen on the gauge surface in the region a small distance away from the necked area (Fig. 13a). On the other hand, the deformed region on the gauge surface of GBE 304L SS is wider (Fig. 13b). Small surface cracks can also be seen on the gauge surface of the GBE Type 304L SS.

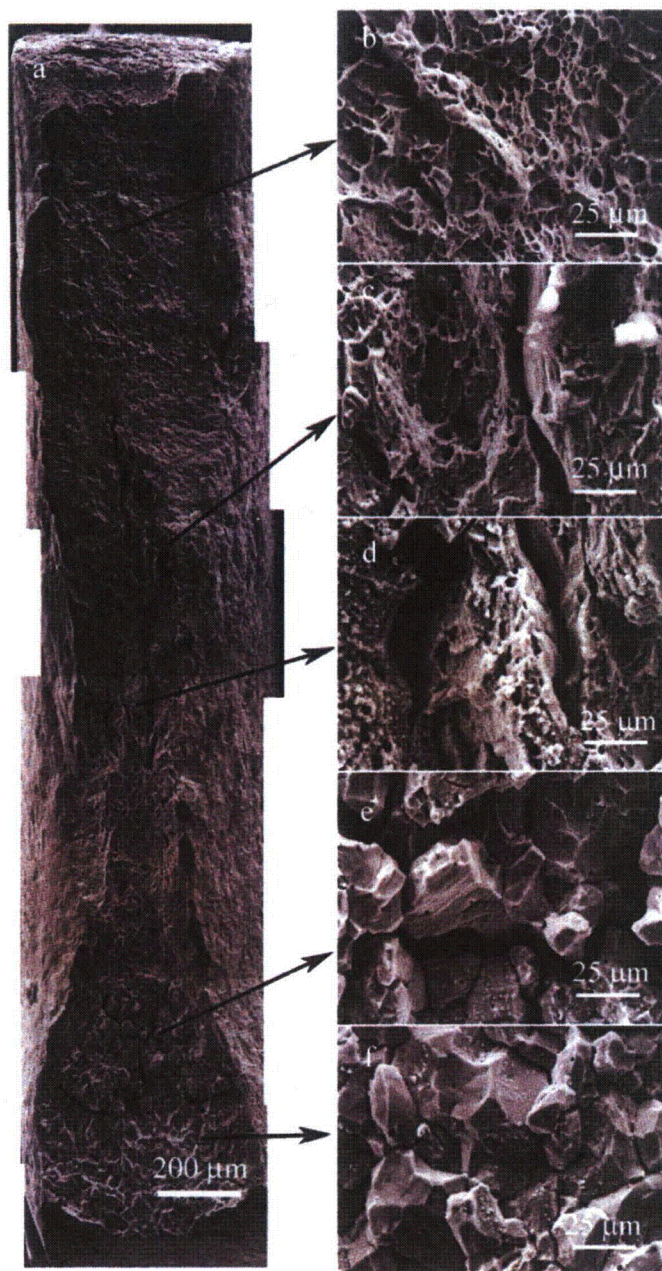


Figure 11.
Fracture surface of Type 304L SS tested in high-DO water at 289°C. (a) fracture surface with central cracks; (b) ductile fracture; (c) and (d) large TG cracks surrounded by ductile fracture area; (e) and (f) IG fracture.

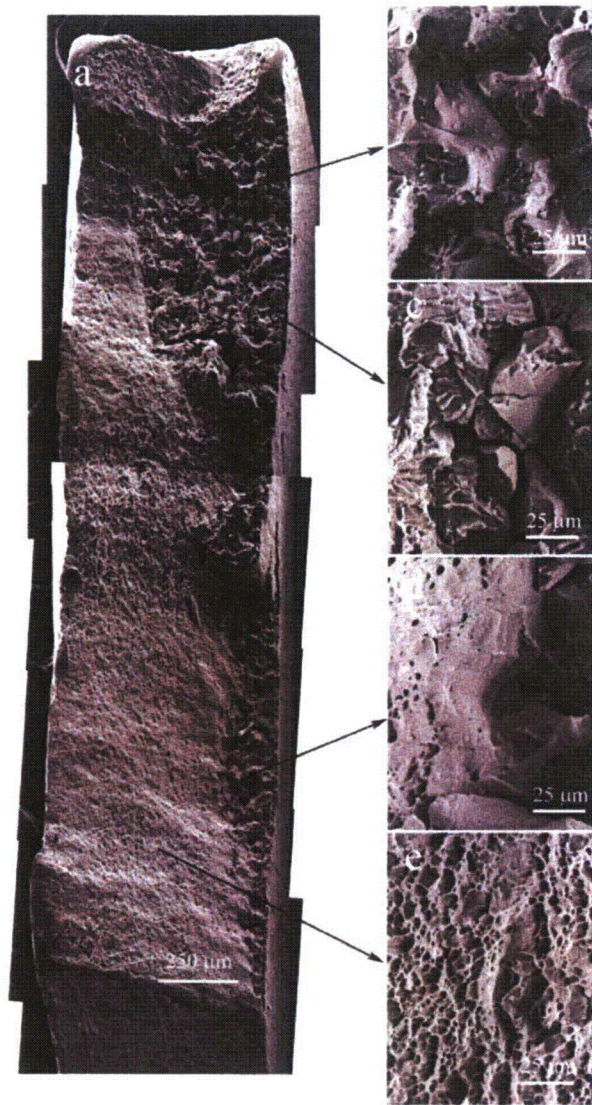


Figure 12.
Fracture surface of irradiated GBE Type 304L SS tested in high-DO water at 289°C. (a) Fracture surface with significant amount of IG cracking; (b) IG fracture; (c) IG and TG fracture; (d) an area between IG and ductile fracture; (e) ductile dimple fracture.

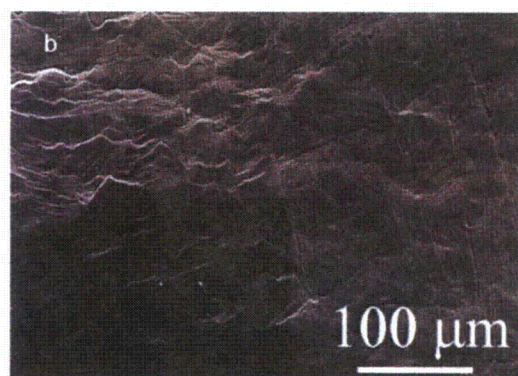
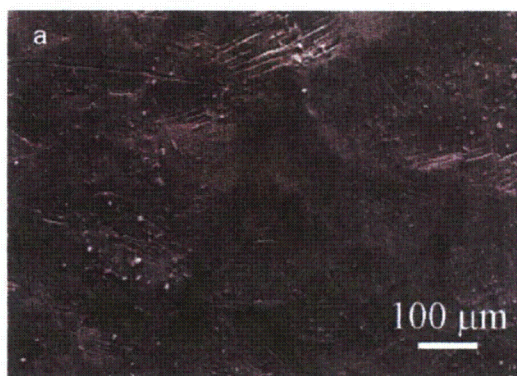


Figure 13. Comparison between gauge surface of Type 304L and GBE Type 304L SSs tested in high-DO water at 289°C. (a) relatively smooth gauge surface for Type 304L SS; and (b) heavily deformed gauge surface of GBE 304L SS.

Two high-purity Type 304L SSs with low-Oxygen (O) content and one high-purity Type 304L SS with high-O content were tested in high-DO water at 289°C.

Figure 14 shows the fracture surfaces of the two low-O content specimens. The fracture surfaces of these two identical specimens are very similar. Both contain one small IG area, and their reduction of area is large. The fracture surface of the high-O specimen is very different from that of the low-O specimens. There are multiple IG cracks visible on the fracture surface (Fig. 15), and most of cracks are appreciably larger than those of the low-O specimens. Two IG cracks at one end of the fracture surface nearly cover the entire cross section of the high-O specimen, and another IG crack initiated from the gauge surface extends to about one-third the specimen thickness. The total IG cracking area is much greater than that in the low-O specimens. The appearance of the gauge surfaces of these two specimens is also similar. Both show moderate plastic deformation and occasional surface cracks (Fig. 16). The gauge section of the high-O specimen also shows more surface cracks (Fig. 16).

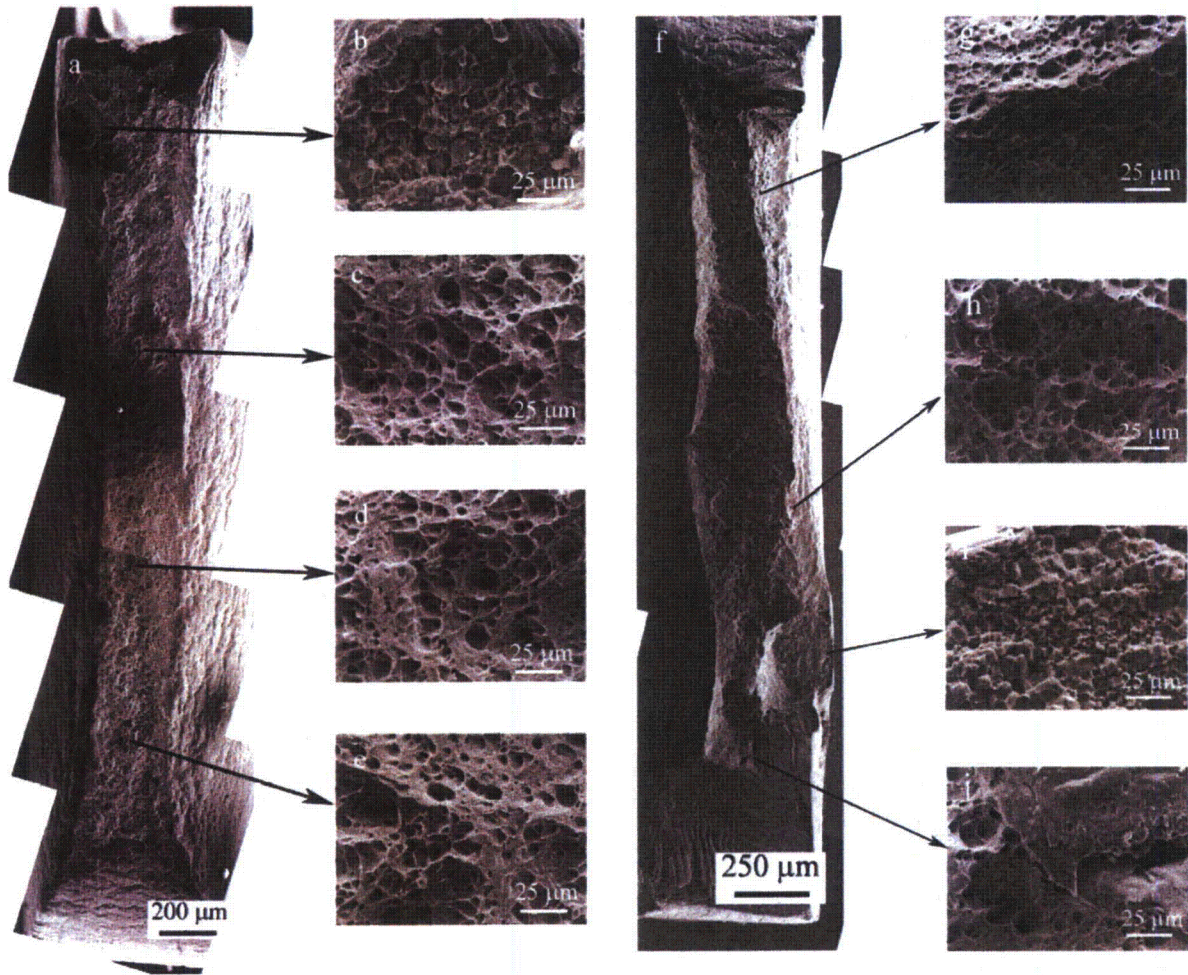


Figure 14. Fracture surfaces of two high-purity Type 304L SSs with low-O content (Heat 327) tested in high-DO water at 289°C. (a) and (f) similar narrow fracture surface for both low-O specimens; (b) and (i) IG fracture in both specimens; (c)-(h) and (j) ductile dimple fracture in both specimens.

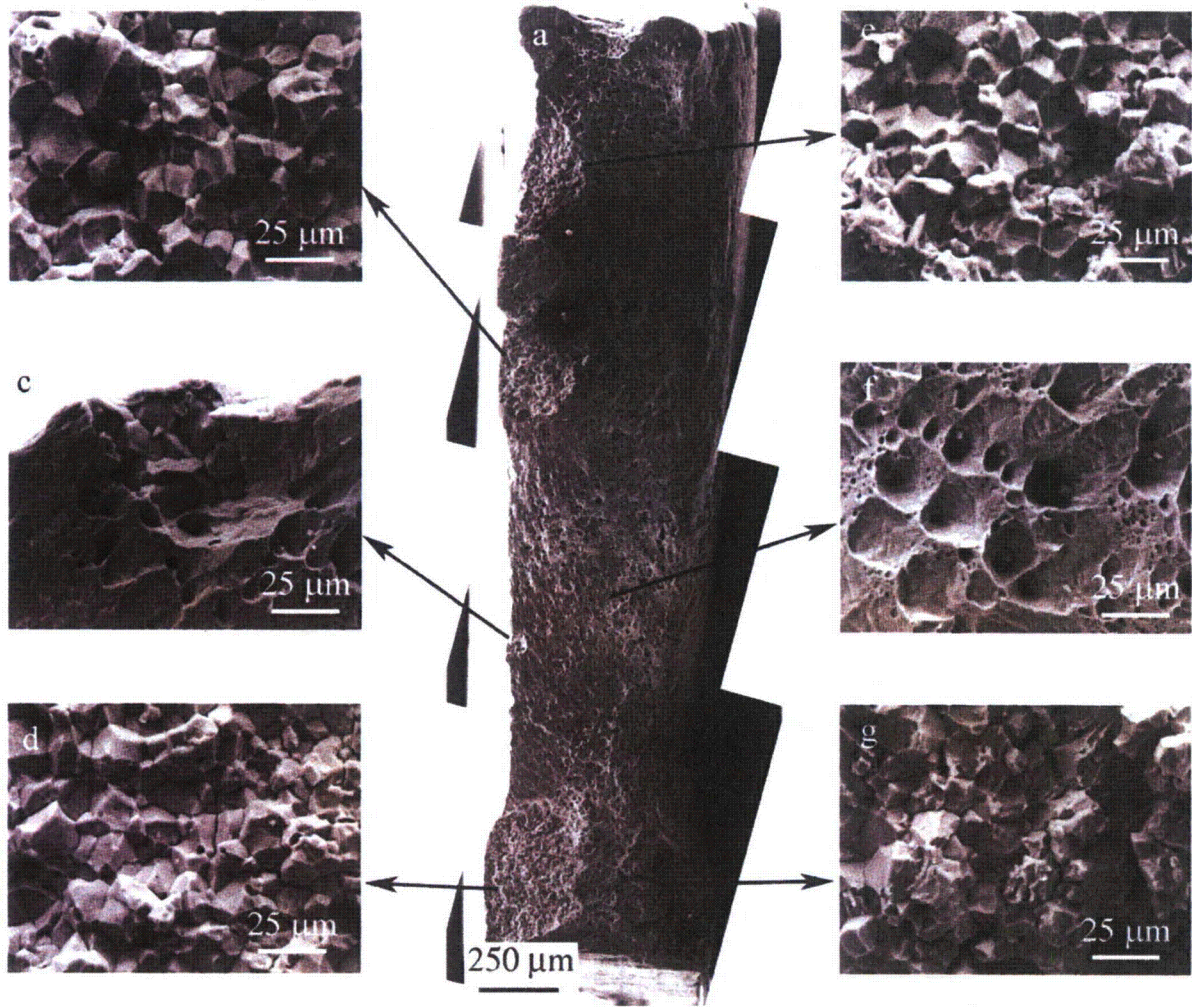


Figure 15. Fracture surface of high-purity Type 304L SS with high-O content (Heat 945) tested in high-DO water at 289°C. (a) fracture surface shows multiple IG areas; (b), (d), (e) and (g) IG fracture; (c) a IG area surrounded by ductile fracture; (f) dimples fracture with inclusions.

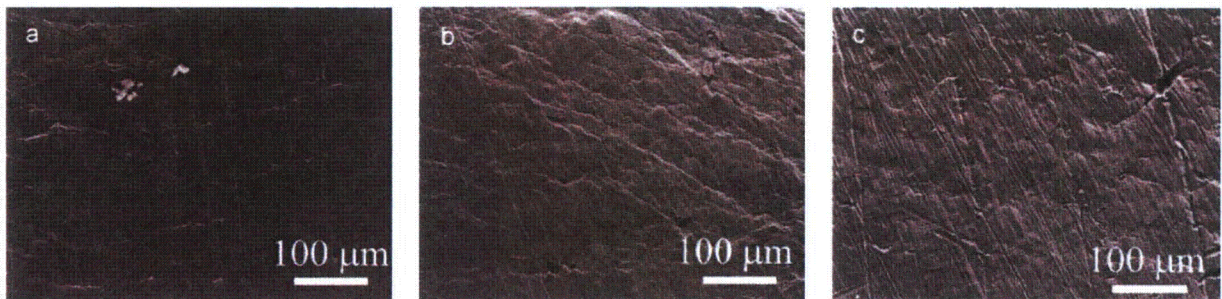


Figure 16. Moderate plastic deformation and occasional surface cracks on the gauge surfaces of high-purity Type 304L SSs: (a) and (b) low-O content (Heat 327) and (c) high-O content (Heat 945).

3.2.4 Irradiated Type 316 and 316L SSs

The fracture surfaces of the Type 316 SS specimens are very different from those of the Type 304 SS specimens. The area of IG cracking is considerably less than that in Type 304 SSs and is often not even detectable. The GBE Type 316 SS has three small IG regions (Fig. 17). Two of the IG regions are so small that they stop at the first grain from the surface. The other IG crack is somewhat larger, but still just a few grains deep. The majority of the non-ductile failure features in GBE Type 316 SS is TG cracking. Two regions of TG cracking can be seen to extend from the small IG cracks, and one TG crack covers nearly half of the entire fracture surface. The gauge surface of the GBE Type 316 SS is shown in Fig. 18. The deformation behavior is similar to that observed in Type 304 SSs.

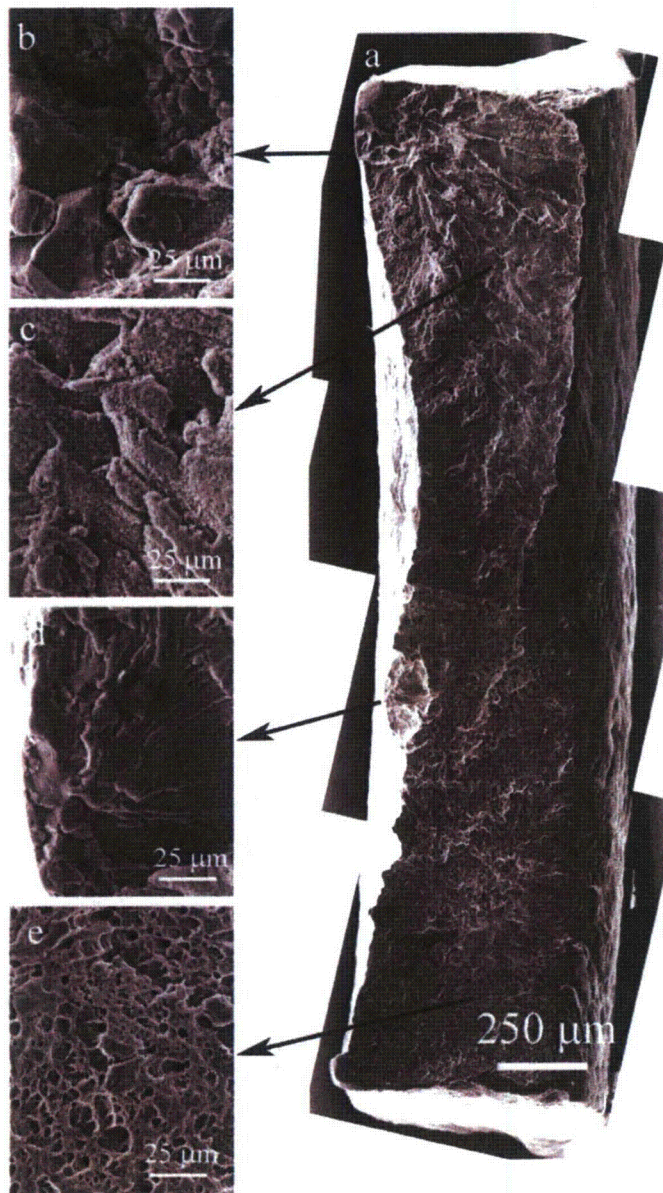


Figure 17.
Fracture surface of GBE Type 316 SS tested in high-DO water at 289°C. (a) fracture surface shows large TG crack area; (b) IG fracture covered with corrosion products; (c) TG cleavage fracture; (d) a small IG area surrounded by TG fracture; (e) ductile fracture.

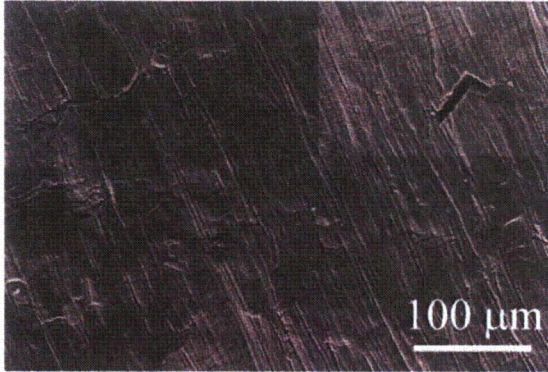


Figure 18.
A surface crack on the gauge surface of GBE Type 316 SS tested in high-DO water at 289°C.

The high-purity Type 316LN SSs, with or without Ti addition, show no IG cracking on the fracture surfaces (Figs. 19 and 20). Several small areas of TG cracking, which are probably unrelated to IASCC, appear in the interior of the specimens. The gauge surface of the Ti-doped specimen shows somewhat more evidence of plastic deformation, as indicated in Fig. 21.

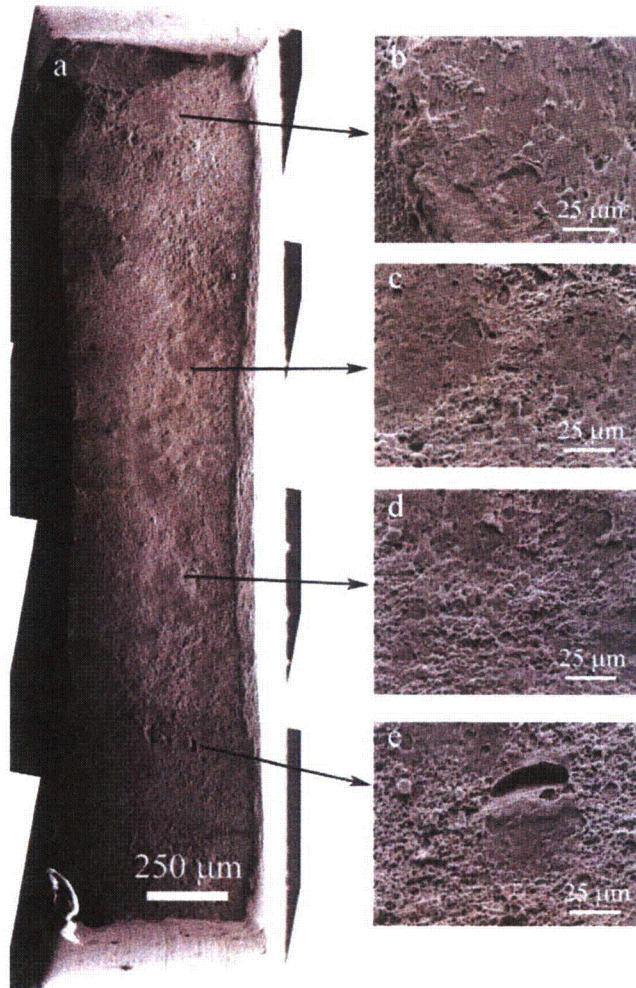


Figure 19.
Fracture surfaces of Type 316LN SS (Heat 623) tested in high-DO water at 289°C. (a) fracture surface; (b) and (c) TG and ductile fracture; (d) ductile fracture; (e) ductile fracture with a deep dimple.

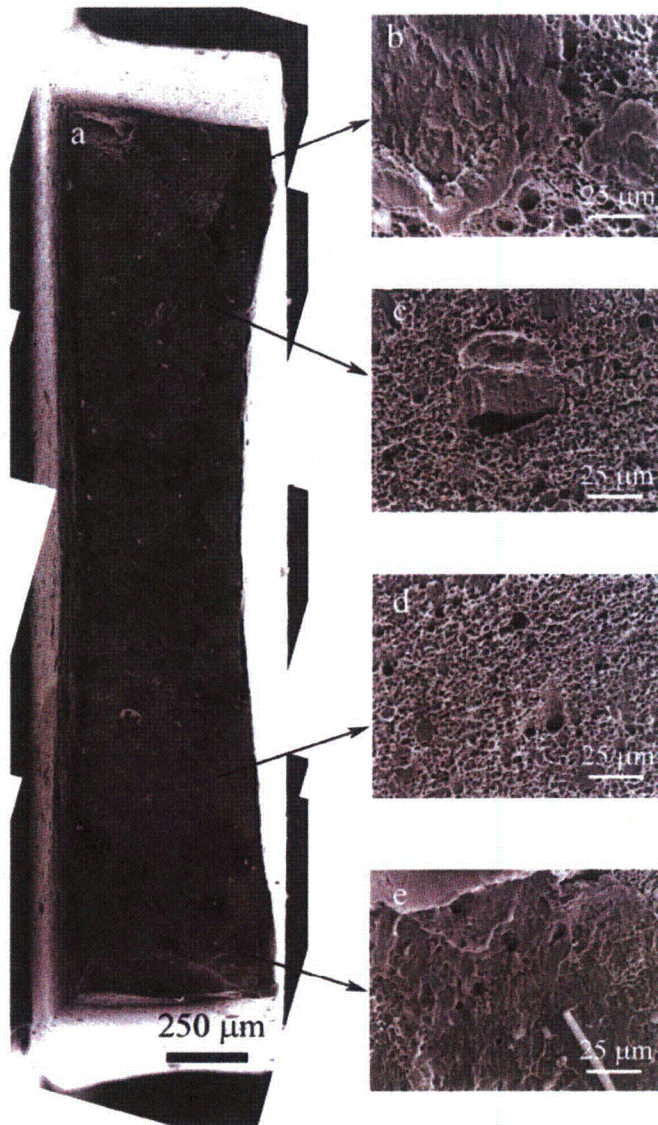


Figure 20. Fracture surfaces of Ti-doped Type 316LN SS (Heat 625) tested in high-DO water at 289°C. (a) fracture surface; (b) and (e) TG and dimple morphology; (c) and (d) ductile fracture with occasionally large dimples.

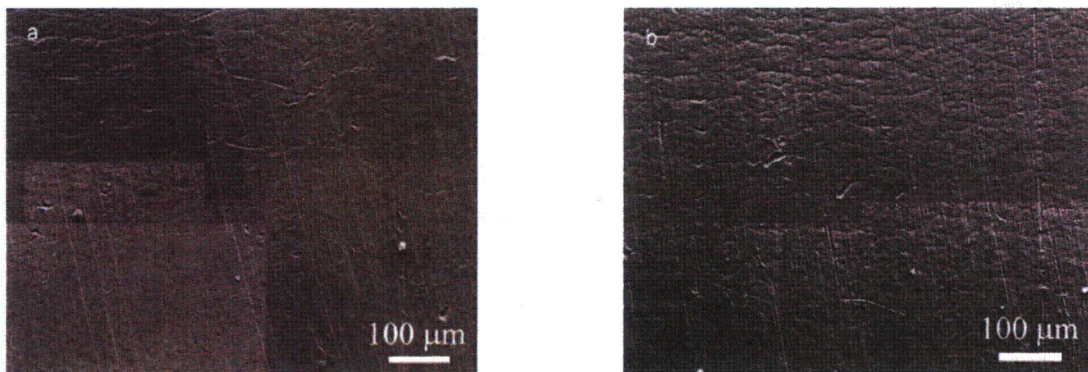


Figure 21. Gauge surfaces of (a) Type 316 LN SS (Heat 623) and (b) Ti-doped Type 316 LN (Heat 625).

3.2.5 Irradiated Alloy 690

Figure 22 shows the fracture surfaces of the Alloy 690 and GBE Alloy 690 specimens. In the Alloy 690 specimen, a small area on the fracture surface shows the typical IG morphology, and the rest of the surface is mainly ductile in appearance. Although a small IG crack initiated on one end of the specimen, TG cracking is not present in the Alloy 690. For GBE Alloy 690, no IG cracking is observed in the entire fracture surface. The gauge surfaces of Alloy 690 and GBE Alloy 690 are shown in Fig. 23. The evidence of plastic deformation is much greater in the GBE Alloy 690. Some surface cracks can be seen on the gauge surface of Alloy 690.



Figure 22. Fracture surfaces of Alloy 690 and GBE Alloy 690 tested in high-DO water at 289°C. (a) and (f) similar fracture surfaces of both alloys; (b) small IG area in the Alloy 690; (c)-(i) ductile fracture in both alloys.

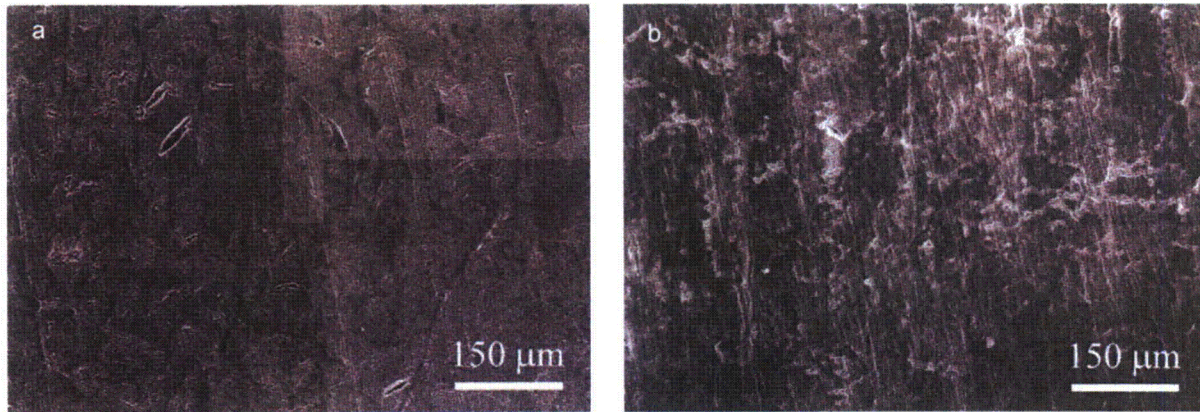


Figure 23. Gauge surfaces of Alloy 690 and GBE Alloy 690 tested in high-DO water at 289°C. (a) surface cracks on the gauge surface of Alloy 690; (b) heavily deformed gauge surface of GBE Alloy 690.

3.3 Measurements of IG and TG Cracking on Fracture Surfaces

To evaluate the fracture morphology quantitatively, the areas of IG and TG cracking were measured from SEM images of the fracture surfaces of the Halden Phase-II specimens. Figure 24 shows schematically how the cracks were characterized on a fracture surface. Four parameters were measured for each fracture surface:

- (a) number of areas of IG and TG cracking,
- (b) length of each IG crack in contact with the aqueous environment (l),
- (c) depth of the IG crack (d), and
- (d) area fraction of IG and TG cracks on the fracture surface.

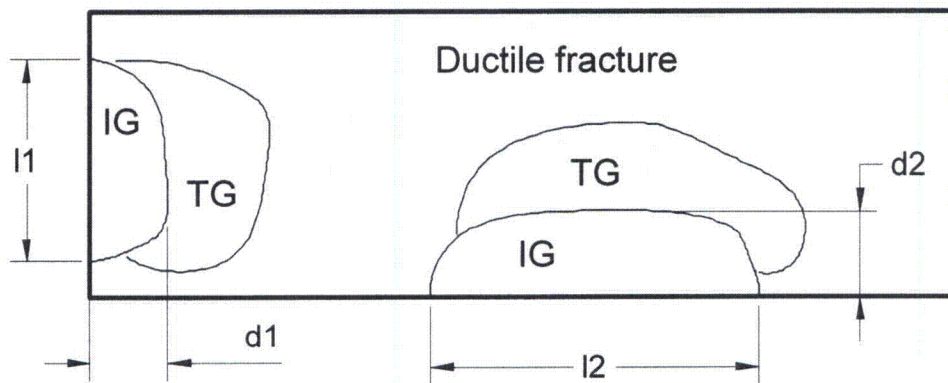


Figure 24. Schematic for fracture surface characterization and measurement.

All measurements were made by pixel counting on composite digital images. A montage of a fracture surface was first constructed by using digital images of at least 120X in magnification. Next, the boundaries that separate IG, TG, and ductile failure regions were defined on the composite image. A

pixel measurement was then conducted for each region. Table 4 summarizes all measurements performed on the fracture surfaces of Halden Phase-II specimens.

Table 4. Measurements of IG and TG cracking^a on the fracture surfaces of Halden Phase-II specimens.

Material	Heat ID	IG				TG		IG+TG Area (%)	
		# of IG Cracks	Length (mm)	Depth (mm)	IG Area (%)	# of TG Cracks	TG Area (%)		
Type 304 SS	333	4	0.14	0.12	1.0	3	3.6		
			0.28	0.09	0.7		5.0		
			0.10	0.09	0.5		1.1		
			0.48	0.32	4.8				
	Sum	1.00	0.62	7.0	9.7	16.7			
	GBE304	1	0.56	0.30	12.5	1	2.1	14.6	
	304L	2	0.28	0.12	1.8	1	8.4		
			1.00	0.59	21.0				
	Sum	1.28	0.71	22.8	8.4	31.2			
	GBE304L	2	1.54	0.50	19.2	-	-		
			1.28	0.18	7.1				
	Sum	2.82	0.68	26.3	-	26.3			
	Type 304L SS	327	1	0.14	0.14	1.4	-	-	1.4
		327 ^b	1	0.29	0.20	2.8	-	-	2.8
945		4	2.64	0.26	10.8	-	-		
	0.40		0.06	0.2					
	2.65		0.29	5.0					
Sum	2.19	0.90	22.0	-	22.0				
	GBE316	3	0.27	0.21	1.8	2	40.0		
			0.07	0.02	-0.1		1.4		
			0.08	0.03	-0.1				
	Sum	0.42	0.26	2.0	41.4	43.4			
	623	-	-	-	-	2	2.1	2.1	
625	-	-	-	-	3	1.8	1.8		
Alloy 690	690	1	0.16	0.09	0.6	-	-	0.6	
	GBE690	-	-	-	-	-	-	-	

^aNumber of cracks and the sum of all cracks in a specimen are in bold.

^bEstimated values were used for the cross-section and IG areas in this specimen.

4 Discussion

4.1 SSRT Tests

4.1.1 Effect of Irradiation and High-DO Water Environment on the SSRT Behavior

Both neutron irradiation and test environment have a large effect on the SSRT behavior of austenitic SSs and Ni alloys. Figure 25 shows the SSRT test results in air and high-DO water for GBE Type 304L SS in the irradiated and nonirradiated conditions. The test on the nonirradiated specimen in high-DO water was initiated at the same strain rate as all other SSRT tests, but this rate was then increased to $8.15 \times 10^{-7} \text{ s}^{-1}$ beyond 16% of strain. At a dose level of 1.96 dpa, irradiation hardening and embrittlement are evident regardless of the test environment. The yield strength of GBE Type 304L SS is increased more than a factor of three, while its elongation is reduced by about one-third in comparison to nonirradiated specimen. The strain hardening observed in the nonirradiated materials is either very limited or completely absent in the irradiated materials. The high-DO environment further reduces the elongation of the material during SSRT testing. The yield strength and strain hardening properties of the irradiated material are unaffected by the high-DO water. The reduction in ductility of the irradiated specimen tested in high-DO water is thus attributed to a synergistic effect of irradiation and corrosive environment.

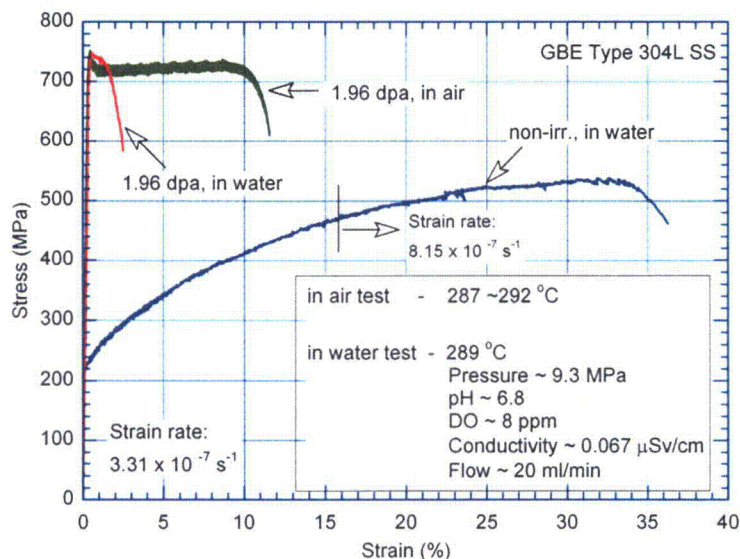


Figure 25. Effects of irradiation and high-DO water on the SSRT behavior of GBE Type 304L SS.

The Halden Phase-II specimens all have irradiation exposures of 1.96 to 2.44 dpa, as shown in Table 2. To help establish the dose dependence of SSRT behavior, some Halden Phase-I SSRT data are plotted along with the current test results in Figs. 26-29. The materials selected from the Halden Phase-I study are commercial heats of Type 304 or 316 SSs. Their chemical compositions are given in Table 5. The SSRT test conditions for Halden Phase-I specimens were similar to those used in the current study.²¹

As shown in Figs. 26 and 27, both the yield strength (YS) and ultimate tensile strength (UTS) obtained from SSRT tests increase with irradiation dose. The increase in YS is more evident than that in UTS. This hardening behavior is not fully saturated at ≈ 3 dpa. Figures 28 and 29 show the decrease in uniform elongation (UE) and total elongation (TE) with an increase in irradiation dose. At ≈ 2 dpa, except

for GBE Alloy 690, the UE and TE of all materials that were investigated decreased to just a few percent elongation.

Table 5. Chemical compositions of commercial heats in Halden Phase-I study.

ANL ID	Composition (wt%)								
	Ni	Si	P	S	Mn	C	N	Cr	Others
C1	8.12	0.50	0.038	0.0020	1.00	0.060	0.060	18.11	O 0.0102, B <0.001
C3	8.91	0.46	0.019	0.0040	1.81	0.016	0.083	18.55	B <0.001
C9	8.75	0.39	0.013	0.0130	1.72	0.062	0.065	18.48	O 0.0102, B <0.001
C10	8.13	0.55	0.033	0.0020	1.00	0.060	0.086	18.19	O 0.0074, B <0.001
C12	8.23	0.47	0.018	0.0020	1.00	0.060	0.070	18.43	B <0.001
C16	12.90	0.38	0.014	0.0020	1.66	0.020	0.011	16.92	Mo 2.30, O 0.0157, B <0.001
C19	8.08	0.45	0.031	0.0030	0.99	0.060	0.070	18.21	O 0.0200, B <0.001
C21	10.24	0.51	0.034	0.0010	1.19	0.060	0.020	16.28	Mo 2.08, O 0.0112, B <0.001

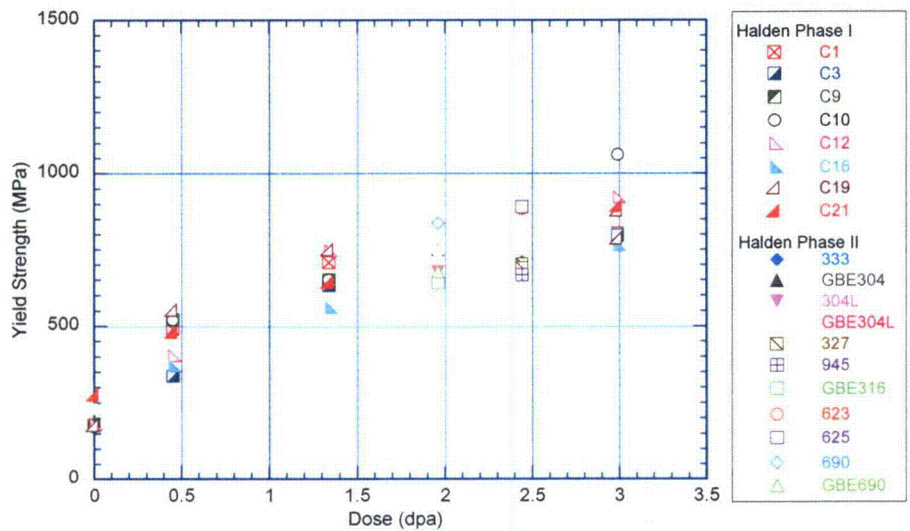


Figure 26. Variation in yield strength with irradiation dose in high-DO water at 289°C.

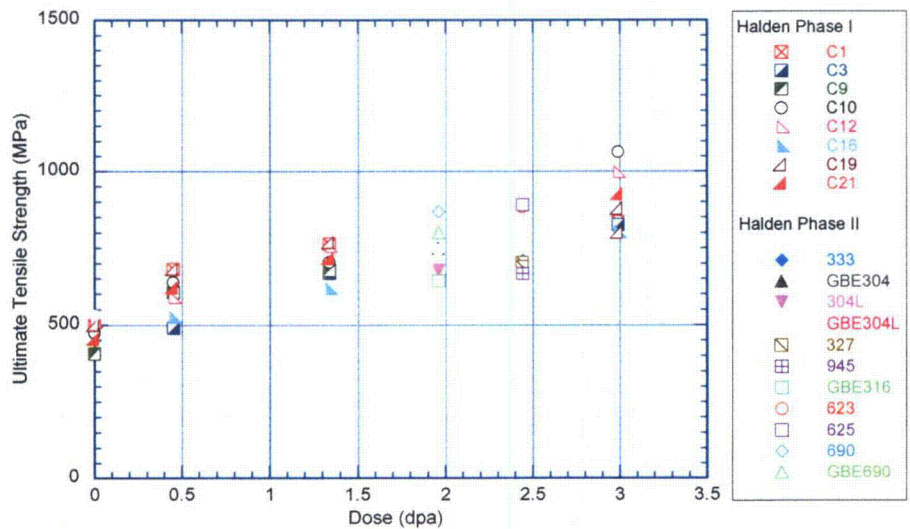


Figure 27. Variation in ultimate tensile strength with irradiation dose in high-DO water at 289°C.

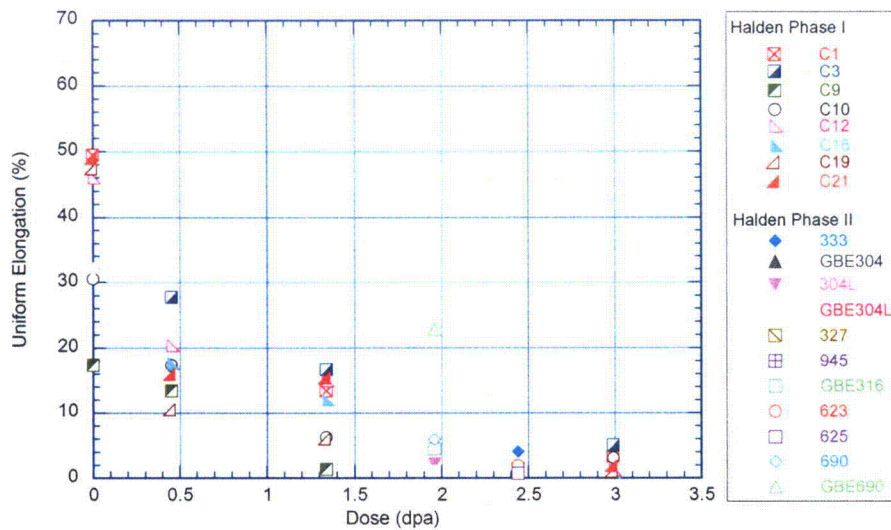


Figure 28. Variation in uniform elongation with irradiation dose in high-DO water at 289°C.

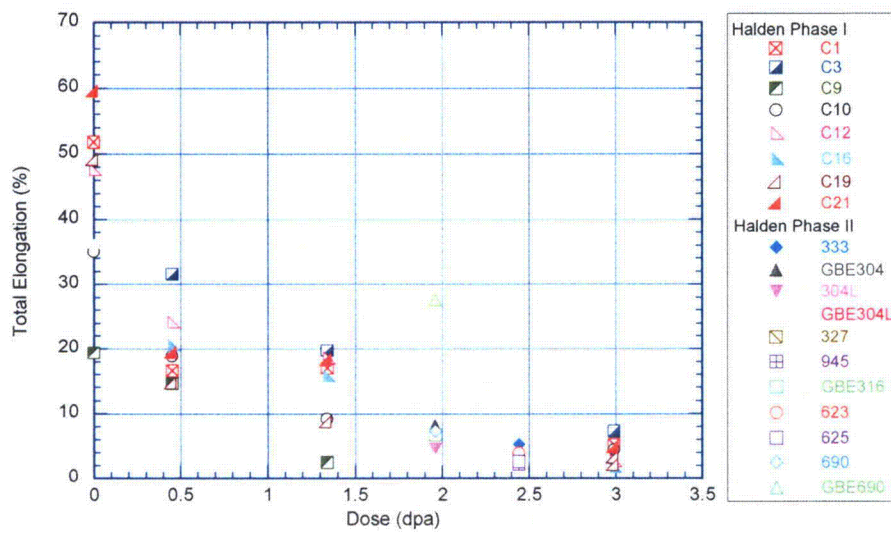


Figure 29. Variation in total elongation with irradiation dose in high-DO water at 289°C.

4.1.2 Influence of GBE Processing on the SSRT Behavior

The GBE processing is a thermomechanical treatment that increases the population of low Σ number CSL boundaries in the materials. Typically, a GBE treatment involves application of one or several iterations of strain-anneal or recrystallization-anneal schedules.²⁹ Thus, in addition to having a different grain boundary structure, the mechanical properties of GBE materials are also different from their baseline materials because of the thermomechanical treatment. The influence of GBE treatment on SSRT behavior is shown in Fig. 4. The SSRT curves on GBE materials are in red, and the SSRT curves for the baseline or similar materials are plotted in the same figure. As shown in Fig. 4, the YS and UTS of Type 304 SS with and without GBE treatment are very similar, but the elongation of GBE Type 304 SS is slightly larger. For Type 304L SS, both the YS and UTS of GBE material are somewhat higher, while their elongations are comparable. For Alloy 690, the YS of GBE material is lower, but the UTS is similar in both materials. The GBE Alloy 690 retains more strain hardening capability after irradiation. This condition leads to a significantly higher elongation compared to the alloy without GBE treatment.

Although four GBE materials were irradiated in the Halden Phase-II study, in only two cases do the baseline alloys, Type 304L SS and Alloy 690, have chemical compositions either identical or very close to their GBE counterparts (Table 1). To isolate the effect of the GBE process, the SSRT properties and tensile properties before irradiation of the baseline alloys and their GBE counterparts were compared.* Table 6 and Fig. 30 summarize the results of this comparison. While the increase in YS can be considered as to be the result of irradiation hardening, the reduction in UE is attributed to both the irradiation embrittlement and cracking behavior in the high-DO aqueous environment. Whether or not the GBE treatment affects irradiation hardening is unclear from the current results. For the Type 304 SS the increase in YS is greater for the GBE material; for Alloy 690 the increase in YS is smaller for the GBE material. For both alloys, the GBE process does appear to result in a smaller reduction in UE in high-DO water, but this effect is more significant in Alloy 690.

Table 6. Comparison of SSRT results with tensile properties obtained before irradiation.

Materials	Non-irr. in Air at Room Temp. ^a			Irr. in High-DO Water at 289°C			Differences		
	YS (MPa)	UTS (MPa)	UE (%)	YS (MPa)	UTS (MPa)	UE (%)	Δ YS (MPa)	Δ UTS (MPa)	Δ UE (%)
304L	308	609	62	677	677	2.18	369	68	59.82
GBE304L	301	634	53	747	747	1.11	446	113	51.89
690	288	654	48	837	868	5.94	549	214	42.06
GBE690	346	697	40	677	801	22.8	331	104	17.20

^aProvided by the supplier of the GBE materials.

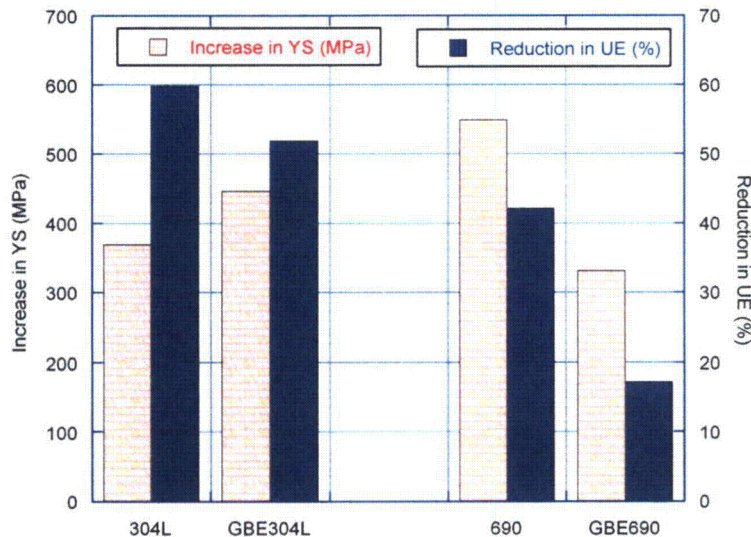


Figure 30. The influence of GBE treatment on the increase in YS and decrease in UE in high-DO water at 289°C.

4.1.3 Influence of Alloying Elements on the SSRT Behavior of Austenitic SSs

As discussed in Section 4.1.1, the increase in YS and UTS in a SSRT test is primarily due to the irradiation hardening, but the loss of ductility results from both irradiation embrittlement and stress corrosion cracking (SCC). To illustrate the influence of alloy elements on IASCC behavior, elongation is the more relevant parameter. Thus, the UE of SSRT specimens tested in the high-DO aqueous environment will be the focus of the remainder of this section.

*Provided by the supplier of the GBE materials.

Figure 31 plots the UE of the Halden Phase-II specimens as a function of several alloying elements. The Type 304 and 316 SSs are represented by circles and squares, respectively. All open symbols are for alloys without GBE treatment, while the closed symbols are for GBE alloys. For major alloying elements such as Chromium (Cr) and Nickel (Ni), no correlation between the UE and the bulk levels of the elements is evident. For the non-GBE alloys, although the data scatter is fairly large, there does seem to be some trend for the UE to increase with the Manganese (Mn) content. The most obvious correlation of the UE with an alloying element is with Carbon (C). As shown in Fig. 31d, there appears to be a nearly linear correlation between C content and the UE for C below 0.06 wt.%. A low-C content is generally associated with poor ductility in high-DO water at the dose level of ≈ 2 dpa, irrespective of whether the material is Type 304 SS or Type 316 SS, with or without GBE treatment.

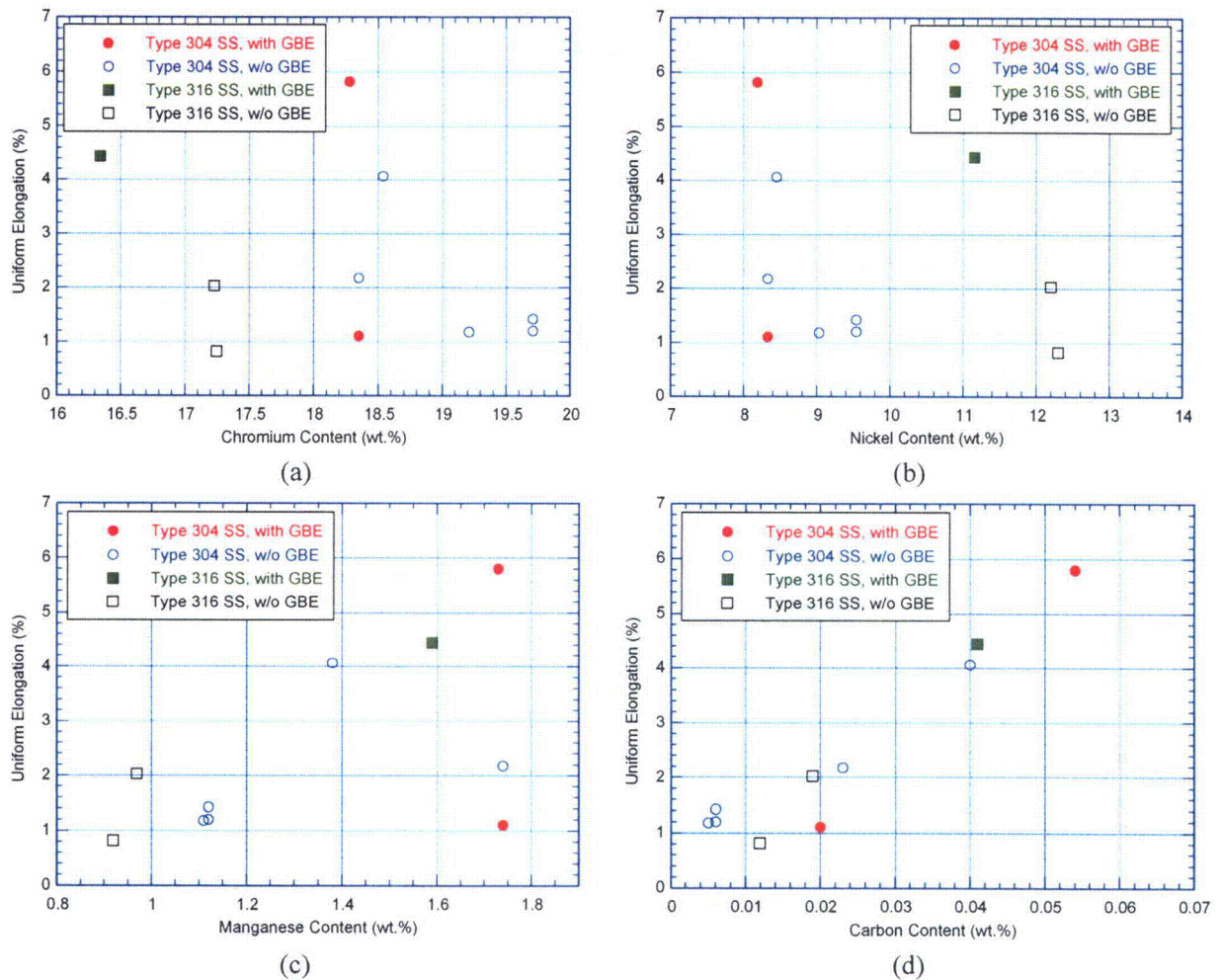


Figure 31. The influence of alloy elements on the uniform elongation for austenitic SSs with and without GBE treatment.

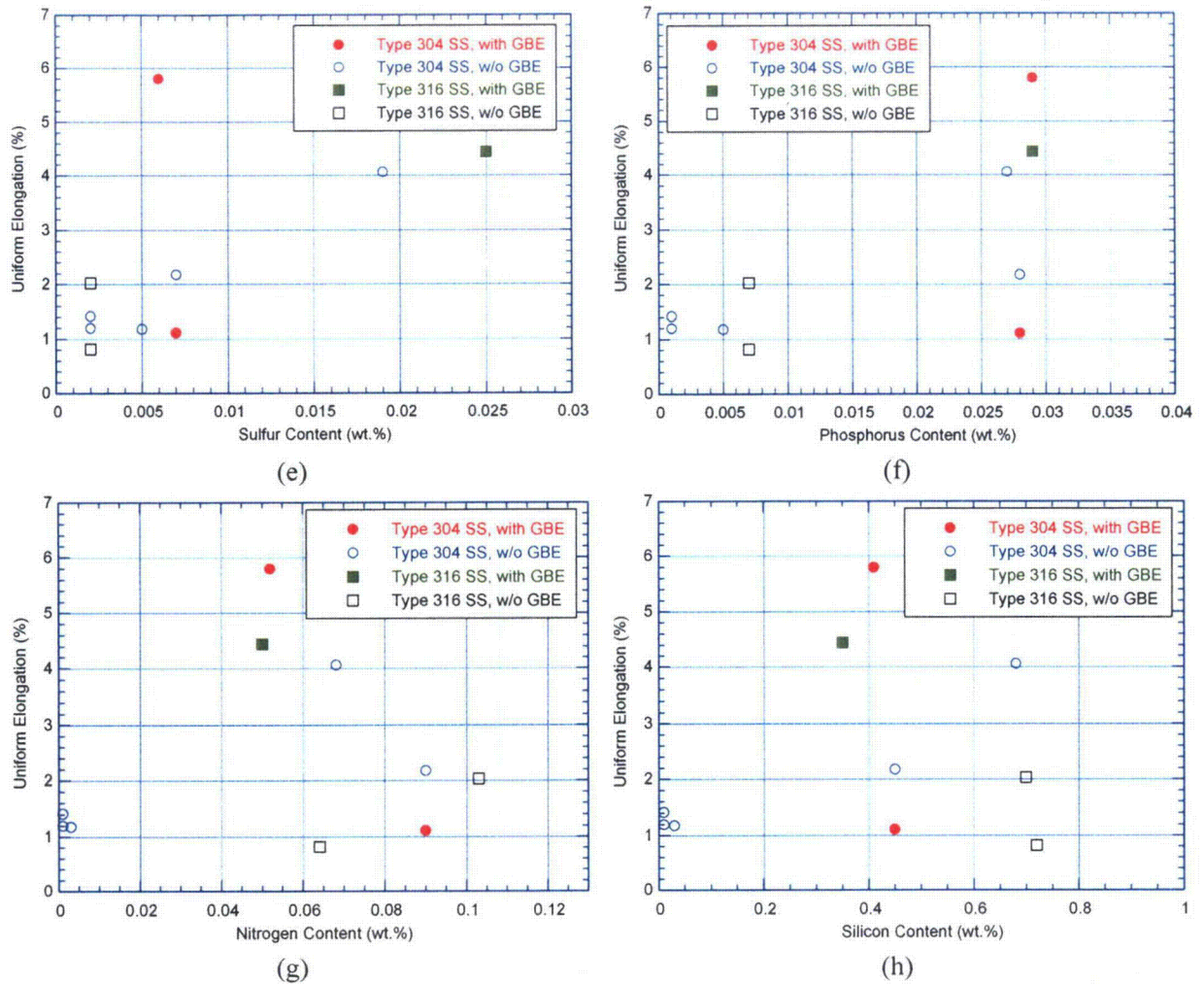


Figure 31. (Contd.)

The correlation of UE with impurity elements, such as Silicon (Si), Sulfur (S), Phosphorus (P) and Nitrogen (N), is more complex due to the interdependence among alloying elements. For example, the austenitic SSs in the Halden Phase-II study with high-Si content usually contain more N, and the high-S or -P contents are typically associated with the high-C content as well. The apparent correlations between the UE and S or P content among non-GBE SSs may be due to the effect of C, as discussed above. More effort is needed to determine the influence of S and P on the SSRT behavior of austenitic SSs in high-DO water.

4.2 Fractographic Analyses

4.2.1 Influence of Irradiation and High-DO Water on the Fracture Morphology

The fractographic observations on the GBE Type 304L SS specimens tested in air and water environments (Fig. 25) illustrate the impact of irradiation and environment on the cracking behavior. The cross sections of the fractured specimens are shown in Figs. 5, 6, and 12. The fracture surface of the nonirradiated GBE Type 304L SS is entirely ductile, although the test was conducted in high-DO water (Fig. 5). The fracture surface of the irradiated GBE Type 304L SS also appears to be completely ductile

when tested in air (Fig. 6). Only on the fracture surface of the irradiated GBE Type 304L SS tested in high-DO water is a considerable amount of IG cracking observed (Fig. 12). The comparisons among these fracture specimens with identical chemical composition show that all three elements—irradiation, corrosive environment, and straining—are required for the occurrence of IASCC.

Necking occurred in all three GBE Type 304L SS specimens discussed above. Figures 7 and 13b show the gauge surfaces of these specimens close to the necked area. Roughness on the gauge surface resulting from large plastic deformation can be seen in the nonirradiated specimen tested in high-DO water (Fig. 7a) and in the irradiated specimen tested in air (Fig. 7b). In contrast, the gauge surface of the irradiated specimen tested in high-DO water is relatively smooth (Fig. 13b). Also, the SEM observations show that the visible deformation area is narrow for irradiated specimens tested in water or air. The difference in the plastic flow visible on the gauge surfaces may indicate localized deformation in irradiated specimens. Small surface cracks can also be seen on the gauge surface of the irradiated specimen tested in high-DO water.

4.2.2 IASCC Susceptibility of Halden Phase-II Specimens

The IASCC susceptibility of the Halden Phase-II specimens can be characterized from the fractographic analysis and SSRT results. Figure 32 shows the area fractions of both IG and TG cracking among Halden Phase-II materials, and Fig. 33 shows the UE from the SSRT tests. The GBE Type 304L SS has the largest IG fraction, while GBE Type 316 SS shows the largest amount of TG cracking. Chung and Shack²¹ argue that such TG cracking is a precursor to IG cracking, which can be triggered by small changes in conditions (e.g. lower strain rate, higher irradiation level, higher potential, etc). Compared to Type 316 SSs and Alloy 690, Type 304 SSs are more vulnerable to IG cracking when tested in high-DO water. At the dose level of ≈ 2 dpa, more than 20% IG cracking can occur during SSRT tests among the susceptible heats of Type 304 SSs. In contrast, failures in Type 316 SSs show mainly TG cracks, which may or may not originate from IG sites. For Alloy 690, the failure appears to be primarily ductile at this dose level, and very little IG cracking is observed.

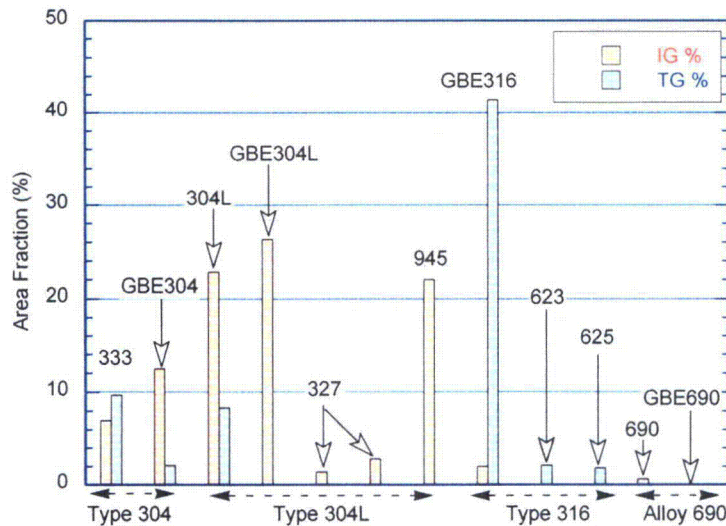


Figure 32. Fraction of IG and TG fracture in the Halden Phase-II specimens tested in high-DO water at 289°C. The identifiers above the bars are the heat IDs.

A higher area fraction of IG or TG is usually associated with a lower uniform elongation, as seen by comparing Figs. 32 and 33. In Fig. 34, the IG fractions of the Halden Phase-II specimens and similar results from the Halden Phase-I specimens²¹ are plotted as a function of the SSRT uniform elongation.

For UE greater than $\approx 10\%$, the corresponding IG fractions are small. So, the materials that are highly resistant to IGSCC can be differentiated from the more susceptible ones by using the UE information. However, UE is not a good indicator of IGSCC susceptibility for $UE < \approx 10\%$, as shown in Fig. 34.

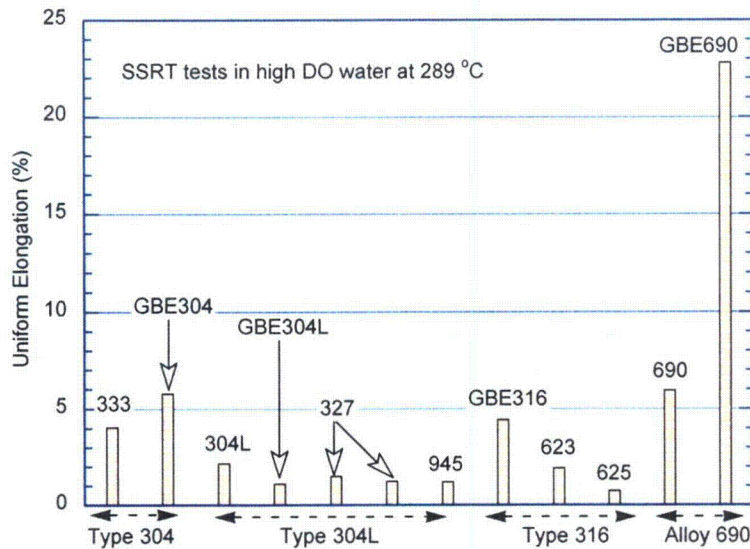


Figure 33. Uniform elongations of the Halden Phase-II specimens tested in high-DO water at 289°C. The identifiers above the bars are the heat IDs.

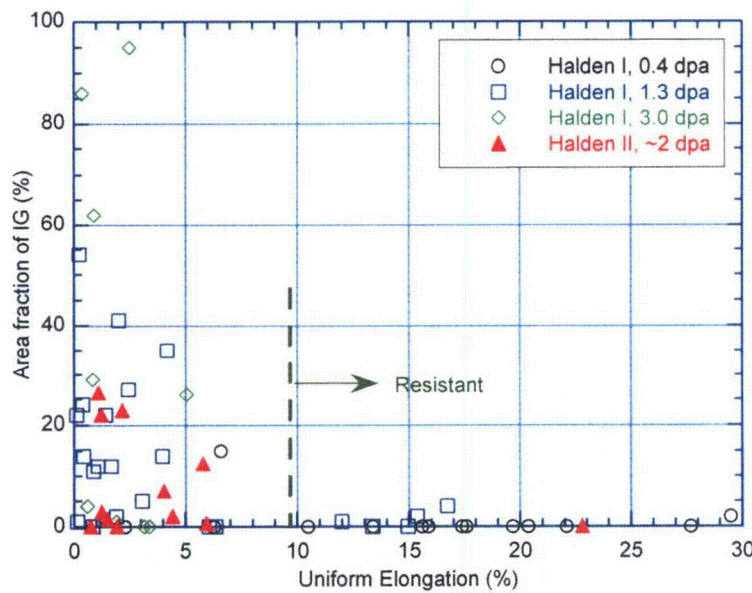


Figure 34. Correlation between IG fraction and UE among Halden Phase-I and Phase-II specimens.

Figure 35 shows the number of IG and TG cracks observed in Halden Phase-II specimens. Very often, multiple IG cracks are present in a specimen. If the IG cracks on the gauge surface are assumed to occur randomly, then the number of IG cracks observed along the periphery of a fracture surface can be considered a measure of susceptibility to IG crack initiation. The more IG cracks observed in a SSRT specimen, the more likely an IG crack can initiate in the material. Because the IG crack initiation is time dependent, a longer SSRT test may allow more IG cracks to initiate; thus, the normalized number of IG cracks is a better representation for the likelihood of IG crack initiation. The time period between the yield and the final load drop is the time period that IG cracks could start. In our constant strain rate test, this time period is equivalent to the UE. Thus, the number of IG cracks normalized by the UE, plotted in

Fig. 36, is a measure of the likelihood of IG crack initiation. As shown, the high-purity Type 304L SS with high-O content (Heat 945) is the most susceptible material for IG crack initiation among all Halden Phase-II specimens. The GBE Type 304L SS also shows a high possibility of IG crack initiation. The likelihood of IG crack initiation is more or less the same for all the other materials (i.e. IG cracking occurs in SSRT tests).

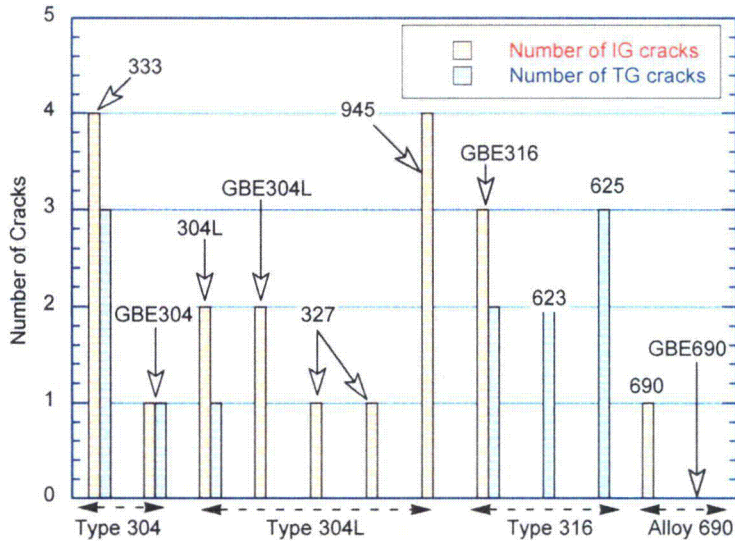


Figure 35. Number of IG and TG cracks observed in Halden Phase-II specimens. The identifiers above the bars are the heat IDs.

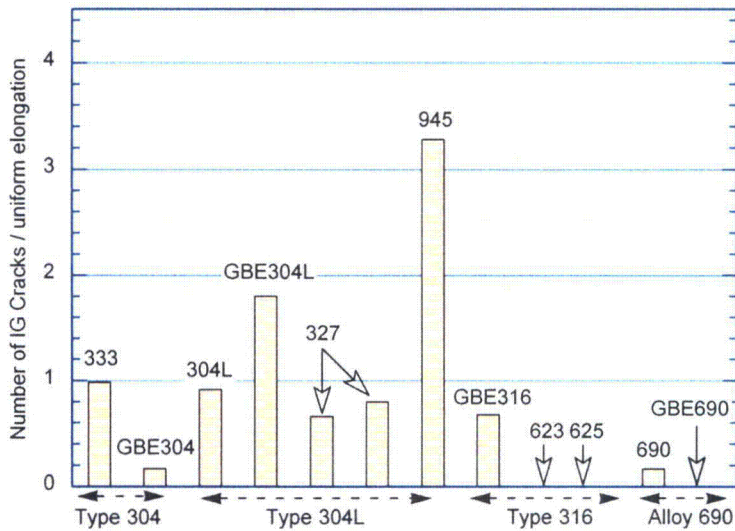


Figure 36. Number of IG cracks normalized by the UE in Halden Phase-II specimens. The identifiers above the bars are the heat IDs.

4.2.3 Effect of GBE Process on the IASCC Behavior

Since the concept of grain boundary design was introduced in the early 1980s,²⁸ many studies have shown the improved resistance of GBE materials to various forms of degradation involving intergranular phenomena,²⁸⁻³⁴ including SCC in Ni alloys²⁷ and austenitic SSs.²⁵ The GBE process increases the population of CSL boundaries. Due to the geometrical symmetry around these boundaries, the free energies of CSL boundaries are much lower than those of random high-angle boundaries. The low CSL boundary energy decreases the driving force for grain-boundary segregation and, therefore, reduces Cr

depletion at the boundaries. One objective of the Halden Phase-II study was to investigate the effect of GBE treatment on the IASCC behavior of neutron-irradiated austenitic SSs and Alloy 690. The percentages of CSL boundaries for these materials, provided by the vendor, are shown in Table 7.

Table 7. Percentages of CSL boundaries (Σ) in GBE materials irradiated in Halden Phase-II study.

Heat ID	Boundary Type (Σ)																
	1	3	5	7	9	11	13	15	17	19	21	23	25	27	29	≤ 29	> 29
GBE 304	1.7	52.0	0.3	0.7	5.3	0.7	0.3	0.3	0.3	0.1	0.2	0.2	0.5	2.7	1.6	66.9	33.1
GBE 304L	1.5	49.3	0.2	0.3	6.0	0.5	0.3	0.2	0.2	0.3	0.2	0.1	0.3	2.6	3.9	66.1	33.9
GBE 316	1.8	52.3	0.5	0.2	4.9	0.5	0.3	0.6	0.1	0.2	0.5	0.2	0.1	2.3	2.0	66.4	33.6
GBE 690	1.2	52.3	0.1	0.2	5.6	0.8	0.3	0.1	0.2	0.1	0.4	0.1	0	3.1	6.0	70.7	29.3

Figure 32 shows that the IG fractions of GBE Type 304 SS and GBE Type 304L SS are about the same as those of their non-GBE counterparts (Heat 333 and Type 304L). The slightly higher values of UE for GBE materials (Fig. 33) are associated with the significantly smaller amounts of TG fracture in these materials compared to the baseline materials. Also, the non-GBE materials (Heat 333 and Type 304L) show a somewhat greater likelihood of IG crack initiation, as illustrated in Fig. 36. However, at this dose level (≈ 2 dpa), overall, the IASCC susceptibility in high-DO water of GBE and non-GBE Type 304 or 304L SSs does not seem to be significantly different.

For the GBE Type 316 SS, the IG fraction is significantly lower than that observed in either the GBE or baseline Type 304 SSs. The major non-ductile fracture mode is TG in the GBE Type 316 SS, although more IG cracks are initiated. However, a direct comparison between GBE and non-GBE Type 316 SSs is not possible because a reference non-GBE Type 316 SS from the same heat or a heat with comparable chemical composition is not available.

For Alloy 690, the difference in the UE of the GBE and non-GBE alloys is considerably larger, as also shown in Fig. 33. Intergranular cracking appears in Alloy 690 but is absent in its GBE counterpart. At ≈ 2 dpa, the GBE treatment appears to significantly increase the IASCC resistance of Alloy 690 in high-DO water.

The reason for the apparent relatively small effect of the GBE process on IASCC susceptibility of austenitic SSs is unclear at present. The effect of CSL boundaries on the IASCC resistance may be overwhelmed by other stronger effects. It is possible that the influence of the GBE process on the IASCC of austenitic SSs may be underestimated in our study. The starting condition of the non-GBE materials can also contribute to the resulting grain-boundary structure after GBE processing.³⁴ The original fraction of CSL boundaries in our test materials is unknown. With only the information of CSL population after GBE treatment, we can only conclude that the current CSL population ($\sim 67\%$ for $\Sigma \leq 29$) is insufficient to reduce the IASCC susceptibility for austenitic SSs. The current GBE treatment for Alloy 690 ($\sim 71\%$ for $\Sigma \leq 29$) appears to result in a higher resistance to IASCC in high-DO water.

4.2.4 Effects of Alloying Elements on the IASCC Behavior of Austenitic SSs

4.2.4.1 Effects of Mo and O

The beneficial effect of Mo on the IASCC behavior of austenitic SSs can be illustrated by comparing the SSRT test results from Type 304 and 316 SSs. Figure 37 compares the IG cracking behavior of Type 304 and 316 SSs. Despite the variability among the same type of SS, the IG cracking in Type 304 SSs appears to be much more extensive than in Type 316 SSs. The IG area fractions of all Type 304 SSs, except the high-purity Type 304L SS with low-O content (Heat 327), are at least a factor

of three higher than those in Type 316 SSs. In the present study, only one out of three Type 316 SSs (GBE Type 316 SS) showed IG fracture, and the resulting IG area fraction was about the same as the lowest fraction observed for Type 304 SS. However, in terms of susceptibility to IG crack initiation, the difference between Type 304 SS and GBE Type 316 SS is less significant. The number of IG cracks per unit UE in GBE Type 316 SS is about the same as in most Type 304 SSs.

Since the main difference between Type 304 and 316 SSs is their Mo content, the difference in IASCC behavior is attributed to the Mo addition in Type 316 SSs. Jenssen et al.³⁵ observed the same beneficial effect of Mo in a dose range (≈ 1.5 dpa) similar to this study. At a higher dose level (≈ 15 dpa), the beneficial effect on IASCC resistance is lost. Grain-boundary microchemical analysis indicates that Mo helps to retain Cr at the grain boundaries^{35,36} and, therefore, improves the IASCC resistance of the austenitic SSs. The Mo enrichment at grain boundaries before irradiation is believed to be responsible for the IASCC mitigation. Sufficiently high levels of neutron irradiation reduce or completely remove Mo enrichment at the grain boundaries. This condition allows Cr depletion to occur.

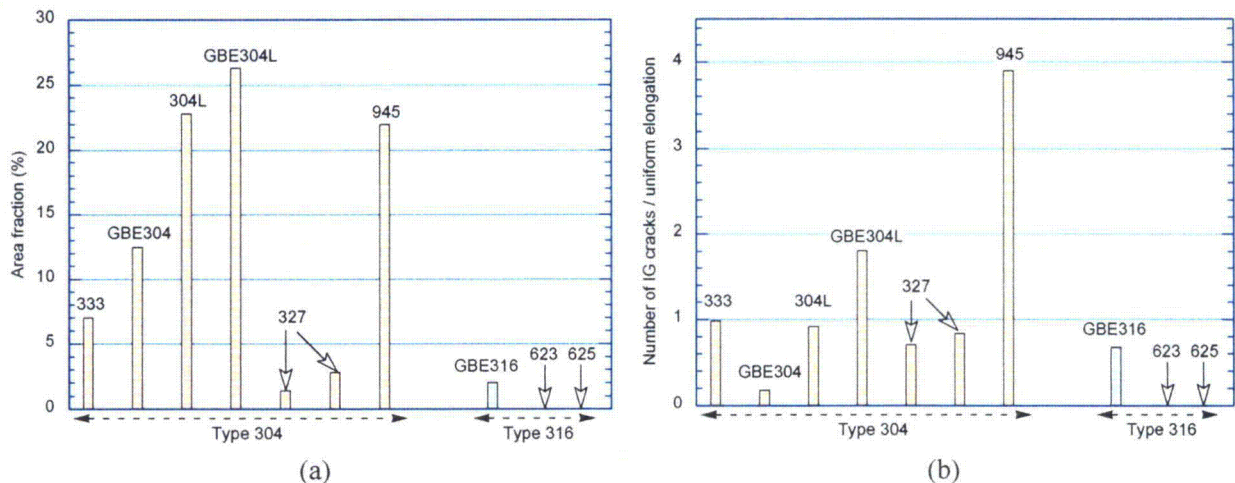


Figure 37. Comparisons of Type 304 and 316 SSs for (a) the IG area fraction and (b) the number of IG cracks normalized by uniform elongation.

The influence of O on the IASCC behavior can be determined by comparison of two heats of high-purity Type 304 SS with different bulk O contents, Heats 327 and 945. The O contents of these two steels are 0.008 and 0.047 wt.%, respectively. As shown in Fig. 37, the combination of IG area fraction and the number of IG cracks per unit UE is much higher in the high-O SS (Heat 945). This finding suggests a deleterious effect of O on the IASCC performance and is consistent with earlier studies with proton irradiation by Cookson et al.³⁷ and with neutron irradiation by Chung et al.^{38,39} The easy crack initiation at the oxide particles is considered responsible for the increased susceptibility of IASCC in high-O SS.³⁷

4.2.4.2 Effects of Cr and Ni

The chemical compositions of Type 304 and Type 316 SSs differ significantly in Cr and Ni contents. However, as previously noted, Mo is the key alloying element that distinguishes Type 316 SS from Type 304 SS. To single out the effects of Cr or Ni, the IG cracking behavior should be compared within the same type of austenitic SS. Figure 38 shows the variations of the IG area fractions and numbers of IG cracks with Cr and Ni contents for Type 304 and 316 SSs. The data sets for the two steels are well apart because of the Mo addition in the Type 316 SS. For the variation in Cr or Ni that occurs

within the specification of a single type of steel, the effects of Cr or Ni on IG cracking are ambiguous. A decreasing trend in IG area fraction may exist with an increase in Cr or Ni content for Type 304 SS (Figs. 38a and 38c). No correlation is apparent between the Cr or Ni contents and the likelihood of IG crack initiation, as represented by the number of IG cracks per unit UE (Figs. 38b and 38d). As suggested in literature²³, greater resistance to IASCC in high-Cr or -Ni SSs could be possible due to the changes in the deformation processes in these materials with increasing Cr and Ni contents.

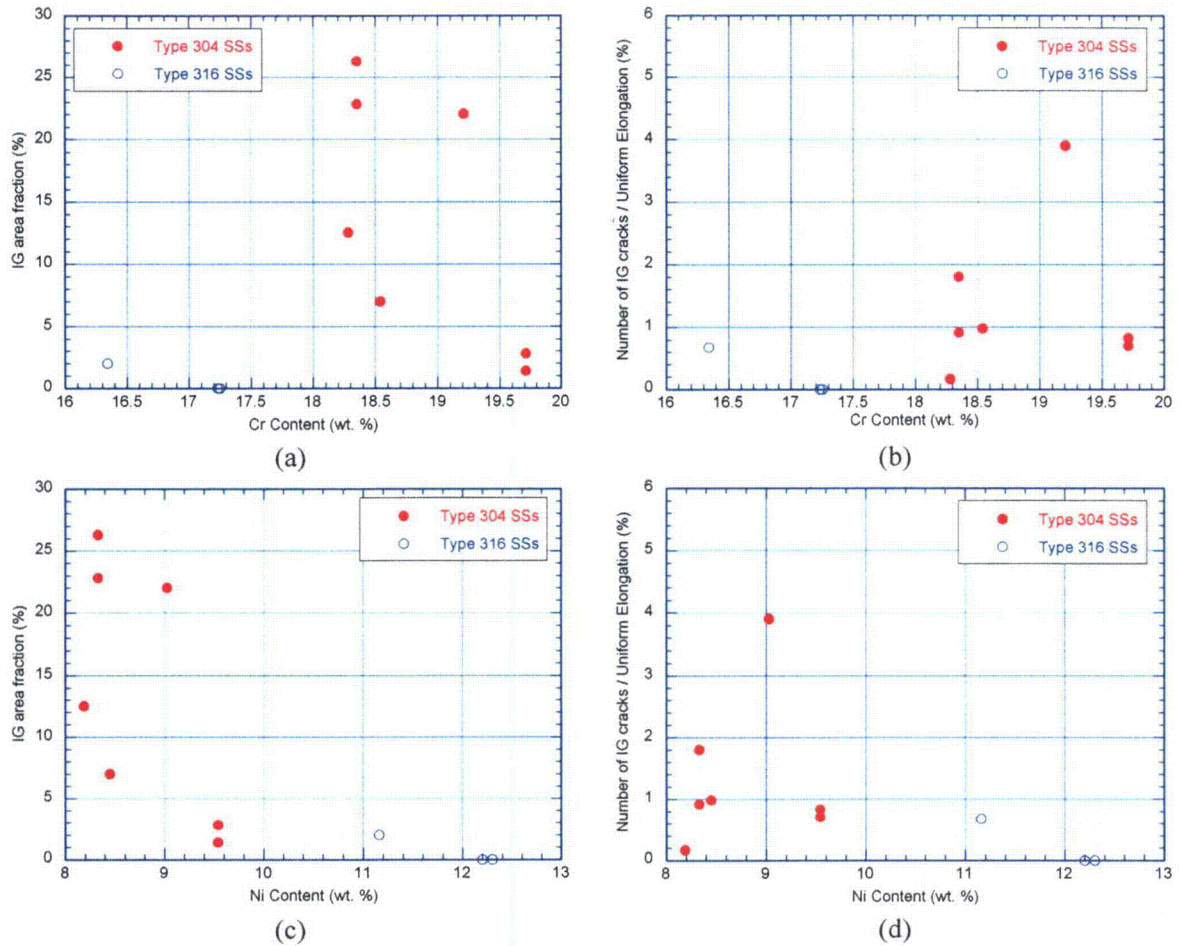


Figure 38. The influence of Cr and Ni content on the IG cracking for austenitic SSs.

4.2.4.3 Effects of C and S

The influence of C content on the IG cracking behavior is illustrated in Fig. 39. Both the IG area fraction and IG crack initiation decrease with an increase in C content, except for the heat of high-purity Type 304L SS with low O. The beneficial effect of C on the resistance to IG cracking is consistent with the results in the SSRT tests, where the UE increases with C content, as shown in Fig. 31d. Halden Phase-I²¹ and several other studies^{40,41} reported a similar behavior (i.e., a minimum C content is required for improved resistance to IASCC). Typically, austenitic SSs with more than 0.04 wt.% C exhibit better IASCC resistant than low-C SSs.

The deleterious effect of S on the IASCC susceptibility of austenitic SSs was discussed in the Halden Phase-I study.²¹ At a dose of ≈ 3 dpa, the percent IG cracking sharply increased in austenitic SSs

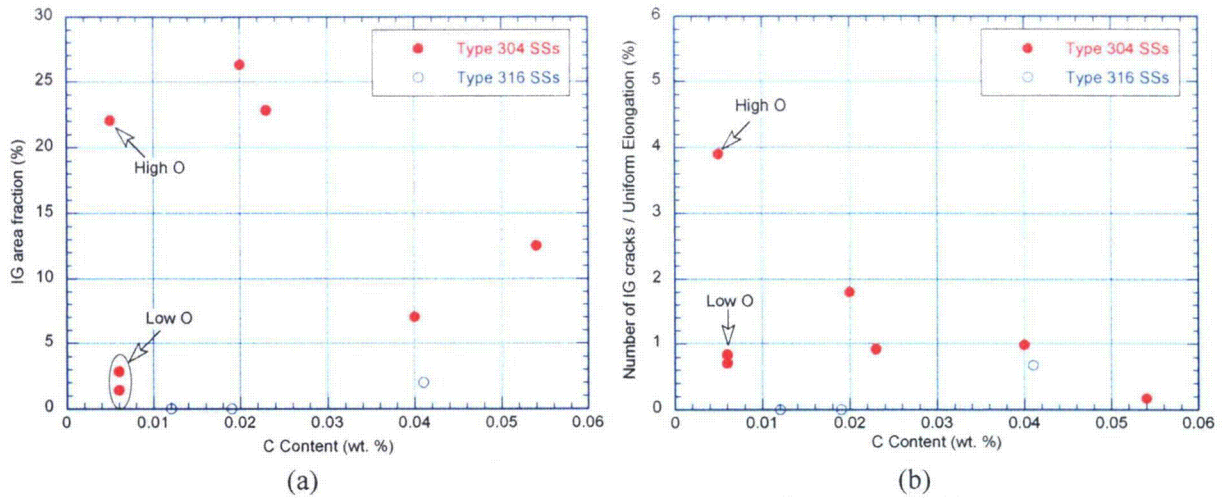


Figure 39. The influence of C content on the IG cracking behavior for austenitic SSs.

for S contents $> \approx 0.002$ wt.%. In Fig. 40a, the IG area fraction and the number of IG cracks are plotted against the S content for the Halden Phase-II specimens (irradiated to ≈ 2 dpa). A steep rise in IG area fraction with S content is indeed observed for the Type 304 SSs; the only exception is the data point for Heat 333 (with 0.019 wt.% S). Unfortunately, no specimens in the Halden Phase-II irradiation have S content below 0.002 wt.%. As a result, the IASCC resistance for the S content below < 0.002 wt.% cannot be verified. The effect of S content on IG crack initiation is less obvious (Fig. 40b).

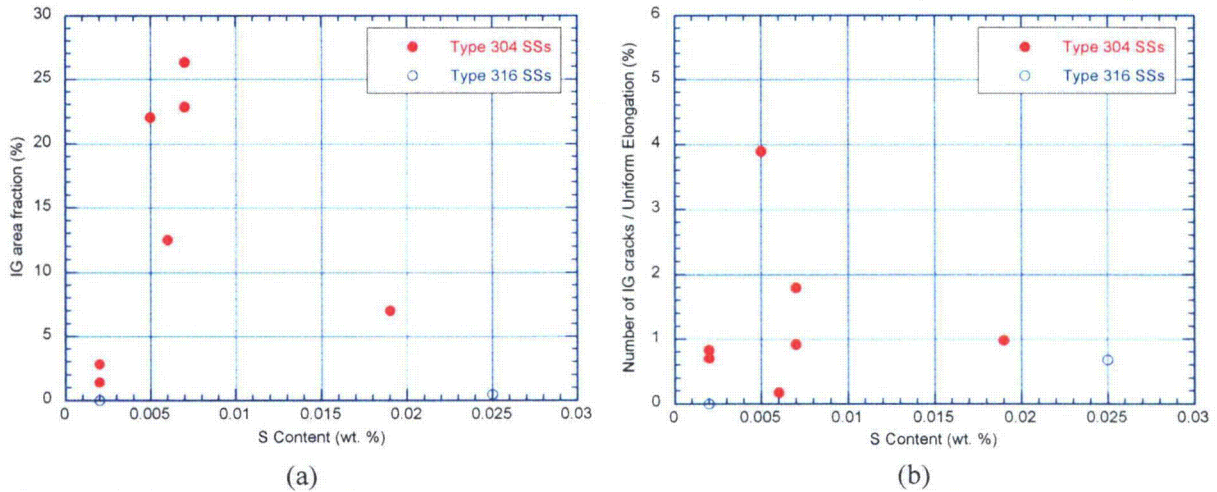


Figure 40. The influence of S content on the IG cracking behavior for austenitic SSs.

In addition to reporting a significant effect of S and C contents on IASCC behavior, the Halden Phase-I study concluded that there was a strong interaction between these elements. A minimum C content was required to suppress IASCC susceptibility even with the S content below 0.002 wt.%.

In the report on the Phase-I work, the strong effects of C and S contents on IASCC behavior and their potential interaction led to the development of the S-C map shown in Fig. 41,²¹ which can be used to determine the IASCC susceptibility for different compositions of austenitic SSs. In Fig. 42, the data from the Halden Phase-II study are also plotted on an S-C map. The line that separates the resistant and susceptible regimes is based on the result of Ref. 21. Although the data are limited in our current study,

they seem consistent with the conclusion of Ref. 21 that the IASCC-resistant regime is located at the low-S and high-C corner of the S-C map. Note that the IASCC-resistant regime in Fig. 42 is based on the data for a 3-dpa irradiation dose, and the position of the boundary could be dose dependent.

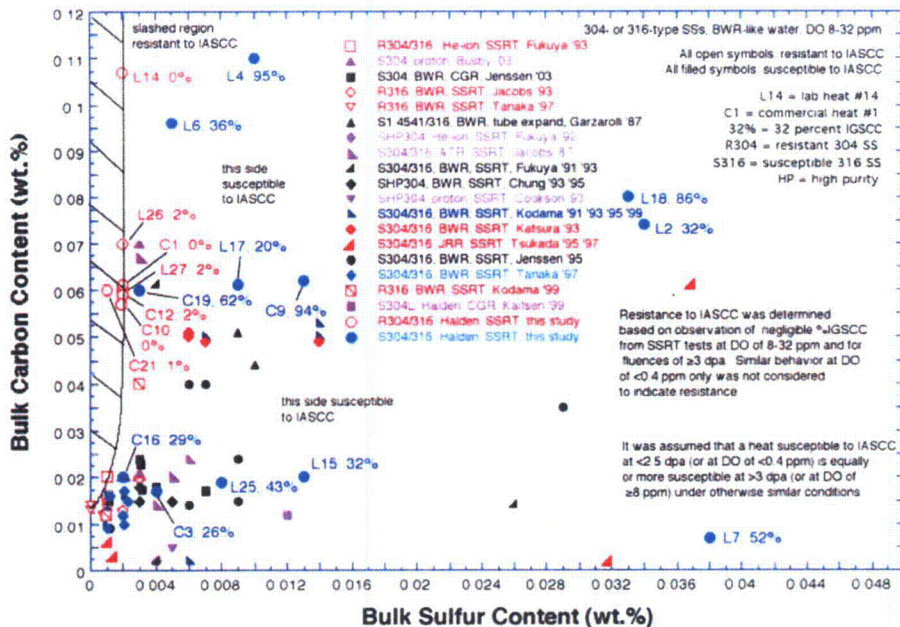


Figure 41. Range of bulk S and C contents in which Type 304 or 316 steels are resistant or susceptible to IASCC in BWR-like oxidizing water.

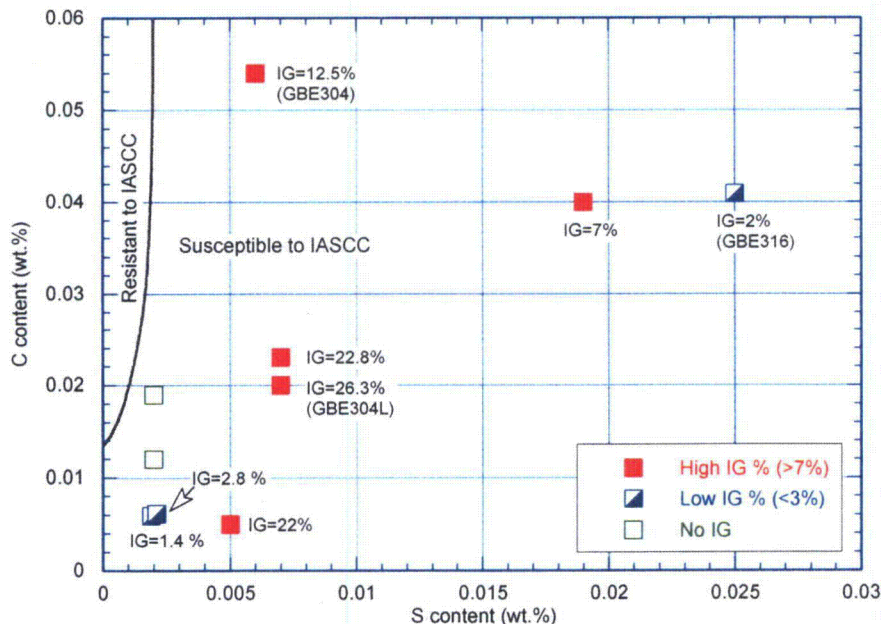


Figure 42. Ranges in the sulfur-carbon content map that austenitic SSs are resistant and susceptible to IASCC in high-DO aqueous environment.

4.2.4.4 Effects of Other Alloying Elements

Figure 43 shows the variation of IG area fraction and normalized number of IG cracks with P content. Neither IG area fraction nor the IG crack initiation seems to correlate with P content in the present study. This observation is consistent with earlier results by Chung et al.,³⁹ Busby and Was,²³ Briant and Andresen.⁴² Detailed analysis of the grain-boundary segregation by Briant⁴³ shows that P could contribute to the IG cracking indirectly by a competitive segregation mechanism between P and S, and P and Sb. This competitive mechanism suggests a beneficial effect of P and may be responsible for the slightly increase in the UE with P content as seen in Fig. 31f. Nevertheless, the potential effect of P on IASCC is clearly secondary and is observed in neither the IG area fraction nor normalized number of IG cracks (Fig. 43).

Figure 44 shows the influence of Mn content on IG cracking in austenitic SSs. Because of the potential effect of O content on the cracking behavior, alloys with high- and low-O content are identified in the plots. If the data point for the high-O content Type 304L SS is excluded, the results suggest an increase of IG area fraction with Mn content (Fig. 44a). The variation in the number of IG cracks, however, is too small to be used to reliably assess any effect of Mn on IG crack initiation.

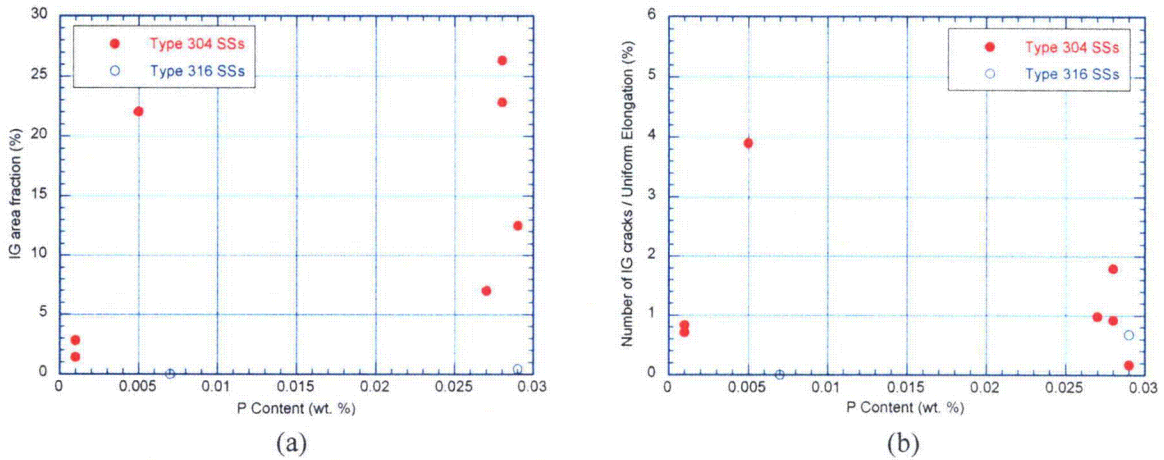


Figure 43. The influence of P content on the IG cracking behavior for austenitic SSs.

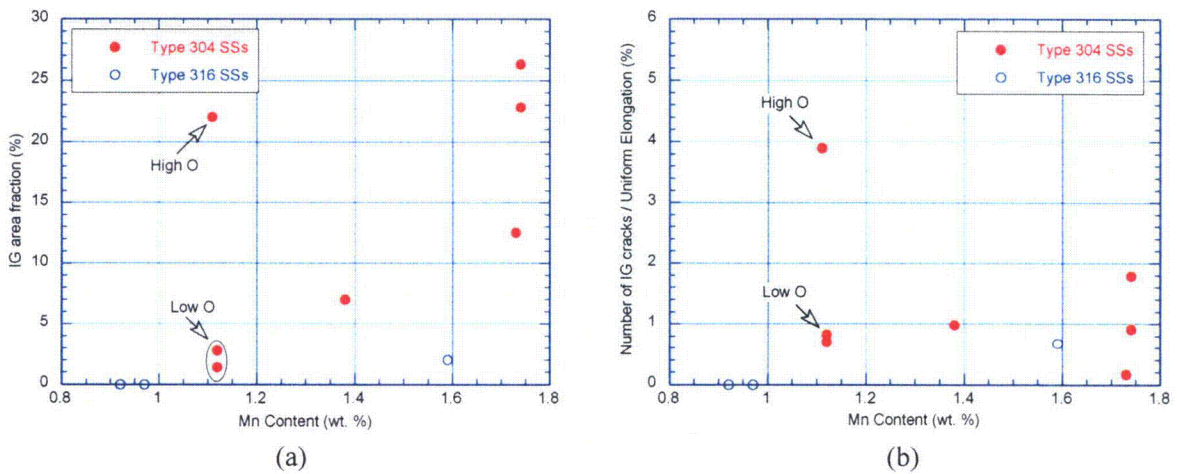


Figure 44. The influence of Mn content on the IG cracking behavior for austenitic SSs.

Figure 45 shows the influence of N content on the IG cracking behavior. With an increase in the N content, the IG area fraction and number of IG cracks both seem to increase for Type 304 SSs, except for the high-O Type 304 SS (Fig. 45a). A similar deleterious effect of N has also been noted by Jacobs⁴⁵ for Type 348 SS. The increase in IG cracking may be related to an increase in the tensile strength of SSs with N addition. The influence of N content on IG initiation is not clear as shown in Fig. 45b.

Figure 46 shows the IG cracking behavior with respect to the Si contents. No obvious dependence can be seen between the IG area fraction and number of IG cracks with Si content. The influence of Si on IG cracking has been an open question. Conflicting results have been reported on the role of Si in IASCC behavior.^{21,23,44,45} Silicon is a major impurity in austenitic SSs and can segregate extensively to the grain boundaries during irradiation. The bulk content of Si cannot characterize the microchemistry at the grain boundaries. This problem might contribute to the conflicting results regarding the influence of Si on IASCC susceptibility.

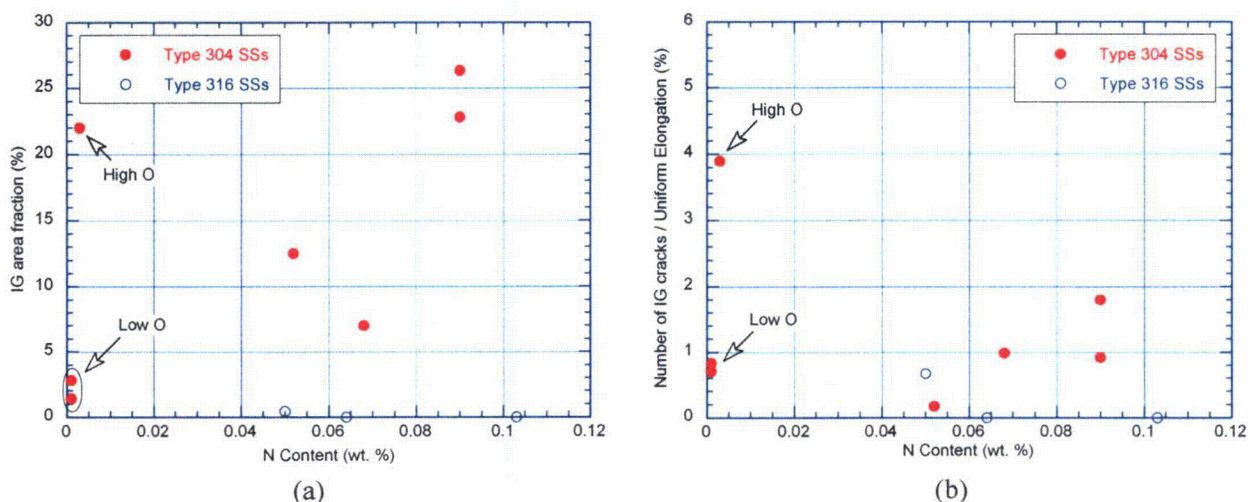


Figure 45. The influence of N content on the IG cracking behavior for austenitic SSs.

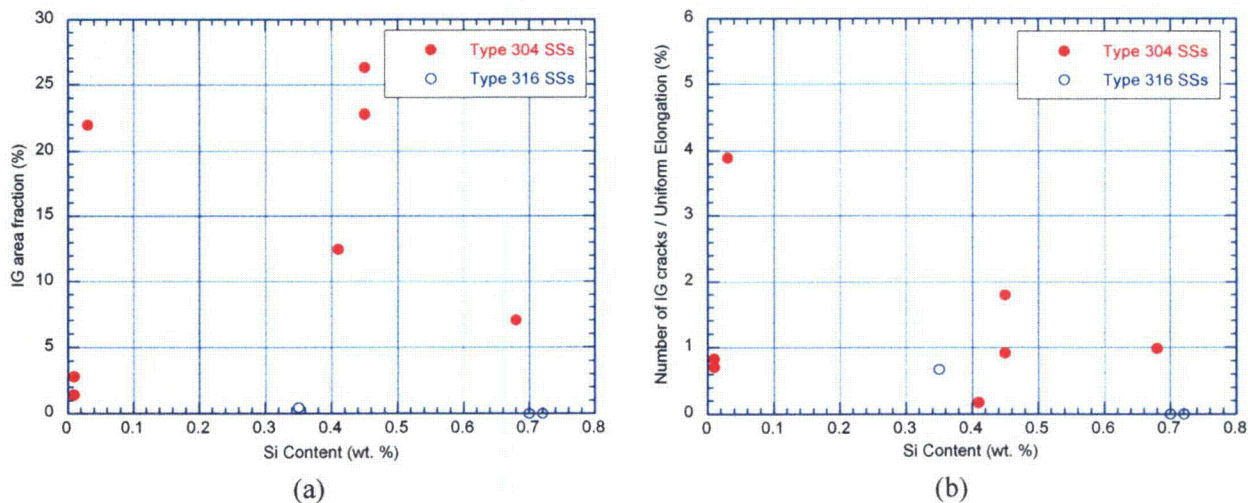


Figure 46. The influence of Si content on the IG cracking behavior for austenitic SSs.

Type 316LN SSs with and without Titanium (Ti) addition (Heat 623 and 625) were investigated in this study to determine the effect of Ti on IASCC susceptibility. The elongation of the Ti-doped Type 316LN SS was slightly lower than that of the base material, as shown in Fig. 4c. Because neither material showed IG cracking, the tests provide no insight on the influence of Ti additions on IASCC behavior. This finding is consistent with the results of Busby and Was.²³ Although Busby and Was²³ found a potential beneficial effect of Ti in reducing RIS, they also found that Ti addition does not change the IASCC behavior of austenitic SSs.

4.2.5 Irradiation Dose and IASCC Behavior

The IASCC behavior is affected by irradiation hardening, embrittlement, radiation-induced microchemistry changes, and radiolysis. All of these processes are dose dependent; and therefore, IASCC behavior varies with irradiation dose as well. The influence of neutron dose on SSRT properties was discussed in Section 4.1.1. Both irradiation hardening and embrittlement respond rapidly to irradiation dose in low dose region. The increase in YS and UTS is evident at ≈ 0.45 dpa as shown in Figs. 26 and 27. The YS and UTS continue to rise with irradiation dose and are not saturated at 3 dpa. Similarly, the elongation also reduces significantly at ≈ 0.45 dpa and continues to drop with neutron fluence. In contrast to these steep changes of strength and elongation at low doses, the occurrence of IASCC requires some dose accumulation or a threshold dose. Figure 47 shows the variation of IG area fraction as a function of irradiation dose for the Halden Phase-II specimens and commercial heats from the Halden Phase-I study. Intergranular cracking is not observed at ≈ 0.45 dpa for the commercial heats of austenitic SSs from the Halden irradiations. Beyond ≈ 0.45 dpa, IG cracking can occur in the most susceptible steels, and the IG area fraction increases gradually with increasing irradiation dose. The SSRT results from the Halden phase I and II study show that IG cracking starts to occur between 0.45 and 1.3 dpa for most austenitic SSs. This dose range seems to be consistent with the threshold value of 0.75 dpa reported by other researchers.^{9,10} However, the Halden SSRT data set is insufficient to determine precisely the IASCC threshold dose at present.

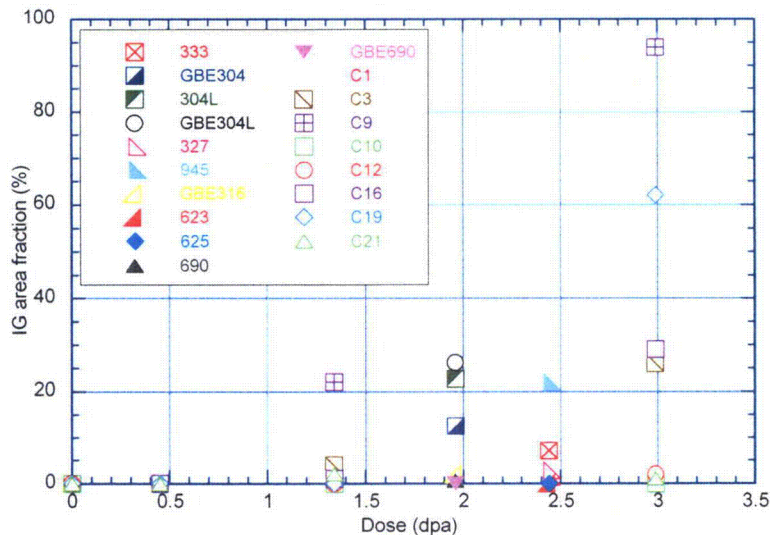


Figure 47. Dose dependence of IG area fraction for Halden Phase-I and Phase-II specimens tested in high-DO water at 289°C.

As discussed in Section 4.2.2, the number of IG cracks per unit UE can be used as a measure of the likelihood of IG crack initiation. The likelihood of initiating an IG crack is expected to increase with increasing irradiation dose. Figure 48 shows that the number of IG cracks varies with irradiation dose.

However, the data are also inadequate to use this measure to independently identify a threshold for IG crack initiation.

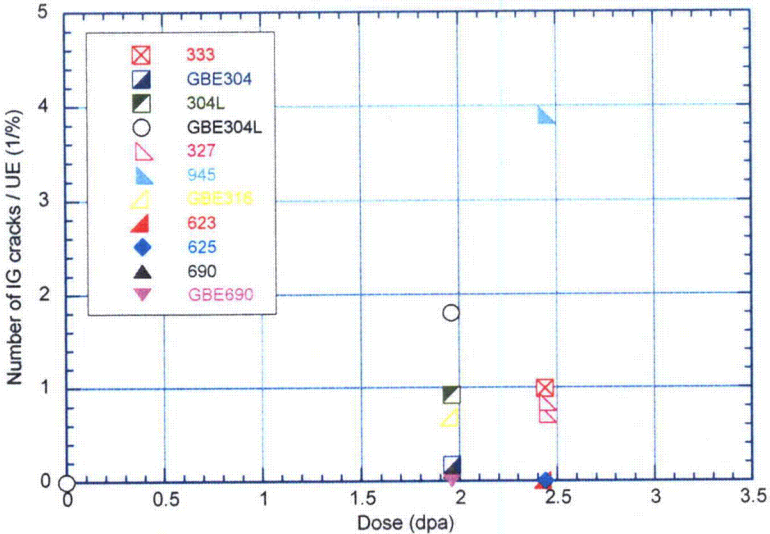


Figure 48.
Dose dependence of number of IG cracks per UE for Halden Phase-II specimens tested in high-DO water at 289°C.

5 Summary

The IASCC behavior of several austenitic SSs and Alloy 690 has been investigated using flat dog-bone tensile specimens irradiated in the Halden heavy boiling water reactor to ≈ 2 dpa. The SSRT tests were conducted in high-DO water at 289°C. Fractographic analyses of the SSRT specimens were performed with an SEM to characterize the fracture morphology and determine the area fraction of brittle fracture (i.e., IG plus TG fracture). The uniform elongation of the SSRT specimens and the fracture characteristics were used to evaluate the IASCC susceptibility of the alloys. The significant results from the present study are summarized as follow:

- (a) Irradiation hardening and embrittlement occurred in all irradiated materials. For austenitic SSs, a small amount of strain hardening remained in the normal-C Type 304 and 316 SSs, but no strain hardening was observed in the low-C SSs (e.g. <0.02 wt.%). For Alloy 690, a considerable amount of strain hardening remained in the GBE alloy, whereas only limited strain hardening occurred in the non-GBE alloy. IG cracking starts to occur between 0.4 and 1.3 dpa for most austenitic SSs in the Halden irradiation programs.
- (b) At a dose of ≈ 2 dpa, a lower C content is usually associated with poor ductility in high-DO water for all austenitic SSs, with or without GBE treatment. The UE obtained from SSRT tests in high-DO water increases linearly with C content below 0.06 wt.%.
- (c) A general correlation appeared to exist between the UE and percent IG fracture. The UE can be correlated with the IASCC susceptibility, but it is not sensitive enough at the low strain range. The IG area fraction and the number of IG cracks per unit UE can be used to assess the IASCC behavior.
- (d) Intergranular cracks initiate on the surface of a SSRT specimen and then extend into the specimen under stress. Transgranular cracks observed in the SSRT specimens may or may not originate from IG crack sites.
- (e) The GBE process used in this study increases the CSL boundaries ($\Sigma < 29$) to about 66% for austenitic SSs and to about 70% for Alloy 690. For Alloy 690, the GBE treatment results in a smaller reduction in UE caused by irradiation and reduces the IASCC susceptibility in high-DO water at ≈ 2 dpa. However, little benefit of the GBE process used in this study was observed for Type 304 or 304L SSs.
- (f) Type 316 SSs are generally more resistant to IASCC than Type 304 SSs. The presence of Mo or the higher Ni concentrations in Type 316 SSs may be responsible for the difference in IASCC susceptibility between Type 304 and 316 SSs.
- (g) The O content is critical for IASCC susceptibility; high-O content contributes to IASCC susceptibility by enhancing IG crack initiation.
- (h) Low-C austenitic SSs are more susceptible to IASCC than the normal-C SSs. An S content below 0.002 wt.% is also a critical requirement for IASCC resistance in austenitic SSs. A minimum C content is needed to suppress IASCC susceptibility in the low-S steels. Thus, there may be a trade-off in minimizing susceptibility to IASCC and minimizing susceptibility to IGSCC resulting from conventional SS sensitization.

References

1. NRC Generic Letter 94-03, "Intergranular Stress Corrosion Cracking of Core Shrouds in Boiling Water Reactors," U.S. Nuclear Regulatory Commission, July 25, 1994.
2. NRC Information Notice 92-57, "Radial Cracking of Shroud Support Access Hole Cover Welds," U.S. Nuclear Regulatory Commission, August 11, 1992.
3. NRC IE Bulletin No. 80-07, "BWR Jet Pump Assembly Failure," U.S. Nuclear Regulatory Commission, April 4, 1980.
4. NRC Information Notice 93-101, "Jet Pump Hold-Down Beam Failure," U.S. Nuclear Regulatory Commission, December 17, 1993.
5. NRC Information Notice 97-02, "Cracks Found in Jet Pump Riser Assembly Elbows at Boiling Water Reactors," U.S. Nuclear Regulatory Commission, February 6, 1997.
6. NRC Information Notice 95-17, "Reactor Vessel Top Guide and Core Plate Cracking," U.S. Nuclear Regulatory Commission, March 10, 1995.
7. NUREG-1544, "Status Report: Intergranular Stress Corrosion Cracking of BWR Core Shrouds and Other Internal Components," U.S. Nuclear Regulatory Commission, March 1996.
8. NRC Information Notice 98-11, "Cracking of Reactor Vessel Internal Baffle Former Bolts in Foreign Plants," U.S. Nuclear Regulatory Commission, March 25, 1998.
9. Jacobs, A. J., G. P. Wozadlo, K. Nakata, T. Yoshida, and I. Masaoka, "Radiation Effects on the Stress Corrosion and Other Selected Properties of Type-304 and Type-316 Stainless Steels," Proc. 3rd Intl. Symp. Environmental Degradation of Materials in Nuclear Power Systems--Water Reactors, G. J. Theus and J. R. Weeks, eds., The Metallurgical Society, Warrendale, PA, pp. 673-680, 1988.
10. Gordon, G. M. and K. S. Brown, "Dependence of Creviced BWR Component IGSCC Behavior on Coolant Chemistry", Proc. 4th Intl. Symp. on Environmental Degradation of Materials in Nuclear Power Systems--Water Reactors, NACE, Houston, TX, pp. 1.4.46-14.62, 1990.
11. Garzarolli, F., D. Alter, P. Dewes, and J. L. Nelson, "Deformability of Austenitic Stainless Steels and Ni-Base Alloys," Proc. 3rd Intl. Symp. on Environmental Degradation of Materials in Nuclear Power Systems--Water Reactors, G. J. Theus and J. R. Weeks, eds., The Metallurgical Society, Warrendale, PA, pp. 657-664, 1988.
12. Chung, H. M., R. V. Strain, and R. W. Clark, "Slow-Strain-Rate-Tensile Test of Model Austenitic Stainless Steels Irradiated in the Halden Reactor," Environmentally Assisted Cracking in Light Water Reactors Semiannual Report July 2000-December 2000, NUREG/CR-4667, Vol. 31, ANL-01/09, pp. 22-32, 2002.
13. Bruemmer, S. M., and Gary S. Was, "Microstructural and Microchemical Mechanisms Controlling Intergranular Stress Corrosion Cracking in Light-Water-Reactor Systems," J. Nucl. Mater., **216**, 348-363, 1994.

14. Scott, P., "A Review of Irradiation Assisted Stress Corrosion Cracking," *J. Nucl. Mater.*, **211**, 101-122, 1994.
15. Osozawa, K., and H. J. Engell, "The Anodic Polarization Curves of Iron-Nickel-Chromium Alloys," *Corr. Sci.*, **6**, 389-393, 1966.
16. Tedmon, C. S., Jr., D. A. Vermilyea, and J. H. Rosolowski, "Intergranular Corrosion of Austenitic Stainless Steel," *J. Electrochem. Soc.*, **118**, 192-202, 1971.
17. Bruemmer S. M., L. A. Charlot and D. G. Atteridge, "Sensitization Development in Austenitic Stainless Steel: Measurement and Prediction of Thermomechanical History Effects," *Corrosion*, **44**, 427, 1987.
18. Andresen, P. L., F. P. Ford, S. M. Murphy, and J. M. Perks, "State of Knowledge of Radiation Effects on Environmental Cracking in Light Water Reactor Core Materials," *Proc. 4th Intl. Symp. on Environmental Degradation of Materials in Nuclear Power Systems--Water Reactors*, NACE, Houston, TX, pp. 1.83-1.121, 1990.
19. Chung, H. M., W. R. Ruther, and R. V. Strain, "Irradiation-Assisted Stress Corrosion Cracking of Model Austenitic Stainless Steels Irradiated in the Halden Reactor," *NUREG/CR-5608*, ANL-98/25, March 1999.
20. Chung, H. M., W. R. Ruther, R. V. Strain, and W. J. Shack, "Irradiation-Assisted Stress Corrosion Cracking of Model Austenitic Stainless Steel Alloys," *NUREG/CR-6687*, ANL-00/21, Oct. 2000.
21. Chung, H. M. and W. J. Shack, "Irradiation-Assisted Stress Corrosion Cracking Behavior of Austenitic Stainless Steels Applicable to LWR Core Internals," *NUREG/CR-6892*, ANL-04/10, Jan. 2006.
22. Chung, H. M., and R. W. Strain, "Slow-Strain-Rate-Tensile Test of Model Austenitic Stainless Steels Irradiated in the Halden Reactor," *Environmentally Assisted Cracking in Light Water Reactors*, Annual Report, January-December 2003, *NUREG/CR-4667*, Vol. 34, ANL-05/17, May 2006.
23. Busby, J. T., and G. S. Was, "Irradiation-Assisted Stress Corrosion Cracking in Model Alloys with Solute Additions," *Proc. of the 11th Int. Symp. on Environmental Degradation of Materials in Nuclear Power Systems--Water Reactors*, NACE, Houston, TX, pp. 995-1014, 2003.
24. Was, G. S., "Recent Developments in Understanding Irradiation Assisted Stress Corrosion Cracking," *Proc. 11th Int. Symp. on Environmental Degradation of Materials in Nuclear Power Systems--Water Reactors*, NACE, Houston, TX, pp. 965-985, 2003.
25. Gertsman, V. Y., and K. Tangri, "Grain Boundary Distributions, Texture and Orientation Correlations in Austenitic Stainless Steels," *Scripta Metallurgica et Materialia*, **33** (7), 1037-1042, 1995.
26. Lin, P., G. Palumbo, U. Erb, and K. T. Aust, "Influence of Grain Boundary Character Distribution on Sensitization and Intergranular Corrosion of Alloy 600," *Scripta Metallurgica et Materialia*, **33** (9), 1387-1392, 1995.

27. Was, G. S., B. Alexandreanu, P. Andresen, and M. Kumar, "Role of Coincident Site Lattice Boundaries in Creep and Stress Corrosion Cracking," *Interfacial Engineering for Optimized Properties III, Materials Research Society Symposium Proceedings, Vol. 819*, pp. 87-100, 2004.
28. Watanabe, T., "Approach to Grain Boundary Design for Strong and Ductile Polycrystals," *Res. Mechanica: Inter. J. Struct. Mech. Mater. Sci.*, **11** (1), 47-84, 1984.
29. Randle, V., "Twinning-Related Grain Boundary Engineering," *Acta Materialia* **52**, 4067-4081, 2004.
30. Kim, H. M., and J. A. Szpunar, "The Effect of Texture and Grain Boundary Structure on the Intergranular Corrosion of Stainless Steel," *Mat. Sci. Forum*, **157-162**, 1997-2004, 1994.
31. Palumbo, G., E. M. Lehockey, and P. Lin, "Applications for Grain Boundary Engineered Materials," *JOM*, **50** (2), 40-43, 1998.
32. Was, G. S., V. Thaveprungsriporn, and D. C. Crawford, "Grain Boundary Misorientation Effects on Creep and Cracking in Ni-Based Alloys," *JOM*, **50** (2), 44-49, 1998.
33. Randle, V., and G. Owen, "Mechanisms of Grain Boundary Engineering," *Acta Materialia* **54**, 1777-1783, 2006.
34. Randle, V., "Twinning-Related Grain Boundary Engineering," *Acta Materialia*, **52**, 4067-4081, 2004.
35. Jenssen, A., L. G. Ljungberg, J. Walmsley, and S. Fisher, "Importance of Molybdenum on Irradiation-Assisted Stress Corrosion Cracking in Austenitic Stainless Steels," *Corrosion*, **54** (1), 48-60, 1998.
36. Cole, J. I., T. R. Allen, G. S. Was, Y. Wang, and E. A. Kenik, "The Effect of Bulk Composition on the Radiation-Induced Microstructures and Segregation Behavior in Model Austenitic Stainless Steel Alloys: A Proton Irradiation Study," *Proc. Tenth Intl. Symp. on Environmental Degradation of Materials in Nuclear Power Systems--Water Reactor*, NACE, Houston, TX, 2001.
37. Cookson, J. M., G. S. Was, and P. L. Andresen, "Oxide-Induced Initiation of Stress Corrosion Cracking in Irradiated Stainless Steels," *Corrosion*, **54** (4), 48-60, 1998.
38. Chung, H. M., W. E. Ruther, J. E. Sanecki, and T. F. Kassner, "Irradiation-Induced Sensitization and Stress Corrosion Cracking of Type 304 Stainless Steel Core: Internal Components," *Proc. of the 5th Int. Symp. on Environmental Degradation of Materials in Nuclear Power Systems--Water Reactors*, D. Cubicciotti, ed., NACE, Houston, TX, p. 795, 1992.
39. Chung, H. M., W. E. Ruther, J. E. Sanecki, A. Hins, N. J. Zaluzec, and T. F. Kassner, "IASCC of Austenitic Stainless Steels: Recent Progress and New Approaches," *J. Nucl. Mater.*, **239**, 61-79, 1996.
40. Tsukada, T., and Y. Miwa, "Stress Corrosion Cracking of Neutron Irradiated Stainless Steels," *Proc. 7th Int. Symp. on Environmental Degradation of Materials in Nuclear Power System--Water Reactors*, August 7-10, 1995, Breckenridge, CO, G Airey et al., eds., NACE, Houston, TX, pp. 1009-1018, 1995.

41. Fukuya, K., S. Shima, K. Nakata, S. Kasahara, A. J. Jacobs, G. P. Wozadlo, S. Suzuki, and M. Kitamura, "Mechanical Properties and IASCC Susceptibility in Irradiated Stainless Steel," Proc. 6th Intl. Symp. on Environmental Degradation of Materials in Nuclear Power Systems--Water Reactors, August 1-5, 1993, San Diego, CA, R. E. Gold and E. P. Simonen, eds., The Minerals, Metals, and Materials Society, Warrendale, PA, pp. 565-572, 1993.
42. Briant, C. L., and P. L. Andresen, "Grain Boundary Segregation in Austenitic Stainless Steels and Its Effect on IG Corrosion and SCC," Met. Trans A., **19A** (3), 495-504, 1988.
43. Briant, C. L., "Competitive Grain Boundary Segregation in Fe-P-S and Fe-P-Sb Alloys," Acta Metallurgica, **36** (7), 1805-1813, 1988.
44. Tsujada, T., Y. Miwa, and H. Nakajima, "Stress Corrosion Cracking of Neutron Irradiated Type 304 Stainless Steels," Proc. 7th Intl. Symp. on Environmental Degradation of Materials in Nuclear Power Systems--Water Reactor, G. Airey et al., eds., NACE, Houston, TX, pp. 1009-1019, 1995.
45. Jacobs, A. J., R. E. Clausing, M. K. Miller, and C. Shepherd, "Influence of Grain Boundary Composition on the IASCC Susceptibility of Type 304 Stainless Steel," Proc. 4th Intl. Symp. on Environmental Degradation of Materials in Nuclear Power Systems--Water Reactors, NACE, Houston, TX, pp. 14.21-14.45, 1990.

Appendix A

Appendix A

Test ID	SSRT001				
Specimen ID	GBE304-02	Test Temp.	289°C	Yield Strength (MPa)	750
Heat ID	GBE304	Test Env.	High-DO Water	Ultimate Tensile Strength (MPa)	750
Material Description	GBE Type 304 SS	Strain Rate	3.31E-7 1/s	Uniform Elongation (%)	5.80
Dose	1.96 dpa			Total Elongation (%)	8.22

Strain (%)	Stress (MPa)						
0.000	0.000	0.166	292.656	2.313	732.661	6.073	734.514
0.082	144.197	0.181	318.048	2.420	731.178	6.175	734.514
0.082	144.382	0.192	337.695	2.514	733.217	6.278	734.329
0.081	142.899	0.200	361.975	2.613	734.143	6.390	731.363
0.082	144.382	0.219	384.587	2.724	731.549	6.491	731.549
0.082	144.011	0.233	408.681	2.818	733.587	6.592	731.734
0.082	144.753	0.249	432.405	2.926	732.105	6.693	732.105
0.082	144.011	0.263	456.314	3.019	734.514	6.806	728.954
0.082	144.197	0.268	483.004	3.125	733.217	6.912	727.842
0.082	144.011	0.285	506.172	3.227	733.217	7.016	727.286
0.082	144.011	0.291	532.490	3.325	734.329	7.125	725.432
0.082	144.938	0.303	557.141	3.426	734.514	7.231	724.135
0.082	144.938	0.314	581.977	3.532	733.217	7.350	719.501
0.082	144.567	0.309	611.261	3.630	734.514	7.454	718.760
0.083	146.421	0.317	637.209	3.735	733.402	7.579	712.458
0.085	148.645	0.324	663.157	3.834	734.329	7.702	706.713
0.084	147.348	0.350	683.915	3.936	734.329	7.858	691.885
0.084	148.274	0.368	706.898	4.037	734.514	8.033	671.868
0.085	149.572	0.406	724.506	4.144	733.031	8.268	635.170
0.086	151.054	0.451	740.074	4.239	734.885	8.561	582.904
0.087	153.464	0.523	748.044	4.340	735.070	10.733	14.827
0.087	152.723	0.621	749.341	4.443	734.699	10.835	14.827
0.089	155.688	0.764	738.036	4.538	736.738	10.942	13.530
0.090	158.839	0.870	736.738	4.650	733.958	11.045	12.974
0.091	159.951	0.981	734.329	4.748	735.070	11.147	13.159
0.093	162.916	1.085	733.587	4.851	734.514	11.252	12.047
0.094	165.326	1.195	731.549	4.951	735.255	11.354	12.047
0.096	169.033	1.290	733.217	5.056	734.329	11.449	13.901
0.096	169.589	1.397	731.919	5.155	735.070	11.550	14.086
0.101	177.744	1.498	732.105	5.258	734.699	11.660	12.047
0.103	180.709	1.602	732.105	5.357	735.441		
0.107	188.308	1.706	731.549	5.460	735.255		
0.116	204.619	1.804	732.475	5.564	734.514		
0.123	216.666	1.905	732.846	5.667	734.143		
0.133	232.976	2.007	732.661	5.763	735.811		
0.143	251.881	2.113	731.549	5.870	734.329		
0.154	270.971	2.211	732.475	5.973	733.958		

Test ID SSRT002

Specimen ID	304L-02	Test Temp.	289°C	Yield Strength (MPa)	677
Heat ID	304L	Test Env.	High-DO Water	Ultimate Tensile Strength (MPa)	677
Material Description	Type 304L SS	Strain Rate	3.31E-7 1/s	Uniform Elongation (%)	2.18
Dose	1.96 dpa			Total Elongation (%)	4.65

Strain (%)	Stress (MPa)						
0.000	0.000	0.180	316.010	0.661	667.235	3.354	517.107
0.074	129.740	0.187	328.984	0.730	663.898	3.460	505.245
0.074	130.111	0.191	335.471	0.794	661.860	3.589	488.193
0.074	130.296	0.170	350.669	0.847	662.416	3.764	460.763
0.074	130.111	0.187	359.380	0.902	662.230	3.887	445.194
0.074	129.925	0.200	369.018	0.961	661.489	4.077	414.056
0.075	132.150	0.208	379.953	1.015	661.674	4.295	376.802
0.075	131.964	0.222	389.220	1.067	662.416	4.539	333.432
0.076	133.447	0.234	399.229	1.130	660.377	5.982	14.827
0.077	135.300	0.239	410.720	1.187	661.118	6.045	12.789
0.078	136.968	0.246	421.655	1.242	661.118	6.108	10.935
0.078	137.524	0.252	432.961	1.314	657.041	6.162	11.306
0.079	138.822	0.269	441.672	1.372	656.485	6.220	10.565
0.080	140.119	0.268	454.461	1.448	651.666	6.273	11.121
0.081	142.158	0.267	467.250	1.520	647.588	6.333	9.823
0.083	145.494	0.272	478.741	1.633	634.429	6.385	10.565
0.084	148.274	0.286	488.193	1.695	632.761	6.438	10.935
0.086	151.981	0.291	499.685	1.779	626.088	6.498	9.823
0.090	158.468	0.286	513.400	1.899	611.076	6.552	10.194
0.094	164.399	0.293	524.520	1.980	605.145	6.609	9.638
0.097	169.959	0.305	534.344	2.048	602.179	6.662	10.009
0.100	176.446	0.296	548.986	2.119	598.658	6.728	7.599
0.105	184.231	0.313	557.697	2.186	595.878	6.786	6.858
0.108	190.718	0.309	571.227	2.237	596.619	6.831	9.267
0.112	197.205	0.325	580.123	2.300	594.765		
0.117	205.731	0.330	591.615	2.368	591.800		
0.122	214.627	0.332	603.847	2.429	590.503		
0.127	223.338	0.345	613.485	2.491	588.834		
0.131	231.123	0.362	622.196	2.563	584.942		
0.136	239.092	0.352	637.024	2.637	580.679		
0.141	247.062	0.366	646.476	2.722	573.822		
0.145	255.032	0.391	653.334	2.794	569.930		
0.150	264.299	0.401	663.713	2.898	558.624		
0.158	277.088	0.425	670.941	2.969	554.917		
0.163	287.096	0.457	676.131	3.093	539.163		
0.171	299.885	0.515	675.390	3.156	537.309		
0.175	307.669	0.610	666.308	3.288	519.516		

Test ID

SSRT003

Specimen ID	GBE304L-06	Test Temp.	289°C	Yield Strength (MPa)	747
Heat ID	GBE304L	Test Env.	High-DO Water	Ultimate Tensile Strength (MPa)	747
Material Description	GBE Type 304L SS	Strain Rate	3.31E-7 1/s	Uniform Elongation (%)	1.11
Dose	1.96 dpa			Total Elongation (%)	2.22

Strain (%)	Stress (MPa)						
0.000	0.000	0.069	121.400	0.111	195.166	0.518	741.742
0.069	120.658	0.070	122.512	0.117	206.101	0.570	746.561
0.069	120.658	0.070	123.809	0.124	218.334	0.662	741.186
0.069	120.473	0.071	124.736	0.131	230.752	0.731	741.742
0.069	120.473	0.071	125.292	0.139	245.209	0.798	743.040
0.068	120.288	0.071	124.736	0.146	256.885	0.873	742.113
0.069	120.473	0.071	125.292	0.155	272.083	0.969	735.626
0.069	120.473	0.071	125.663	0.162	284.316	1.037	736.367
0.069	120.844	0.071	125.106	0.170	298.958	1.117	734.143
0.069	120.473	0.072	126.033	0.153	317.678	1.192	733.217
0.069	120.658	0.071	125.477	0.170	331.764	1.253	735.811
0.069	120.844	0.071	125.292	0.178	348.074	1.335	733.031
0.069	121.214	0.072	126.219	0.196	361.975	1.420	729.510
0.069	120.658	0.071	125.477	0.208	377.358	1.528	719.872
0.069	120.844	0.072	126.960	0.210	395.336	1.600	719.687
0.069	120.844	0.073	127.701	0.249	403.677	1.715	708.381
0.069	120.844	0.073	128.257	0.260	419.431	1.836	695.592
0.069	120.844	0.073	128.628	0.266	436.483	1.972	678.540
0.069	121.029	0.074	129.555	0.269	454.090	2.145	652.222
0.069	120.658	0.074	129.369	0.267	473.181	2.310	627.757
0.069	120.658	0.074	129.369	0.287	486.711	4.722	19.090
0.069	120.473	0.074	129.740	0.285	505.616	4.801	17.237
0.068	120.288	0.074	129.740	0.285	524.150	4.882	14.457
0.068	120.288	0.074	130.296	0.322	533.046	4.964	11.677
0.069	120.473	0.074	130.111	0.327	550.283	5.021	15.569
0.068	120.102	0.074	130.852	0.304	574.934	5.091	15.939
0.069	120.473	0.074	130.296	0.326	587.722	5.167	14.642
0.069	120.658	0.075	131.964	0.319	607.925	5.257	9.638
0.069	120.658	0.076	133.076	0.328	624.235	5.307	15.383
0.069	120.473	0.076	134.188	0.336	640.731	5.373	16.681
0.069	120.473	0.078	137.154	0.340	658.153	5.471	9.638
0.068	120.288	0.080	140.305	0.344	675.575	5.517	16.310
0.069	120.658	0.083	146.050	0.361	689.661	5.591	15.569
0.069	120.844	0.087	152.352	0.401	697.816	5.667	14.457
0.068	120.288	0.091	160.322	0.421	711.346	5.737	14.642
0.069	120.658	0.098	171.813	0.417	730.807	5.822	11.121
0.069	120.658	0.105	184.231	0.461	737.850		

Test ID SSRT004

Specimen ID	333-04	Test Temp.	289°C	Yield Strength (MPa)	711
Heat ID	ABB 333	Test Env.	High-DO Water	Ultimate Tensile Strength (MPa)	711
Material Description	Type 304 SS from ABB	Strain Rate	3.31E-7 1/s	Uniform Elongation (%)	4.06
Dose	2.44 dpa			Total Elongation (%)	5.34

Strain (%)	Stress (MPa)						
0.000	0.000	0.171	299.885	1.273	706.713	3.917	704.859
0.069	120.844	0.179	314.342	1.349	705.415	3.980	706.898
0.070	122.882	0.187	328.057	1.422	704.859	4.054	706.342
0.071	123.994	0.196	343.811	1.496	704.118	4.125	706.342
0.071	125.663	0.205	360.492	1.569	703.562	4.197	706.157
0.072	126.775	0.212	371.983	1.644	702.450	4.265	707.083
0.073	127.701	0.220	386.811	1.711	703.747	4.341	705.601
0.073	127.887	0.231	402.750	1.786	702.635	4.411	706.157
0.073	128.443	0.234	421.655	1.853	703.932	4.485	705.230
0.073	129.184	0.251	436.483	1.921	704.859	4.561	704.674
0.074	129.925	0.265	452.422	1.991	705.045	4.633	704.488
0.075	131.223	0.272	470.400	2.069	703.376	4.712	702.264
0.076	133.076	0.277	488.564	2.137	704.118	4.798	698.372
0.077	135.300	0.286	505.986	2.208	704.303	4.878	695.963
0.077	135.671	0.289	524.706	2.277	704.859	4.961	692.627
0.078	137.710	0.301	541.201	2.350	704.488	5.057	685.769
0.079	139.749	0.317	556.585	2.414	706.342	5.148	680.209
0.081	142.899	0.323	574.748	2.488	705.601	5.245	673.166
0.079	139.378	0.340	589.761	2.562	705.045	5.348	664.269
0.082	144.197	0.352	606.071	2.632	705.415	5.459	653.334
0.084	147.162	0.363	623.123	2.701	705.971	5.585	638.321
0.087	153.649	0.367	641.657	2.775	705.045	6.774	328.428
0.091	160.136	0.374	659.450	2.845	705.415	7.979	14.457
0.094	165.697	0.385	676.131	2.913	706.342		
0.097	169.774	0.415	687.622	2.991	704.674		
0.100	175.890	0.433	702.264	3.066	703.562		
0.104	182.563	0.484	708.010	3.126	706.527		
0.107	188.679	0.547	710.419	3.200	705.786		
0.111	194.610	0.626	708.195	3.270	706.157		
0.117	205.731	0.703	706.527	3.346	705.045		
0.122	214.442	0.775	706.342	3.418	704.859		
0.127	223.153	0.851	705.045	3.488	705.045		
0.134	236.312	0.921	705.415	3.556	705.971		
0.141	248.730	0.990	705.971	3.632	704.674		
0.149	262.260	1.073	702.820	3.695	706.898		
0.156	274.678	1.133	705.786	3.771	705.601		
0.163	287.096	1.205	705.786	3.839	706.713		

Test ID SSRT005

Specimen ID	690-01	Test Temp.	289°C	Yield Strength (MPa)	837
Heat ID	690	Test Env.	High-DO Water	Ultimate Tensile Strength (MPa)	868
Material Description	Alloy 690	Strain Rate	3.31E-7 1/s	Uniform Elongation (%)	5.94
Dose	1.96 dpa			Total Elongation (%)	7.29

Strain (%)	Stress (MPa)						
0.000	0.000	0.074	146.792	0.778	850.724	4.561	847.388
0.065	129.925	0.077	153.835	0.866	854.616	4.699	837.194
0.066	130.481	0.083	165.326	0.959	857.026	4.772	845.349
0.066	130.481	0.090	178.300	1.061	857.026	4.860	849.241
0.066	130.667	0.096	191.274	1.159	858.879	4.957	850.724
0.066	130.667	0.103	204.433	1.247	862.586	5.082	844.052
0.066	130.481	0.112	221.670	1.349	862.771	5.176	846.276
0.066	130.667	0.118	235.200	1.435	867.034	5.303	839.233
0.066	130.852	0.128	254.105	1.554	862.401	5.389	843.496
0.066	130.852	0.137	273.010	1.655	862.401	5.494	842.754
0.066	131.408	0.148	294.510	1.747	865.366	5.638	830.892
0.066	131.037	0.159	315.083	1.831	870.370	5.717	837.379
0.066	131.223	0.168	333.432	1.935	869.814	5.805	841.272
0.066	131.223	0.178	352.893	2.065	861.659	5.914	839.233
0.067	132.335	0.188	374.207	2.174	859.621	6.007	841.642
0.067	133.632	0.200	397.375	2.256	865.366	6.112	840.716
0.067	133.818	0.212	419.987	2.358	865.366	6.256	828.668
0.068	134.930	0.223	443.155	2.464	864.069	6.362	827.742
0.068	135.300	0.234	465.211	2.589	857.396	6.459	829.039
0.068	135.300	0.245	487.267	2.687	858.694	6.532	837.194
0.069	136.042	0.254	509.322	2.762	866.108	6.713	814.768
0.069	136.227	0.264	535.270	2.884	860.362	6.775	825.888
0.069	136.968	0.286	557.697	2.996	857.582	6.878	825.703
0.069	137.710	0.299	582.904	3.098	857.582	7.013	816.250
0.070	138.822	0.305	609.964	3.223	851.095	7.142	808.651
0.070	139.193	0.317	635.356	3.306	856.284	7.282	797.716
0.071	140.119	0.329	660.933	3.397	859.435	7.430	784.742
0.071	140.490	0.345	685.213	3.503	858.323	7.586	769.544
0.071	140.305	0.359	710.049	3.640	848.129	10.347	17.422
0.070	139.934	0.370	735.626	3.696	861.103		
0.071	140.861	0.400	756.014	3.805	859.250		
0.071	141.046	0.418	779.738	3.946	848.129		
0.071	141.417	0.457	797.345	4.037	851.651		
0.072	143.270	0.501	813.655	4.114	858.694		
0.071	141.046	0.555	827.371	4.233	853.690		
0.072	142.343	0.617	838.491	4.325	856.470		
0.073	144.011	0.699	844.052	4.424	857.396		

Test ID SSRT006

Specimen ID	GBE690-12	Test Temp.	289°C	Yield Strength (MPa)	677
Heat ID	GBE690	Test Env.	High-DO Water	Ultimate Tensile Strength (MPa)	801
Material Description	GBE Alloy 690	Strain Rate	3.31E-7 1/s	Uniform Elongation (%)	22.8
Dose	1.96 dpa			Total Elongation (%)	27.6

Strain (%)	Stress (MPa)						
0.000	0.000	4.216	736.182	12.416	769.544	20.618	789.561
0.067	133.076	4.419	738.592	12.623	771.212	20.826	791.044
0.069	137.339	4.612	743.596	12.837	771.212	21.008	798.457
0.073	145.124	4.851	737.665	13.028	776.402	21.219	799.013
0.076	151.796	5.053	740.445	13.262	771.768	21.496	784.371
0.080	158.468	5.269	739.889	13.479	771.027	21.659	796.233
0.085	169.218	5.458	745.820	13.699	769.544	21.908	788.078
0.094	187.196	5.679	743.967	13.892	774.548	22.098	793.453
0.104	206.657	5.906	741.001	14.109	773.807	22.330	789.190
0.116	230.011	6.105	744.337	14.306	777.699	22.511	796.975
0.130	258.739	6.302	748.415	14.524	776.587	22.769	786.595
0.150	296.919	6.531	745.449	14.720	780.850	22.950	794.194
0.177	352.152	6.734	748.044	14.945	778.255	23.156	796.233
0.194	385.699	6.939	750.083	15.122	787.337	23.386	792.341
0.201	424.621	7.159	748.600	15.370	779.367	23.586	796.233
0.241	465.211	7.387	745.264	15.573	781.962	23.823	790.858
0.252	512.473	7.568	752.863	15.760	788.263	24.046	788.820
0.277	556.399	7.761	757.867	16.012	779.367	24.276	784.927
0.287	603.847	7.998	752.307	16.207	783.630	24.500	782.703
0.342	640.916	8.180	759.721	16.411	786.039	24.698	786.410
0.441	667.605	8.430	751.380	16.644	781.591	24.902	788.634
0.590	682.803	8.594	763.057	16.841	785.483	25.113	789.190
0.760	692.997	8.831	757.682	17.060	784.371	25.362	781.035
0.958	696.704	9.042	758.238	17.230	794.380	25.590	777.884
1.148	703.006	9.254	758.609	17.464	789.746	25.808	776.772
1.343	707.454	9.434	766.949	17.715	781.035	26.046	771.212
1.549	709.122	9.692	756.570	17.898	788.263	26.234	777.143
1.734	715.980	9.897	758.609	18.128	784.927	26.484	768.988
1.946	716.350	10.059	770.841	18.330	787.707	26.693	769.915
2.157	717.092	10.327	758.238	18.547	786.966	26.939	762.501
2.362	719.131	10.536	759.350	18.762	786.781	27.170	758.423
2.557	723.393	10.732	763.428	18.970	788.078	27.442	744.893
2.785	720.057	10.923	768.802	19.193	786.039	27.729	727.842
2.976	725.432	11.125	771.583	19.406	786.039	28.015	710.975
3.186	726.359	11.355	767.690	19.642	781.035	31.176	24.465
3.394	727.656	11.559	770.100	19.791	796.048	31.396	22.983
3.571	736.367	11.799	763.984	19.966	805.130	31.608	23.353
3.804	732.475	11.990	769.173	20.213	797.345		
4.024	730.993	12.221	765.281	20.452	791.600		

Test ID SSRT007

Specimen ID	GBE304L-05	Test Temp.	289°C	Yield Strength (MPa)	231
Heat ID	GBE304L	Test Env.	High-DO Water	Ultimate Tensile Strength (MPa)	532
Material Description	Non-Irr. GBE304L	Strain Rate	3.31E-7 1/s	Uniform Elongation (%)	32.2
Dose	-		(8.15E-7 1/s)	Total Elongation (%)	36.1

Strain (%)	Stress (MPa)						
0.000	0.000	9.187	402.936	19.587	494.310	27.177	524.150
0.074	129.369	9.531	406.828	19.781	495.051	27.372	524.891
0.076	133.818	9.887	410.164	19.968	496.163	27.594	524.335
0.078	136.968	10.243	413.500	20.187	495.792	27.809	524.150
0.083	145.680	10.575	417.948	20.358	497.646	28.012	524.520
0.090	157.541	10.896	422.953	20.544	498.758	28.230	524.150
0.099	173.296	11.240	426.845	20.743	499.314	28.417	525.633
0.110	192.942	11.600	429.996	20.930	500.426	28.652	524.520
0.011	212.403	11.960	433.146	21.105	502.094	28.787	528.042
0.200	223.524	12.324	436.112	21.339	500.982	28.957	529.895
0.389	234.644	12.672	439.819	21.490	503.762	29.208	528.042
0.677	241.131	13.096	440.004	21.712	503.206	29.486	524.891
0.869	252.252	13.317	449.642	21.928	503.391	29.673	526.003
1.086	262.075	13.697	451.866	22.075	506.357	29.867	526.745
1.430	265.967	14.021	456.685	22.281	506.542	29.967	531.934
1.679	274.308	14.425	457.797	22.500	506.172	30.289	526.745
1.904	283.760	14.809	459.836	22.559	513.215	30.440	529.525
2.272	286.540	15.117	465.396	22.766	513.400	30.682	528.042
2.510	295.437	15.533	465.952	22.984	513.029	30.885	528.783
2.795	302.109	15.838	471.698	23.131	515.995	31.060	530.451
3.139	306.001	16.057	471.883	23.692	499.685	31.278	530.081
3.391	314.156	16.254	471.142	23.513	517.848	31.437	532.490
3.767	316.566	16.398	472.810	23.711	518.404	31.592	535.085
4.004	325.462	16.531	475.034	23.947	517.663	31.878	531.564
4.368	328.428	16.676	476.702	24.134	518.775	32.117	530.266
4.720	331.949	16.833	477.814	24.328	519.516	32.212	535.641
4.945	341.402	17.009	477.999	24.515	520.628	32.387	537.309
5.249	347.147	17.358	480.409	24.726	520.628	32.804	527.671
5.570	352.152	17.521	482.633	24.920	521.370	32.860	534.900
5.878	357.712	17.712	483.560	25.103	522.667	33.043	536.197
6.230	361.233	17.898	484.672	25.337	521.555	33.412	528.783
6.499	368.647	18.093	485.413	25.568	520.628	33.595	530.081
6.873	371.242	18.296	485.784	25.743	522.296	33.837	528.598
7.161	377.729	18.435	489.120	25.969	521.555	34.163	523.223
7.529	380.509	18.621	490.232	26.124	524.150	34.605	512.473
7.849	385.513	18.832	490.232	26.418	520.258	34.887	509.137
8.165	390.703	19.007	491.900	26.545	524.150	35.507	490.047
8.502	394.966	19.178	493.754	26.756	524.150	45.682	25.763
8.847	398.858	19.396	493.383	26.986	523.223	45.932	23.909

Test ID SSRT009

Specimen ID	GBE316-12	Test Temp.	289°C	Yield Strength (MPa)	640
Heat ID	GBE316	Test Env.	High-DO Water	Ultimate Tensile Strength (MPa)	644
Material Description	GBE Type 316 SS	Strain Rate	3.31E-7 1/s	Uniform Elongation (%)	4.44
Dose	1.96 dpa			Total Elongation (%)	6.80

Strain (%)	Stress (MPa)						
0.000	0.000	0.303	530.081	2.074	652.407	4.289	663.898
0.092	161.248	0.305	544.723	2.137	651.851	4.351	663.713
0.087	152.352	0.312	558.438	2.192	653.334	4.409	664.640
0.090	157.541	0.319	571.968	2.258	652.222	4.471	664.269
0.093	163.472	0.328	585.128	2.322	651.480	4.526	665.752
0.098	171.813	0.340	597.175	2.375	653.334	4.584	666.679
0.102	179.041	0.356	608.481	2.437	653.334	4.649	665.566
0.107	187.567	0.370	620.343	2.503	652.036	4.715	664.269
0.111	195.907	0.392	629.981	2.557	653.890	4.768	666.308
0.114	201.282	0.423	637.394	2.614	654.817	4.838	664.269
0.119	209.808	0.476	639.433	2.681	653.334	4.902	663.342
0.125	219.075	0.526	642.213	2.739	654.446	4.979	659.450
0.130	229.084	0.579	644.252	2.798	655.002	5.050	657.041
0.135	237.980	0.635	645.549	2.857	655.558	5.139	650.183
0.142	249.472	0.696	645.549	2.921	654.817	5.221	644.808
0.148	260.592	0.761	644.623	2.982	654.817	5.321	635.170
0.154	270.045	0.815	646.291	3.039	655.743	5.427	623.864
0.159	280.424	0.876	646.291	3.093	657.597	5.572	603.106
0.167	292.842	0.932	647.774	3.160	656.114	5.741	576.231
0.172	301.738	0.991	648.144	3.217	657.041	5.895	552.878
0.178	312.859	1.055	647.403	3.274	658.153	6.035	533.417
0.184	323.609	1.120	646.476	3.342	656.485	6.168	515.253
0.191	335.471	1.169	649.442	3.399	657.411	6.301	497.460
0.198	347.703	1.235	648.330	3.453	659.079	6.448	475.961
0.205	359.936	1.294	648.886	3.519	657.967	6.641	443.155
0.212	373.281	1.367	645.735	3.577	658.709	6.831	410.905
0.218	383.845	1.416	648.886	3.628	661.118	8.537	0.927
0.218	398.858	1.472	650.183	3.690	661.118	8.602	0.000
0.236	409.793	1.536	649.442	3.754	660.192	8.664	-0.371
0.237	424.806	1.598	649.256	3.808	662.045	8.716	2.039
0.252	436.112	1.652	650.924	3.877	660.006		
0.251	451.681	1.715	650.368	3.931	661.860		
0.264	463.728	1.771	651.851	3.989	662.601		
0.271	477.073	1.832	651.851	4.049	662.786		
0.280	490.047	1.901	649.812	4.113	662.045		
0.286	503.762	1.972	647.403	4.177	661.489		
0.290	518.033	2.023	649.812	4.233	662.786		

Test ID SSRT010

Specimen ID	945-02	Test Temp.	289°C	Yield Strength (MPa)	666
Heat ID	945	Test Env.	High-DO Water	Ultimate Tensile Strength (MPa)	666
Material Description	High-Purity Type 304L SS with High-O	Strain Rate	3.31E-7 1/s	Uniform Elongation (%)	1.22
Dose	2.44 dpa			Total Elongation (%)	2.20

Strain (%)	Stress (MPa)						
0.000	0.000	0.116	203.507	0.259	461.504	0.785	580.679
0.076	134.188	0.120	210.920	0.266	468.362	0.826	579.197
0.077	134.744	0.123	216.666	0.268	476.517	0.868	577.343
0.077	135.300	0.126	221.855	0.265	485.784	0.909	575.675
0.077	135.856	0.130	227.786	0.264	494.866	0.946	575.119
0.077	135.856	0.133	234.088	0.268	502.465	0.987	573.451
0.078	136.783	0.136	239.278	0.270	510.620	1.021	573.636
0.078	137.710	0.139	244.653	0.268	519.702	1.064	571.598
0.079	138.822	0.142	249.472	0.273	526.930	1.096	572.154
0.080	140.119	0.146	257.071	0.274	535.456	1.139	570.115
0.081	141.602	0.151	265.226	0.280	542.499	1.178	569.003
0.082	144.938	0.155	272.454	0.290	548.615	1.219	567.520
0.084	148.089	0.159	278.941	0.295	556.214	1.259	566.037
0.086	150.684	0.163	286.911	0.303	562.701	1.295	565.667
0.087	153.279	0.167	293.027	0.312	569.188	1.339	563.443
0.089	156.059	0.171	300.441	0.302	580.309	1.382	561.404
0.090	157.541	0.175	307.855	0.302	588.834	1.424	559.365
0.083	145.865	0.179	314.156	0.306	596.434	1.468	557.141
0.084	146.977	0.183	321.941	0.306	605.145	1.511	554.917
0.084	148.274	0.186	327.686	0.307	613.670	1.552	553.434
0.085	149.757	0.190	334.173	0.312	620.899	1.600	550.098
0.086	151.240	0.189	340.660	0.309	630.351	1.652	545.650
0.087	153.279	0.199	346.962	0.315	637.394	1.705	541.201
0.088	154.576	0.198	355.858	0.314	646.476	1.754	537.494
0.090	157.727	0.194	365.496	0.317	654.261	1.817	530.451
0.091	160.136	0.196	373.466	0.326	660.562	1.884	522.482
0.091	160.692	0.211	378.285	0.342	665.196	1.956	513.215
0.093	163.843	0.219	384.957	0.351	666.493	2.015	507.098
0.095	167.179	0.230	390.888	0.352	666.864	2.081	499.129
0.096	168.662	0.233	398.858	0.594	606.998	2.153	489.861
0.098	173.110	0.239	406.086	0.650	593.468	2.223	481.150
0.100	176.446	0.240	414.241	0.651	593.839	2.322	465.025
0.102	179.968	0.248	421.099	0.663	591.244	4.118	25.577
0.105	184.602	0.248	429.625	0.676	588.464	4.162	23.168
0.108	189.420	0.249	438.151	0.673	589.947	4.198	22.797
0.110	193.869	0.253	445.750	0.690	587.166	4.236	22.056
0.114	199.985	0.248	455.573	0.741	583.089	4.274	21.129

Test ID SSRT011

Specimen ID	327-01	Test Temp.	289°C	Yield Strength (MPa)	703
Heat ID	327	Test Env.	High-DO Water	Ultimate Tensile Strength (MPa)	703
Material Description	High-Purity Type 304L SS with Low-O	Strain Rate	3.31E-7 1/s	Uniform Elongation (%)	1.51
Dose	2.44 dpa			Total Elongation (%)	3.10

Strain (%)	Stress (MPa)						
0.000	0.000	0.120	210.550	0.296	523.408	0.830	607.739
0.081	143.270	0.124	218.149	0.302	533.417	0.897	600.696
0.082	144.197	0.128	224.265	0.303	544.723	0.954	596.434
0.083	145.124	0.132	231.864	0.314	553.249	1.005	594.024
0.083	145.124	0.136	238.351	0.317	563.999	1.056	591.429
0.083	145.494	0.140	245.579	0.325	573.451	1.107	588.834
0.083	146.050	0.144	253.364	0.331	583.274	1.161	585.498
0.083	146.236	0.148	260.778	0.341	592.171	1.211	583.274
0.084	146.977	0.152	267.821	0.344	603.106	1.264	580.123
0.083	146.606	0.156	275.049	0.350	612.929	1.316	577.529
0.083	146.606	0.162	284.501	0.351	624.235	1.370	574.007
0.084	147.348	0.165	290.432	0.364	632.390	1.420	571.783
0.084	147.718	0.170	298.402	0.365	643.696	1.473	568.817
0.084	147.904	0.175	307.669	0.370	653.705	1.531	564.369
0.084	147.718	0.180	316.195	0.378	663.157	1.590	559.550
0.084	147.718	0.183	322.497	0.389	671.868	1.640	557.326
0.084	147.718	0.189	331.579	0.391	682.803	1.699	552.693
0.084	148.274	0.193	339.548	0.409	689.290	1.761	546.947
0.084	148.274	0.198	347.518	0.421	697.631	1.815	543.796
0.084	148.274	0.203	356.229	0.442	703.562	1.878	537.865
0.084	147.718	0.208	365.496	0.442	703.562	1.936	533.417
0.085	148.645	0.213	374.763	0.444	703.562	1.996	528.227
0.085	149.016	0.218	383.845	0.445	703.747	2.068	520.072
0.086	151.425	0.223	391.259	0.445	704.488	2.133	513.585
0.087	153.835	0.228	400.526	0.448	704.118	2.200	506.728
0.089	156.800	0.233	409.793	0.449	704.488	2.272	498.387
0.091	159.580	0.238	418.134	0.453	703.932	2.351	488.193
0.092	162.360	0.243	427.215	0.453	704.488	2.423	479.853
0.095	166.994	0.248	436.853	0.456	704.118	2.501	469.659
0.097	170.515	0.254	445.935	0.472	700.411	2.579	459.650
0.099	174.037	0.259	455.202	0.781	615.339	2.681	443.155
0.102	178.856	0.264	464.840	0.792	612.929	2.770	429.996
0.104	183.490	0.269	473.551	0.799	611.446	2.869	414.241
0.107	187.938	0.276	484.486	0.806	610.149	2.974	396.634
0.111	194.981	0.280	493.012	0.812	609.037	3.096	374.578
0.114	200.541	0.287	502.835	0.818	607.925	4.479	3.336
0.117	204.989	0.291	513.400	0.822	608.110	4.525	2.039

Test ID SSRT012

Specimen ID	623-01	Test Temp.	289°C	Yield Strength (MPa)	883
Heat ID	623	Test Env.	High-DO Water	Ultimate Tensile Strength (MPa)	883
Material Description	Type 316LN SS	Strain Rate	3.31E-7 1/s	Uniform Elongation (%)	1.94
Dose	2.44 dpa			Total Elongation (%)	4.00

Strain (%)	Stress (MPa)						
0.000	0.000	0.201	353.078	0.514	834.970	2.450	859.064
0.072	127.331	0.207	364.570	0.529	846.647	2.511	857.026
0.076	134.374	0.214	375.875	0.561	853.504	2.569	856.099
0.077	134.930	0.221	388.108	0.573	866.478	2.628	854.616
0.077	134.744	0.227	398.858	0.615	870.185	2.696	850.724
0.077	134.930	0.234	410.535	0.655	874.633	2.752	849.983
0.077	134.930	0.241	423.509	0.690	880.564	2.813	848.129
0.077	134.559	0.247	434.629	0.757	876.672	2.880	844.422
0.077	136.227	0.254	446.676	0.801	879.823	2.939	842.940
0.077	135.671	0.261	459.094	0.865	877.043	3.006	839.233
0.080	139.934	0.270	473.922	0.931	873.521	3.073	835.526
0.079	139.193	0.277	486.896	0.985	873.707	3.135	833.116
0.079	139.378	0.285	501.723	1.050	870.556	3.197	830.707
0.080	140.490	0.292	514.141	1.108	869.258	3.257	829.224
0.083	145.865	0.300	528.227	1.165	868.702	3.326	824.591
0.086	150.684	0.308	541.016	1.218	868.888	3.396	819.957
0.090	159.024	0.315	553.805	1.266	870.926	3.462	816.621
0.095	166.253	0.321	563.999	1.324	869.814	3.522	814.953
0.100	175.520	0.340	574.192	1.381	869.258	3.597	808.651
0.103	181.265	0.336	591.800	1.433	869.814	3.661	805.686
0.109	190.903	0.345	605.515	1.488	870.000	3.733	800.311
0.113	199.244	0.351	620.157	1.536	872.038	3.801	796.419
0.118	208.140	0.357	634.985	1.597	870.000	3.864	793.824
0.124	217.778	0.359	650.739	1.657	868.332	3.935	788.634
0.128	224.636	0.375	662.416	1.721	865.551	4.008	783.074
0.134	235.200	0.387	675.204	1.766	868.332	4.083	776.772
0.139	243.541	0.392	690.402	1.819	868.702	4.167	768.061
0.144	253.178	0.385	708.937	1.878	867.405	4.246	760.462
0.149	261.148	0.401	720.428	1.936	866.478	4.375	738.036
0.155	272.639	0.405	735.997	1.991	866.108	6.886	-6.487
0.159	279.868	0.420	747.673	2.049	865.181	6.941	-6.672
0.165	290.247	0.436	759.350	2.103	865.366		
0.170	298.402	0.444	773.621	2.166	862.771		
0.177	310.449	0.453	787.337	2.214	864.625		
0.181	318.975	0.461	801.237	2.277	862.030		
0.188	331.393	0.481	811.802	2.327	863.327		
0.194	341.031	0.492	824.961	2.395	859.250		

Test ID SSRT013

Specimen ID	625-01	Test Temp.	289°C	Yield Strength (MPa)	890
Heat ID	625	Test Env.	High-DO Water	Ultimate Tensile Strength (MPa)	890
Material Description	Type 316LN, Ti doped	Strain Rate	3.31E-7 1/s	Uniform Elongation (%)	0.75
Dose	2.44 dpa			Total Elongation (%)	2.59

Strain (%)	Stress (MPa)						
0.000	0.000	0.075	132.520	0.273	481.521	0.971	880.194
0.067	118.249	0.077	134.559	0.283	495.051	1.010	885.198
0.068	118.990	0.078	137.339	0.293	508.210	1.061	886.681
0.068	119.546	0.078	137.524	0.299	522.667	1.144	879.267
0.068	119.732	0.080	141.231	0.305	537.309	1.188	882.788
0.068	120.288	0.084	147.904	0.313	551.025	1.271	875.189
0.069	120.473	0.087	153.835	0.314	566.964	1.337	872.224
0.068	120.102	0.092	161.063	0.326	579.567	1.401	870.185
0.069	120.844	0.096	168.662	0.334	593.653	1.476	864.995
0.069	121.214	0.100	175.334	0.340	608.110	1.548	860.362
0.070	122.512	0.104	182.377	0.343	623.494	1.622	855.358
0.070	122.326	0.108	189.420	0.357	635.541	1.703	848.315
0.070	122.326	0.112	197.390	0.355	652.222	1.775	843.866
0.070	122.697	0.117	205.175	0.366	665.381	1.857	836.453
0.070	122.697	0.123	216.666	0.382	676.872	1.935	830.336
0.070	122.697	0.128	225.562	0.404	686.881	2.021	821.996
0.070	123.068	0.134	235.942	0.413	700.411	2.098	816.065
0.070	123.438	0.139	244.282	0.431	711.346	2.185	807.354
0.071	124.736	0.146	256.515	0.457	720.243	2.265	800.496
0.071	125.663	0.151	265.596	0.458	735.997	2.350	792.341
0.072	126.775	0.157	276.161	0.457	752.492	2.434	784.371
0.072	127.145	0.164	288.394	0.461	767.505	2.501	781.220
0.073	127.516	0.171	299.885	0.469	781.406	2.569	778.070
0.073	128.443	0.177	311.005	0.449	803.462	2.663	767.320
0.073	127.701	0.183	322.126	0.466	814.768	2.759	755.828
0.073	128.443	0.189	331.764	0.481	826.629	2.869	740.630
0.073	128.257	0.195	342.143	0.501	837.009	2.980	725.062
0.073	128.813	0.201	353.078	0.509	850.909	5.502	18.349
0.074	129.555	0.207	363.643	0.531	860.733	5.560	17.793
0.074	130.296	0.213	374.022	0.568	866.478	5.621	16.681
0.074	130.481	0.221	388.849	0.599	873.521	5.681	15.569
0.075	131.037	0.223	399.043	0.641	877.784	5.737	15.569
0.075	131.037	0.227	413.871	0.688	880.379	5.794	15.383
0.075	132.150	0.241	426.289	0.711	890.202	5.854	14.457
0.076	134.003	0.248	440.375	0.772	888.719	5.907	15.569
0.079	138.080	0.263	452.237	0.822	890.573	5.968	14.086
0.076	133.262	0.271	465.952	0.892	886.681	6.021	15.198

Test ID SSRT015

Specimen ID	327-03	Test Temp.	289°C	Yield Strength (MPa)	690
Heat ID	327	Test Env.	High-DO Water	Ultimate Tensile Strength (MPa)	690
Material Description	High-Purity Type 304L SS with Low-O	Strain Rate	3.31E-7 1/s	Uniform Elongation (%)	1.25
Dose	2.44 dpa			Total Elongation (%)	2.59

Strain (%)	Stress (MPa)						
0.000	0.000	0.100	176.076	0.250	447.047	0.727	593.468
0.076	134.003	0.102	179.041	0.258	455.758	0.796	585.869
0.076	134.188	0.105	184.416	0.259	466.508	0.848	582.904
0.076	133.818	0.108	189.606	0.270	474.663	0.900	579.753
0.076	134.003	0.110	194.239	0.276	483.930	0.951	576.973
0.076	133.818	0.114	199.985	0.284	492.827	1.005	573.451
0.076	134.374	0.117	206.472	0.288	502.835	1.055	571.042
0.076	134.003	0.121	212.588	0.295	511.917	1.109	567.335
0.076	134.188	0.125	219.446	0.298	522.111	1.159	564.925
0.076	133.632	0.128	225.006	0.306	530.822	1.215	560.662
0.076	133.447	0.131	230.752	0.308	541.387	1.269	557.141
0.076	133.818	0.136	238.536	0.311	551.581	1.328	552.137
0.076	134.188	0.139	244.838	0.313	562.145	1.386	547.688
0.077	134.559	0.143	251.140	0.315	572.524	1.440	543.981
0.077	135.115	0.146	256.700	0.318	582.718	1.496	539.904
0.077	135.671	0.150	263.002	0.319	593.283	1.550	536.197
0.077	135.486	0.154	271.157	0.300	609.778	1.614	530.081
0.077	135.486	0.159	278.941	0.300	620.899	1.677	523.964
0.077	136.042	0.163	286.169	0.293	633.687	1.734	519.702
0.077	135.486	0.168	294.695	0.301	642.584	1.811	509.878
0.078	136.783	0.172	302.294	0.311	650.924	1.884	501.167
0.080	139.934	0.176	308.967	0.324	658.523	1.960	491.529
0.081	142.714	0.181	318.234	0.323	669.644	2.040	480.965
0.082	144.382	0.186	327.316	0.342	675.575	2.117	471.142
0.083	145.124	0.190	334.359	0.349	684.657	2.222	453.905
0.083	146.606	0.195	342.328	0.352	687.252	2.349	430.552
0.084	147.348	0.199	350.669	0.351	687.993	2.492	402.750
0.084	147.904	0.203	356.970	0.352	688.178	3.996	7.599
0.084	148.089	0.208	365.867	0.349	689.661	4.040	6.672
0.085	148.830	0.214	375.875	0.349	690.217	4.085	5.746
0.085	150.313	0.218	383.475	0.352	689.846	4.124	6.116
0.087	153.279	0.224	393.854	0.355	689.661	4.167	5.375
0.089	156.429	0.228	401.638	0.356	690.032	4.203	6.672
0.091	159.766	0.233	410.349	0.360	689.290	4.246	6.116
0.093	162.916	0.238	418.134	0.668	606.813	4.288	5.931
0.095	166.809	0.241	427.586	0.697	599.399	4.328	5.931
0.097	170.330	0.243	437.965	0.708	596.990	4.370	5.560

Test ID SSRT016

Specimen ID	GBE304L-07	Test Temp.	290°C	Yield Strength (MPa)	750
Heat ID	GBE304L	Test Env.	Air	Ultimate Tensile Strength (MPa)	750
Material Description	GBE Type 304L SS	Strain Rate	3.31E-7 1/s	Uniform Elongation (%)	9.41
Dose	1.96			Total Elongation (%)	11.3

Strain (%)	Stress (MPa)						
0.000	0.000	0.063	110.300	1.665	712.600	5.511	721.400
0.000	-0.700	0.080	141.200	1.729	724.700	5.585	730.600
0.000	0.700	0.089	155.900	1.884	709.700	5.726	719.700
0.000	0.400	0.102	179.400	1.951	721.200	5.838	717.500
0.000	0.700	0.115	202.800	2.081	713.600	5.906	728.400
0.001	2.400	0.128	224.800	2.169	718.600	6.023	724.700
0.001	1.900	0.141	248.700	2.282	716.000	6.159	715.600
0.000	0.400	0.152	272.100	2.387	716.000	6.226	726.700
0.000	-0.200	0.154	302.700	2.477	720.200	6.326	728.200
0.000	0.700	0.191	322.900	2.603	713.900	6.513	715.200
0.001	2.600	0.175	358.800	2.666	726.400	6.582	726.000
0.001	2.200	0.215	377.900	2.813	713.800	6.661	733.600
0.000	0.000	0.202	413.100	2.870	728.000	6.850	717.500
0.000	0.700	0.245	429.600	3.027	712.500	7.117	714.900
0.001	1.900	0.238	433.500	3.098	722.500	7.354	721.000
0.001	2.200	0.210	459.500	3.232	713.900	7.578	731.200
0.001	2.200	0.258	476.300	3.296	726.000	7.834	731.500
0.000	0.400	0.233	515.100	3.435	715.600	8.128	720.800
0.001	0.900	0.274	534.000	3.502	726.900	8.394	718.600
0.001	2.200	0.261	569.000	3.621	722.700	8.620	729.500
0.000	0.700	0.283	593.800	3.733	720.600	8.900	722.800
0.002	3.000	0.299	620.300	3.850	716.900	9.183	715.400
0.001	2.200	0.314	646.800	3.921	727.100	9.437	716.400
0.001	1.100	0.330	673.400	4.065	715.200	9.667	724.700
0.001	0.900	0.341	701.300	4.177	713.200	9.924	724.900
0.005	8.900	0.391	717.500	4.245	723.900	10.238	708.400
0.007	11.900	0.416	741.400	4.335	728.400	10.529	698.600
0.007	12.400	0.583	722.700	4.464	721.200	10.784	699.300
0.012	21.900	0.663	730.300	4.586	716.000	11.153	666.300
0.015	25.600	0.818	715.400	4.647	729.100		
0.014	23.900	0.903	721.200	4.772	723.000		
0.020	35.000	1.033	713.800	4.904	714.900		
0.028	49.300	1.107	722.800	4.967	727.300		
0.030	52.500	1.258	709.100	5.109	716.200		
0.035	62.300	1.305	726.400	5.205	718.900		
0.043	75.100	1.456	712.500	5.278	728.400		
0.058	102.100	1.519	724.900	5.420	717.100		

NRC FORM 335 (9-2004) NRCMD 3.7		U.S. NUCLEAR REGULATORY COMMISSION		1. REPORT NUMBER (Assigned by NRC, Add Vol., Supp., Rev., and Addendum Numbers, if any.) NUREG/CR-6965	
BIBLIOGRAPHIC DATA SHEET <i>(See instructions on the reverse)</i>					
2. TITLE AND SUBTITLE Irradiation-Assisted Stress Corrosion Cracking of Austenitic Stainless Steels and Alloy 690 from Halden Phase-II Irradiations				3. DATE REPORT PUBLISHED	
				MONTH September	YEAR 2008
5. AUTHOR(S) Y. Chen, O. K. Chopra, W. K. Soppet, N. L. Dietz Rago and W. J. Shack				4. FIN OR GRANT NUMBER Y6388	
				6. TYPE OF REPORT Technical	
8. PERFORMING ORGANIZATION - NAME AND ADDRESS <i>(If NRC, provide Division, Office or Region, U.S. Nuclear Regulatory Commission, and mailing address; if contractor, provide name and mailing address.)</i> Argonne National Laboratory 9700 South Cass Avenue Argonne, IL 60439				7. PERIOD COVERED <i>(Inclusive Dates)</i>	
				9. SPONSORING ORGANIZATION - NAME AND ADDRESS <i>(If NRC, type "Same as above"; if contractor, provide NRC Division, Office or Region, U.S. Nuclear Regulatory Commission, and mailing address.)</i> Division of Engineering Office of Nuclear Regulatory Research US Nuclear Regulatory Commission Washington, DC 20555-0001	
10. SUPPLEMENTARY NOTES Appajosula S. Rao, Program Manager					
11. ABSTRACT <i>(200 words or less)</i> This work is an ongoing effort at Argonne National Laboratory on the mechanistic study of irradiation-assisted stress corrosion cracking (IASCC) in the core internals of light water reactors. Phase II in this effort focused on determining the influence of grain boundary engineering (GBE), alloying elements, and neutron dose on the IASCC susceptibility of austenitic stainless steels (SSs) and Alloy 690. Flat dog-bone specimens irradiated in the Halden boiling heavy water reactor to neutron doses of ~2 displacements per atom (dpa) were subjected to slow strain rate tensile (SSRT) tests in high dissolved oxygen water at 289°C. The areas of the fracture surfaces with brittle fracture morphology (intergranular and transgranular cleavage cracking) were measured with a scanning electron microscope. All materials showed significant irradiation hardening and loss of ductility. Some strain hardening was observed in the normal-carbon (C) content SSs (Types 304 and 316) and Alloy 690, but not in the low-C content SSs (Types 304L and 316L). The area fraction of the intergranular cracking increased with decreasing uniform elongation and was used to rank the IASCC susceptibility of the alloys. The GBE process did not seem to have a significant effect on the IASCC behavior of Type 304 and 304L SSs, at least at a dose level of about ~2 dpa, but did affect the cracking behavior of Alloy 690. A minimum-C content and a low-sulfur (S) content (<0.002 wt.%) may be required for IASCC resistance. By analysis of the results from the Halden Phase-II specimens along with previous results on Halden Phase-I specimens, the effect of neutron dose on IASCC behavior was determined. While irradiation hardening and embrittlement start below 0.4 dpa, IG cracking appears between 0.4 and 1.3 dpa for most commercial austenitic SSs in this study.					
12. KEY WORDS/DESCRIPTORS <i>(List words or phrases that will assist researchers in locating the report.)</i> Irradiation assisted stress corrosion cracking (IASCC), Stainless steels, irradiation hardening, Inter granular cracking				13. AVAILABILITY STATEMENT unlimited	
				14. SECURITY CLASSIFICATION <i>(This Page)</i> unclassified	
				<i>(This Report)</i> unclassified	
				15. NUMBER OF PAGES	
16. PRICE					





UNITED STATES
NUCLEAR REGULATORY COMMISSION
WASHINGTON, DC 20555-0001

OFFICIAL BUSINESS